Thesis for the degree of Doctor of Philosophy

High Spectral Efficiency Transmission using Optical Frequency Combs

Mikael Mazur

Photonics Laboratory
Department of Microtechnology and Nanoscience – MC2
Chalmers University of Technology
Göteborg, Sweden 2019

High Spectral Efficiency Transmission using Optical Frequency Combs

Mikael Mazur

Göteborg, September 2019

ISBN 978-91-7905-163-1

Doktorsavhandlingar vid Chalmers tekniska högskola
Ny serie nr 4630
ISSN 0346-718X

Technical Report MC2-419
ISSN 1652-0769

Photonics Laboratory
Department of Microtechnology and Nanoscience – MC2
Chalmers University of Technology
SE-412 96 Göteborg
Sweden
Telephone: +46 (0)31-772 1000

Printed by Chalmers Reproservice, Chalmers University of Technology
Göteborg, Sweden, September 2019

High Spectral Efficiency Transmission using Optical Frequency Combs

Mikael Mazur
Photonics Laboratory
Department of Microtechnology and Nanoscience – MC2
Chalmers University of Technology, SE-412 96 Göteborg, Sweden

Abstract

Modern long-haul optical communication systems transmit data on all available single-mode fiber dimensions, time, polarization, wavelength, phase and amplitude. Powerful digital signal processing and forward error correction has pushed the per-channel throughput towards its theoretical limits and the bandwidth is limited by the erbium-doped fiber amplifiers. Maximizing the spectral efficiency (SE), i.e. the throughput normalized to bandwidth, is therefore of indisputable importance. Even more so in optical networks as large routing guard-bands drastically reduce the SE of traditional WDM systems. Flex-grid networks with optical superchannels can overcome this limitation. Superchannels consist of multiple tightly packed WDM channels routed as a unit. A comb-based superchannel is formed by encoding independent information onto lines from an optical frequency comb, a multi-wavelength light source fully determined by its center frequency and line spacing.

This thesis studies the generation, transmission and detection of comb-based superchannels. Focus is on profiting from unique frequency comb properties to realize systems with capabilities beyond that of conventional systems using arrays of independent lasers. Digital, analog and optical processing schemes are proposed, and combined, to increase the system SE. Superchannel modulation is investigated and a scheme capable of encoding independent information onto the lines from a frequency comb in a single waveguide structure is demonstrated. By combining overhead-optimized pilot-based DSP with a 22 GHz-spaced soliton microcomb, superchannel transmission with record SE for distances up to 3000 km is realized, closing the performance gap between chip-scale and bulk-optic combs in optical communications. The use of two optical pilot tones (PTs) to phase-lock a transmitter and receiver comb pair is studied, realizing self-homodyne detection of a 50×20Gbaud PM-64QAM superchannel with 4% pilot overhead. The PT gains are furthermore analyzed and a complexity-performance trade-off using a single PT and low complexity DSP is proposed. The scheme is used to demonstrate 12 bits/s/Hz SE over the full C-band using $3 \times 50 \times 24$ GBaud PM-256QAM superchannels and DSP-complexity reduction at distances exceeding 1000 km is shown. Finally, a comb-enabled multi-channel joint equalization scheme capable of mitigating inter-channel crosstalk and thereby minimizing the SE loss from spectral guard bands is demonstrated.

Keywords: Coherent optical communication, Optical frequency combs, Superchannels

List of Papers

This thesis is based on the following appended papers:

[I] **M. Mazur**, N. K. Fontaine, H. Chen, R. Ryf, D. T. Neilson, G. Raybon, A. Adamiecke, S. Cortselli and J. Schröder,"Multi-wavelength arbitrary waveform generation through spectro-temporal unitary transformations", Manuscript under Review, 2019

[II] **M. Mazur**, J. Schröder, A. Lorences-Riesgo, T. Yoshida, M. Karlsson and P. Andrekson,"Overhead-optimization of pilot-based digital signal processing for flexible high spectral efficiency transmission",*Optics Express*, Vol. 27, no. 17, pp. 24654–24669, 2019.

[III] **M. Mazur***, M.-G. Suh*, A. Fülöp, J. Schröder, V. Torres-Company, M. Karlsson, K. J. Vahala and P. A. Andrekson, "High spectral efficiency coherent superchannel transmission with soliton microcombs", Manuscript under Review, 2019

[IV] **M. Mazur**, A. Lorences-Riesgo, J. Schröder, P. A. Andrekson and M. Karlsson, "10 Tb/s self-homodyne PM-64QAM superchannel transmission with 4% spectral overhead",*Journal of Lightwave Technology*, Vol. 36, no. 16, pp. 3176-3184, 2018.

[V] **M. Mazur**, A. Lorences-Riesgo, J. Schröder, P. A. Andrekson and M. Karlsson, "High Spectral Efficiency PM-128QAM Comb-Based Superchannel Transmission Enabled by a Single Shared Optical Pilot Tone", *Journal of Lightwave Technology* , Vol. 36, no. 6, pp. 1318 - 1325, 2018.

[VI] **M. Mazur**, J. Schröder, A. Lorences-Riesgo, M. Karlsson and P. A. Andrekson, "Experimental Investigation of Link Impairments in Pilot Tone Aided Superchannel Transmission", *IEEE Photonics Technology Letters*, Vol. 31, no. 6, pp.459–462, 2019

[VII] **M. Mazur**, J. Schröder, A. Lorences-Riesgo, T. Yoshida, M. Karlsson and P. Andrekson, “12 bits/s/Hz Spectral Efficiency Over the C-band Based on Comb-Based Superchannels”, *Journal of Lightwave Technology*, Vol. 37, no. 2, pp. 411–417, 2019.

[VIII] **M. Mazur**, J. Schröder, M. Karlsson and P. Andrekson,"Joint Superchannel Digital Signal Processing for Ultimate Bandwidth Utilization",*Manuscript Submitted*, 2019.

Related publications by the author not included in the thesis:

Journal papers

[A] B. Foo, M. Karlsson, K. Vijayan, **M. Mazur**, P. A. Andrekson,"An Analysis of Nonlinearity Mitigation Using Phase-Sensitive Optical Parametric Amplifiers", *Optics Express*, Special Issue: Nonlinear Optics, Accepted, 2019.

[B] A. Nazemosadat, **M. Mazur**, S. Kruk, I. Kravchenko, J. Carpenter, J. Schröder, P. A. Andrekson and Y. Kivshar,"Dielectric Broadband Metasurfaces for Fiber Mode-Multiplexed Communications", *Advanced Optical Materials*, Special Issue: Metamaterials and Metasurfaces, Vol. 7, no. 14, pp. 1801679, 2019.

[C] V. Torres-Company, J. Schröder, A. Fülöp, **M. Mazur**, L. Lundberg, O. Helgason, M. Karlsson and P. A. Andrekson,"Laser Frequency Combs for Coherent Optical Communications", *Journal of Lightwave Technology*, Vol. 37, no. 7, pp. 1663–1670, 2019.

[D] C. Fougstedt, L. Svensson, **M. Mazur**, M. Karlsson and P. Larsson-Edefors, "ASIC Implementation of Time-Domain Digital Back Propagation for Coherent Receivers", *IEEE Photonics Technology Letters*, Vol. 30, no. 13, pp. 1179–1182, 2018.

[E] **M. Mazur** and M. Karlsson, "Correlation Metric for Polarization Changes", *IEEE Photonics Technology Letters*, Vol. 30, no. 17, pp. 1575–1578, 2018.

[F] A. Fülöp, **M. Mazur**, A. Lorences-Riesgo, P-H. Wang, Xi Xuan, D. E. Leaird, M. Qi, P. A. Andrekson, A. M. Weiner and V. Torres-Company, "High-order coherent communications using mode-locked dark-pulse Kerr combs from microresonators", *Nature Communications* , Vol. 9, Paper. 1598, 2018.

[G] L. Lundberg, M. Karlsson, A. Lorences-Riesgo, **M. Mazur**, V. Torres-Company, J. Schröder and P. A. Andrekson Frequency Comb-Based Transmission Systems Enabling Joint Signal Processing", *Applied Sciences*, Special Issue: DSP for Next Generation Fibre Communication Systems, 2018.

[H] A. Fülöp, **M. Mazur**, A. Lorences-Riesgo, T. A. Eriksson, P-H. Wang, Xi Xuan, D. E. Leaird, M. Qi, P. A. Andrekson, A. M. Weiner and V. Torres-Company, "Long-haul coherent communiations using microresonator-based frequency combs", *Optics Express* , Vol. 25, no. 22, pp. 26678-26688, 2017.

[I] A. Lorences-Riesgo, **M. Mazur**, T. A. Eriksson, P. A. Andrekson and M. Karlsson, "Self-homodyne 24×32-QAM superchannel receiver enabled by all-optical comb regeneration using Brillouin amplification", *Optics Express* , Vol. 24, no. 26, pp. 29714-29723, 2016.

Invited and upgraded conference papers

[J] **M. Mazur**, N. K. Fontaine, R. Ryf, H. Chen, D. T. Neilson and J. Carpenter, "Reduced footprint multiplane light propagation mode multiplexers", *Proceedings of European on Optical Communication (ECOC)*, Paper. W.2.C.4, 2019.

[K] **M. Mazur**, J. Schröder, A. Lorences-Riesgo, M. Karlsson and P. A. Andrekson, "Frequency Comb Based High-Spectral Efficiency Transmission", *OSA Advanced Photonics Congress*, Paper SpTh1E.1, 2019.

[L] R. Ryf, N. K. Fontaine, S. Wittek, K. Choutagunta, **M. Mazur**, H. Chen and J. C. Alvarado-Zacarias, ""Recent Advances in Mode-Multiplexed Transmission over Multimode Fibers, *Proceedings of Conference on Lasers and Electro-Optics (CLEO)*, Paper. SM1G.1, 2019.

[M] K., Choutagunta, R. Ryf, N. K. Fontaine, S. Wittek, J. C. Alvarado-Zacarias, **M. Mazur**, H. Chen, R.-J. Essiambre, R. Amezcua Correa, T. Hayashi, Y. Tamura, T. Hasegawa, T. Taru and J. M. Kahn, "Modal Dynamics in Spatially Multiplexed Links", *Proceedings of Optical Fiber Communications Conference (OFC)*, Paper. M2I.2, 2019.

[N] A. Fülöp, **M. Mazur**, A. Lorences-Riesgo, P-H. Wang, Yi Xuan, D. E. Leaird, M. Qi, P. A. Andrekson, A. M. Weiner and V. Torres-Company, "PM-64QAM Coherent Optical Communications Using a Dark-Pulse Microresonator Frequency Comb", *Proceedings of Conference on Lasers and Electro-Optics (CLEO)*, Paper. SW3C.1, 2018.

[O] A. Fülöp, **M. Mazur**, A. Lorences-Riesgo, T. A. Eriksson, P-H. Wang, Yi Xuan, D. E. Leaird, M. Qi, P. A. Andrekson, A. M. Weiner and V. Torres-Company, "Microresonator frequency combs for long-haul coherent communications", *International conference on Laser Optics (ICLO)*, 2018.

[P] **M. Mazur**, A. Lorences-Riesgo, Jochen Schröder, P. Andrekson and M. Karlsson, "10.3 bits/s/Hz spectral efficiency 54×24 Gbaud PM-128QAM superchannel transmission using single pilot", *Proceedings of European on Optical Communication (ECOC)*, Paper. M.1.F.5, 2017.

Regular conference papers

[Q] B. Foo, M. Karlsson, K. Vijayan , **M. Mazur** and P. A. Andrekson, "Combining phase-sensitive amplifiers with DSP for improved nonlinearity mitigation", *Proceedings of European on Optical Communication (ECOC)*, Paper. Tu.3.B.2, 2019.

[R] **M. Mazur**, M.-G. Suh, A. Fülöp, J. Schröder, V. Torres-Company, M. Karlsson, K. J. Vahala and P. A. Andrekson, "High Spectral Efficiency Superchannel Transmission using a Soliton Microcomb", *Proceedings of European on Optical Communication (ECOC)*, Paper. W.1.A.5, 2019.

[S] T. Yoshida, **M. Mazur**, J. Schröder, M. Karlsson and E. Agrell, "Performance Monitoring for Live Systems with Soft FEC", *Proceedings of European on Optical Communication (ECOC)*, **Top Scored** Paper. W.3.D.5, 2019.

[T] A. Mirani, **M. Mazur**, E. Agrell, B. Foo, J. Schröder, P. A. Andrekson and M. Karlsson, "Comparison of uniform cross QAM and probabilistically shaped QAM formats under the impact of transmitter impairments", *Proceedings of European on Optical Communication (ECOC)*, Paper. Th.2.B.3, 2019.

[U] S., Wittek, R.Ryf, N. K. Fontaine, K. Choutagunta, **M. Mazur**, H. Chen, J. C. Alvarado-Zacarias, M. Capuzzo, R. Kopf, Al Tate, H. Safar, C. Bolle, D. T. Neilson, E. Burrows, K. Kim, M. Bigot-Astruc, F. Achten, P. Sillard, A. Amezcua-Correa, J. M. Kahn, J. Schröder, R. Amezcua-Correa, J. Carpenter, "Mode-Multiplexed Transmission Within and Across Mode Groups of a Multimode-Fiber", *Proceedings of Optical Fiber Communications Conference (OFC)*, Paper. M2I.2, 2019.

[V] **M. Mazur**, N. K. Fontaine, R. Ryf, H. Chen, D. T. Neilson, M. Bigot, F. Achten, P. Sillard, A. Amezcua-Corra, J. Schröder and J. Carpenter "Characterization of Long Multi-Mode Fiber Links using Digital Holograph", *Proceedings of Optical Fiber Communications Conference (OFC)*, **Top Scored** Paper. W4C.5, 2019.

[X] **M. Mazur**, N. K. Fontaine, R. Ryf, D. T. Neilson, H. Chen, G. Raybon, A. Adamiecki, S. Corteselli and J. Schröder "Optical Arbitrary Waveform Generator Based on Time-Domain Multiplane Light Conversion", *Proceedings of Optical Fiber Communications Conference (OFC)*, Paper. M1B.3, 2019.

[Y] R., Ryf, N. K. Fontaine, S. Wittek, K. Choutagunta, **M. Mazur,** H. Chen, J. C. Alvarado-Zacarias, R. Amezcua-Correa, M. Capuzzo, R. Kopf, Al Tate, H. Safar, C. Bolle, D. T. Neilson, E. Burrows, K. Kim, M. Bigot-Astruc, F. Achten, P. Sillard, A. Amezcua-Correa, J. M. Kahn, J. Schröder and J. Carpenter, "High-Spectral-Efficiency Mode-Multiplexed Transmission over Graded-Index Multimode Fiber", *Proceedings of European on Optical Communication (ECOC)*, **Post Deadline** Paper. Th3B.1, 2018.

[Z] L. Lundberg, E. Börjeson, C. Fougstedt, **M. Mazur**, M. Karlsson, P. A. Andrekson and P. Larsson-Edefors, "Power consumption savings through joint carrier recovery for spectral and spatial superchannels", *Proceedings of European on Optical Communication (ECOC)*, 2018.

[AA] **M. Mazur**, J. Schröder, A. Lorences-Riesgo, M. Karrlson and P. A. Andrekson, "Optimization of Low-Complexity Pilot-Based DSP for High Spectral Efficiency 51×24 Gbaud PM-64QAM Transmission", *Proceedings of European on Optical Communication (ECOC)*, Paper. MoF4.2, 2018.

[AB] L. Lundberg, **M. Mazur**, A. Fülöp, V. Torres-Company, M. Karlsson and P. Andrekson, "Phase Correlation Between Lines of Electro-Optical Frequency Combs", *Proceedings of Conference on Lasers and Electro-Optics (CLEO)*, Paper. JW2A.149, 2018.

[AC] **M. Mazur**, J. Schröder, A. Lorences-Riesgo, T. Yoshida, M. Karlsson and P. A. Andrekson, "11.5 bits/s/Hz PM-256QAM Comb-Based Superchannel Transmission by Combining Optical and Digital Pilots", *Proceedings of the Optical Fiber Conference (OFC)*, **Top Scored** Paper. M1G.2, 2018.

[AD] C. Fougstedt, L. Svensson, **M. Mazur**, M. Karlsson and P. Larsson-Edefors, "Finite-Precision Optimization of Time-Domain Digital Back Propagation by Inter-Symbol Interference Minimization, *Proceedings of European on Optical Communication (ECOC)*, Paper. W.1.D.2, 2017.

[AE] L. Lundberg, **M. Mazur**, A. Lorences-Riesgo, M. Karlsson and P. Andrekson, "Joint carrier recovery for DSP complexity reduction in frequency comb-based superchannel transceivers", *Proceedings of European on Optical Communication (ECOC)*, Paper. Th.1.D.3, 2017.

[AF] A. Fülöp, **M. Mazur**, A. Lorences-Riesgo, P-H. Wang, Xi Xuan, D. E. Leaird, M. Qi, P. A. Andrekson, A. M. Weiner and V. Torres-Company, "Frequency noise of a normal dispersion microresonator-based frequency comb", *Proceedings of the Optical Fiber Conference (OFC)*, Paper. W.2.A.6, 2017.

[AG] **M. Mazur**, A. Lorences-Riesgo, M. Karlsson and P. Andrekson, "10 Tb/s self-homodyne PM-64QAM superchannel transmission with 4% spectral overhead", *Proceedings of the Optical Fiber Conference (OFC)*, Paper. Th.3.F.4, 2017.

[AH] C. Fougstedt, **M. Mazur**,L. Svensson, H. Eliasson, M. Karlsson and P. Larsson-Edefors, "Time-domain digital back propagation: Algorithm and finite-precision implementation aspects, *Proceedings of the Optical Fiber Conference (OFC)*, Paper. W.1.G.4, 2017.

[AI] A. Fülöp, **M. Mazur**, T. A. Eriksson, P. A. Andrekson, P-H. Wang, Xi Xuan, D. E. Leaird, M. Qi, A. M. Weiner and V. Torres-Company, "Long-haul coherent transmission using a silicon nitride microresonator-based frequency comb as WDM source", *Proceedings of Conference on Lasers and Electro-Optics (CLEO)*, Paper. SMF.2, 2016.

[AJ] A. Lorences-Riesgo, T. A. Eriksson, **M. Mazur**, P. A. Andrekson and M. Karlsson, "Quadrature decompossion of a 20 Gbaud 16-QAM signal into 2×4-PAM signals", *Proceedings of European on Optical Communication (ECOC)*, Paper. Tu.1.E.3, 2016.

[AK] T. Fehenberger, **M. Mazur**, T. A. Eriksson, M. Karlsson and N. Hanik, "Experimental analysis of correlations in the nonlinear phase noise in optical fiber systems", *Proceedings of European on Optical Communication (ECOC)*, Paper. W.1.D.4, 2016.

[AL] **M. Mazur**, T. Taunay, T. Geisler, L. Gruener-Nielsen, M. Karlsson and P. A. Andrekson, "Measurements of temperature-induced polarization drift and correlation in a 7-core fiber", *Proceedings of European on Optical Communication (ECOC)*, Paper. W.1.B.2, 2016.

Other published work

[α] J. Schröder and M. Mazur," *QAMPy a DSP chain for optical communications*, DOI: 10.5281/zenodo.1195720, 2018.

Contents

Dedicated to my parents, Eva and Ulf Mazur

Acknowledgements

First, I would like to thank my examiner Prof. Peter A. Andrekson for accepting me as a PhD student and for your continuous support. My main supervisor, Prof. Magnus Karlsson, deserves endless thanks for always being open to discuss ideas, for your support and for always taking your time to discuss related, and unrelated, theoretical aspects of my work. Limitless thank you to Dr. Jochen Schröder for all the time and effort you have devoted to my projects and for teaching me invaluable skills about programming and Python. You have always taken your time to discuss my somewhat crazy ideas and encouraged me to push the boundaries. Dr. Abel Lorences-Riesgo deserves a very special thank you. You shared invaluable knowledge about the role as a researcher and about fiber optics. Despite leaving the group, you have always devoted time to my work and your continuous support has been invaluable. To all my supervisors, thank you very much for allowing me to try out my own ideas and allowing me to tackle problem that I found interesting, without directly questioning the relevance of the problem itself.

Thank you Dr. Nicolas K. Fontaine, Dr. Ronald Ryf, Dr. Haoshuo Chen and Dr. David T. Neilson for allowing me do to do an internship at Bell Labs as part of my studies. You taught me endless things and all our discussions drove my motivation to unforeseen levels, even after the internship. Especially thank you for allowing me to work on topics outside coherent transmission, broadening my knowledge and spearheading my interest for other areas in optics, including developing a special interest for multi-mode technologies. Thank you all other colleagues for making the internship such an enjoyable time.

Thank you Dr. Tobias Eriksson for motivating and teaching me. Over overlap was short but you got me into building a 600 km long interferometer for measuring the nonlinear memory. Thank you Dr. Attila Fülöp for very interesting collaborations and for teaching about microcombs. Many thanks to Christoffer Fougstedt for very fruitful collaborations and for teaching me about hardware considerations and to Dr. Lars Lundberg for interesting discussions and collaborations on joint DSP. Thank you Tsuyoshi Yoshida for sharing your deep knowledge on the design of high performance DSP and thank you Dr. Myoung-Gyun Suh for a very successful collaboration on microcombs, I really learned a lot from working with both of you. Thank you Dr. Benjamin Foo for inspiring collaborations and for teaching me

about PSAs. Thank you Dr. Elham Nazemosadat for always being open to share your deep knowledge on SDM. Thank you Prof. Anders Larsson for sharing a lot of knowledge on VCSELs and short-reach optical communications and Dr. Erik Haglund for taking your time to explain laser fabrication to me. Thank you Prof. Victor Torres-Company for sharing your knowledge on various frequency combs and their properties. Thank you Dr. Henrik Eliasson for being a superb office mate and thank you Ali Mirani for ensuring that this did not change when Henrik graduated. Thank you very much Ravikiran Kakarla for all interesting discussions on various problems and for making it very easy to share the lab. Special thanks to Dr. Emanuel Haglund for making the time at the photonics lab much funnier and to Ewa Simpanen for funny times, endless discussions and continuous support. Thank you Filip Hjort for lots of interesting discussions on research and for taking your time to help me. Thank you all other colleges for contributing to an interesting working environment. Extra thank you to Dr. Christian Haffner for your spot-on feedback and all interesting discussions over the years. Talking to you is always a true joy and your way of doing research and viewing problems has always inspired me. Thank you to Jeanette Träff for your superb way of administrating the lab and for rescuing me when being lost in the jungle of administrative duties and thank you Henric Fjellstedt for handling our IT infrastructure in a superb way.

I would like to thank my friends outside the world of fiber-optic research for your support. Thank you all diving friends for our underwater experiences. Special thanks to Lena for always being so supportive and for sharing your advises on how to handle various situations in life. Thank you Madeleine for our somewhat philosophical discussions about life, and for the mutual understanding of the various challenges inherent to graduate studies. Finally, I would like to thank my family for your endless support and for your understanding of the many hours spent in the lab. This work would not have been possible without you. My deepest thank you to Zoe for your love, acceptance and all the happiness you bring to me. Despite living being far away, you have always been supporting me throughout this work. Thank you to Ida and Fredrik for all your support and for accepting my somewhat strange way of being. Seeing your hard work and passion in all your do is an incredible source of inspiration for me. Finally, thank you mum and dad for always standing by my side, no matter what, and for always supporting me to follow my own path and doing stuff my way.

Mikael Mazur

Gothenburg
September, 2019

Chapter 1

Introduction

This chapter starts with an historical overview of optical communication systems, focusing on key events that enabled the high performance multi-Tb/s optical transmission systems available today. The work in this thesis is then summarized and a thesis outlook is provided.

1.1 Historical Overview

From a holistic perspective, any form of communication using light falls under the optical communication umbrella. This would include anything from the ancient use of smoke signals to more modern communication using Morse-signaling with light. These traditional systems used air as the communication medium with the information speed mainly being limited by the light source or the human operating it. With this in mind, it is clear that optical communication dates back thousands of years.

The era of more modern communication began around 1830 with the invent of the electromagnetic telegraph [1]. Following its invention, engineers devoted large resources to increase the transmission speed of telegraph systems, which were on the order of 10 bits/s. The next major leap towards modern communication systems took place in 1876, with the invent of the telephone by Alexander Graham Bell [2]. Four years later, he and S. Tainter invented the Photophone, highlighting early ideas of optical communications [3]. Analog communication systems then developed fast, and the introduction of microwave carrier frequencies allowed for throughput equivalent to bit-rates beyond 100 Mbit/s around 1970 [4]. While these speeds were truly amazing at the time, systems were strongly limited by densely spaced repeaters, typically a few kilometers apart, arising from the use of coaxial cables as the transmission waveguide. It was clear that in order to scale the system

throughput by orders of magnitude, different waveguides and much higher carrier frequencies were needed.

Parallel to the development of advanced microwave communication systems, the era of modern optical communication began. However, although the potential for optical communications was realized early, optical systems require coherent light sources and low-loss waveguides. The development of coherent light sources would change the world forever, enabling endless applications beyond communication. For their pioneering work and extraordinary achievements Charles H. Townes, Nicolay G. Basov and Aleksandr M. Prokhorov were awarded the Nobel price in physics 1964 for the innovation of the maser and the laser [5]. While the benefit of having narrow-band continuous wave (CW) light sources was clear at the time, performance was far away from today's lasers. As a result, information transmission using a pure noise carrier of varying bandwidth was also investigated [6]. In 1966, Charles K. Kao published pioneering work, in which he realized that optical fibers at that time were loss-limited by impurities in the glass, not by intrinsic losses [7] (reprinted 20 years later available in [8]). Important to emphasize here is that at the time optical fibres were loss limited (>1000 dB/km), making Kao's revolutionary insights anything but obvious. In fact, at the same time, free-space propagation using sequences of gas lenses to form an optical transmission line were investigated as an alternative approach [9]. Transmission distances reaching about 800 m with about 120 m lens separation was demonstrated in [10, 11]. In parallel, Kao's work continued with analyzing the loss mechanisms of fibers, knowledge essential to fabricate low-loss fibers [12, 13]. Multiple advancements improved fiber technology to reduce losses to below 20 dB/km [14, 15]. Following this pioneering work, from around 1970 to around 1990, systems were mainly improved through improving the optical fiber, including going from multi-mode (MMF) to single-mode fibers (SMF) [16]. During this time, the loss of optical fibers dropped with 5 orders of magnitude in dB, in line with Kao's pioneering understanding of the true potential for optical fibers. For this, he was awarded the Nobel price for the pioneering work on realizing the potential of optical fibers as a transmission medium in 2009.

A next big game-changer in the field of fiber-optic communication was the introduction of optical amplifiers in the telecommunication band (C-band) in the late 1980s [17, 18]. Previously, systems were limited to single-span and electrical regeneration. The invention of the Erbium-doped fiber amplifier (EDFA) changed this by allowing direct amplification in the optical domain around 1550 nm, which corresponds to the wavelength with lowest propagation loss in SMF. To improve noise characteristics of EDFAs, much efforts were devoted to developing pump lasers around 980 nm [19, 20]. Major breakthroughs were achieved using high efficiency quantum well-based lasers [21] and application to EDFA pumping was investigated in [22]. The use of EDFAs boosted system experiments using solitons with propagation distances reaching 10000 km [23, 24].

The introduction of the EDFA allowed system to span significantly longer distances without being limited by fiber loss. With the loss problem out of the way

the next big limiting factor is dispersive broadening. Dispersive pulse broadening in SMF cause temporal overlap, making consecutive pulses indistinguishable. Dispersive broadening also have a quadratic dependence on the temporal pulse width, making it even more severe as the symbol rate increases. Two techniques existed to avoid dispersive broadening, transmission around the zero dispersion wavelength of 1310 nm or using soliton waveforms. Soliton waveforms are incompatible with lumped amplification (to mention one issue) and moving away from 1310 nm was necessary to exploit the potential for the combination of low-loss SMF and EDFAs [25]. Large resources were therefore devoted to finding ways of compensating for the fiber dispersion. One solution of the problem with dispersive broadening was dispersion-shifted fiber (DSF) with zero-dispersion around 1550 nm, developed around 1980 [26–28]. However, already at this time, most fiber deployed was SMF and upgrade-paths were sought to allow compatibility with already existing infrastructure. Optical dispersion compensation was therefore heavily investigated and a dispersion compensating fiber using a higher-order mode was proposed in [29]. Still, mode-shifting required additional components and was not fully compatible with the installed single-mode technology. The issue was solved in 1992 with the introduction of the dispersion-compensating fiber (DCF) [30]. Following this, the potential for combining SMF, DCF and EDFAs for improving both system throughput and reach was quickly realized. In addition to the low noise figure provided by EDFAs pumped around 980 nm, the EDFAs provided broad-band gain spanning the around 30 nm within the C-band. While wavelength-division multiplexing (WDM) previously had been demonstrated, the birth of the EDFAs and the development of DCF draw increased attention to research on WDM [31]. This is also clearly reflected in record experiments from the early 1990s, which became increasingly focused on multi-span WDM transmission [32, 33]. With this new shift in system design, nonlinear effects started to be an increasingly limiting factor for systems and it was realized that the use of DSF represented a worst-case scenario by maintaining phase-coherence among channels over long distances, causing severe nonlinear distortions [34, 35]. Even with the combination of SMF-DCF, nonlinearities posed large limitations on the reachable system throughput. All-optical nonlinearity compensation based on mid-span spectral inversion via optical phase conjugation was investigated to simultaneously compensate both dispersion and fiber nonlinearities [36, 37]. At this time it was also clear that ther penalties from nonlinearities was dependent on dispersion, requiring a general approach to optimizing WDM systems [38, 39].

With the bandwidth of the C-band occupied using WDM, system designers turned their attention to the idea of coherent transmission using both the amplitude and the phase, together with advanced modulation formats to improve the spectral-efficiency (SE) [25]. While previous formats relied on direct-detection (DD), the introduction of coherent technologies enabled drastic increase in the channel throughput [40]. Early experiments with differential quadrature phase shift keying (D-QPSK) using optical delay-based receivers marks an early start

of experiments with coherent formats [41]. However, these systems were still DD systems but expanded with new optical modulators and receiver front-ends. High speed digital-to-analog converters (DACs) with multi-bit resolution were first introduced in optical communication in 2005, when commercial transceivers capable of electronic pre-compensation of dispersion were introduced [42]. Three years later, analog-to-digital converters (ADCs) were added to the receiver [43]. The ability to compensate the dispersion digitally using pre or post compensation also significantly increased the system tolerance to fiber nonlinearities [44]. The combination of high speed, high resolution DACs and ADCs marks the starting point of coherent optical communication systems using digital signal processing (DSP) implemented in high-speed application-specific integrated circuits (ASICs) [45, 46]. As both laser quality and DSP performance improved, differential formats were replaced and the modulation order grew quickly [40]. With the introduction of coherent technologies, the optical communication community also started to increasingly connect with the fields of communication and information theory [47], applying advanced modulation and forward error correction (FEC) coding schemes to improve transmission performance [48]. While the required bit to error rate (BER) target of around 10^{-15} have been remained untouched throughout the years of development, these schemes have enabled new ways of ensuring the performance [49]. A first glimpse on the gains can be found by the implication of replacing the use of on-off keying (OOK) with binary phase shift keying (BPSK), which results in a 3 dB sensitivity gain [50].

Today, SMF with 0.14dB/km loss have been demonstrated [51] and formats reaching 4096-QAM are being evaluated in optical communication systems [52, 53]. In single-span experiments using Raman amplification, a SE exceeding 17 bits/s/Hz have been demonstrated using low baud-rate carriers [54]. A SE of 14.1 bits/s/Hz over 500 km of Raman-amplified link was demonstrated for a 5 channel system in [55]. Combining state-of-the-art communication techniques using rate-adaptive FEC [56, 57], constellation shaping [58, 59] and powerful DSP to combat both linear and nonlinear impairments [60], system throughput has reached 25.4 Tb/s over 10000 km [61]. Adding EDFAs with capabilities of L-band amplification, state-of-the-art results exceeding 70 Tb/s system throughput over 7600 km [62] and 51 Tb/s over 17000 km [63]. DAC and ADC bandwidth (BW) have improved tremendously over the years and record demonstrations include a 100 GHz BW DAC [64] and a >110 GHz BW ADC [65]. As a result of this, record symbol-rate is now reaching 192 Gbaud [66] and PM-1024QAM at 66 Gbaud have been demonstrated using powerful FEC [67].

As transceivers are operating increasingly close to the bounds using shaping, focus are shifting back to the fiber itself and concerns are raising that we are running out of capacity in SMF [68]. The capacity of the fiber channel (capacity is strictly defined within information theory [47]) is still unknown and research efforts are ongoing to produce better bounds [69–71]. Such lower bounds have shown that the capacity does not decay at high launch power but instead flattens out [70]. However,

even if there is plenty of capacity left, it is becoming increasingly challenging to exploit the full capacity of SMF, requiring transmission technologies beyond what is reachable with systems optimized for a linear channel. One approach to develop communication schemes tailored to the nonlinear channel is to use the nonlinear Fourier transform (NFT) [72, 73]. This can be viewed as new generation of soliton communications using using properties of integratable (exactly solvable) nonlinear equations [74]. Although tailored methods are being developed to increase the performance of NFT communication [75, 76], there are still many challenges and obstacles to be overcome before NFT-based transmission is practical [77]. We also note that NFT can be used to estimate the capacity of the nonlinear fiber channel [78].

In addition to the concern of fiber capacity, power consumption is becoming increasingly important as the internet traffic grows. While bulk components normally have been used, work on integrated optics followed its electrical counterparty. Photonic integration has a long history and investigations on integrated circuitry dates back to around 1970 [79, 80] and the need for scaling down component size to maximize performance was realized early [81]. Today, the ability to increase performance and reduce power consumption is still a major drive behind photonic integration [82, 83]. Multiple platforms exist, with two of the most popular once being silicon photonics [84] and InP [85]. Complete transceivers can then be designed on a microscale, realizing equivalent performance to systems built using bulk-optic components but with significantly less power consumption [86]. Today, integrated transceivers have reached 100 Gbaud [87] and enabled multi-Tb/s throughput at record-low energy consumption of <0.1W/Gbit at 200 Gbit/s [88]. In addition, development of novel components [89, 90], waveguides [91, 92], bonding techniques [93, 94] and passive components can further enable efficiency gains not feasible on a macroscale [95].

While integrated photonics provides a path towards smaller, more effective optical transponders necessary to reduce the energy per bit, it does not provide any means of increasing the system throughput. The bandwidth in the wavelength domain is limited by the amplifier gain bandwidth, which for EDFAs is limited by the erbium atoms. When this is fully occupied by WDM channels, each using dual polarization coherent transmission, no further dimensions are left in SMF. To further increase the system throughput, one then have to go outside the signal space dimensions provided by SMF [96, 97]. Such spatial multiplexing, refereed to as space division multiplexing (SDM), use multiple spatial paths to increase the information throughput. Important to note here is that the idea of SDM is nothing new and it was indeed considered for free-space optical communications already in 1968, before high quality SMF was available [98]. SDM technologies has enabled current record throughput exceeding 10 Pb/s [99] over a 10 km fiber containing 19 cores, each supporting 6 modes. System throughput of 159 Tb/s over 1045 km using 3-mode transmission was demonstrated in [100] and simultaneous transmission over 45 spatial modes was demonstrated in [101]. Moreover, recent results using

few-mode fiber (FMF) [102] and coupled-core multi-core fiber (CC-MCF) [103] have shown that the use of SDM-fibers can outperform classical SMFs by providing additional gain due to improved tolerance to fiber nonlinearities. However, while SDM have been successful in enabling record-breaking transmission results, lots of work remains before its fully understood and considered as a reasonable alternative to SMF in long-haul optical communication links.

1.2 This Thesis

The focus of this thesis is on developing schemes enabling high SE transmission using optical superchannels with multi-Tb/s throughput. A superchannel consists of a set of WDM channels, treated and routed as a single unit. Densely packed superchannaels can therefore be used to maximize the SE of WDM systems and to realize effective channel throughput far beyond that of a single optical carrier. We focus the work around comb-based superchannels, which are formed by modulating multiple lines all originating from a common optical frequency comb. Frequency combs are multi-wavelength light sources with intrinsic phase-locking between the lines. As such, a frequency comb can be characterized using information from only two lines and a grid formed by a comb is orders of magnitude more stable compared to the grid from a laser array. This thesis focus on these unique aspects of frequency combs and how they can be exploited to increase the performance of transmission systems in ways not feasible using laser arrays. First, in Paper I, the fundamentals of arbitrary waveform generation is investigated and a new multi-wavelength modulation scheme is described. The proposed modulation structure is in principle capable of loss-less modulation. Moreover it can also encode different waveforms on multiple spectrally separated laser lines. The method developed allows for arbitrary temporal waveform generation with implications beyond superchannel transmission.

Paper II investigates high performance signal processing for high SE transmission. The aim of the paper is to present a complete pilot-based DSP chain with focus on low overhead processing. The performance of the individual pilot-based algorithms are compared to that of comparable conventional blind DSP algorithms. A full pilot overhead optimization is then performed and the sensitivity of the found optimum is investigated by varying the propagation distance. In Paper III, the line stability of frequency combs is used to optimize the channel separation, realizing sub-GHz inter-channel guardbands. The dense packing of wavelength channels within the superchannel is combined with the high performance low-overhead DSP developed in Paper II to create a high SE superchannel. The comb-based superchannel is formed using lines originating from an optimized soliton microcomb. Optimizing both the symbol rate on the 22.1 GHz grid provided by the microcomb and the pilot-based DSP presented in Paper II, transmission performance directly comparable to that of bulk-optic frequency combs is realized. The insights gained in Paper III are key to

understand path towards realization of superchannel transceivers using integrated photonics without sacrificing performance.

Paper IV presents a self-homodyne comb-based superchannel receiver. Using two unmodulated pilot tones (PTs) from the transmitter comb, a phase-locked receiver comb is generated, avoiding the need for any dedicated DSP-block to compensate frequency offsets and track the laser phase noise. The scheme used two electro-optic (EO) frequency combs and a combination of optical injection locking (OIL) and an electrical phase-locked loop. A hybrid scheme using a single optical PT and slow DSP for residual tracking was developed in Paper V. In contrast to the dual PT scheme, the smaller overhead enabled higher spectral efficiency, exploiting that the majority of the gain from the two PT scheme can be recovered with a single PT. In Paper VI, the single PT scheme reported in Paper V was used for multi-span transmission. This study focused on investigating its sensitivity to distortions from the link, including fiber nonlinearities and amplifier noise. The results shows a strong resilience, highlighting that the single PT scheme can be exploited to reduce DSP complexity even at distances reaching 1000 km. The single PT scheme was further enhanced in Paper VII by replacing the previously used blind DSP with a pilot-based DSP. This enabled a further increase in modulation order, realizing a spectral efficiency of 12 bits/s/Hz over the full C-band using three comb-based superchannels. Finally, in Paper VIII, the pilot-based DSP is expanded to build a superchannel DSP to improve the performance of comb-based superchannels. The proposed methods exploit frequency locking to enable multi-channel equalization via spectral stitching of the different channels, all detected on individual receivers.

This thesis is organized as follows. Chapter 2 is focused on the basics of coherent optical communication. The key building blocks of a single channel transmission system are introduced together with channel models. Following this, Chapter 3 is devoted to DSP with focus on describing standard blind methods used to compensate various impairments faced in optical communications. Models for transceiver impairments and non-ideal lasers are introduced and discussed. Optical frequency combs are introduced in Chapter 4. The basics of principle behind combs, different generation techniques are discussed, especially focusing on EO frequency combs. New results and insights on EO-comb generation with arbitrary shape are also presented. Multi-channel transmission and the role of frequency combs in optical communications is discussed in-depth in Chapter 5.

Chapter 2

Optical Communication Systems

Optical communication systems comes in different flavors depending on target application. This chapter discusses concepts of coherent optical communication systems, which are the typical systems used for distances exceeding 10 km. An overview of a single channel coherent optical communication system can be seen in Fig. 2.1. From a systems perspective, an optical communication system can be divided into three key parts; the transmitter, the optical channel and the receiver. The systems under consideration in this thesis belongs to the category of software-defined transceivers [104]. The purpose of this chapter is to go through the key components of such a system and review the different functionalities needed in order to transport information over the optical fiber. We also discuss challenges related to optical modulation in relation to the results presented in Paper I, where we present a transmitter configuration.

2.1 Transmitter

The role of the transmitter is to encode the information onto the optical carrier wave. Its operation can roughly be divided into functions implemented in the digital, electrical and optical domain, as illustrated in Fig. 2.2. Operations in the digital domain are characterized by discrete-time representations of bits or complex symbols at a fixed oversampling rate. This discrete digital signal is then converted to continuous analog electrical signals through the use of DACs. The resulting signal spectrum is DC-centered. Finally, a dual-polarization optical IQ-modulator attach the electrical signal to its optical carrier wave, resulting in an effective up-conversion

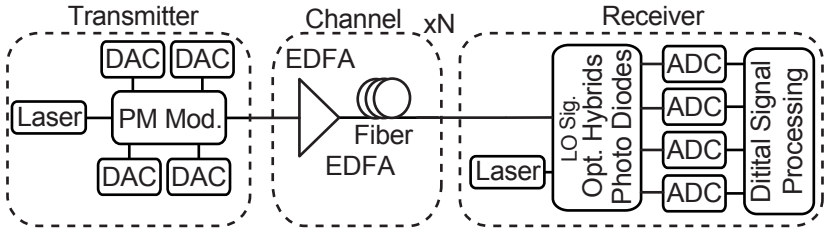

Fig. 2.1. Overview of a coherent optical communication system. DACs are used to convert information symbols to analog electrical signals, which are modulated onto the lightwave carrier using an optical modulator. After propagation through the link consisting of spans with optical fiber and optical amplifiers, the signal is detected using an optical receiver. The receiver consists of an optical hybrid and balanced detectors, enabling extraction of both the amplitude and the phase of the signal. After sampling using the receiver ADCs, DSP is used to recover the data.

of the signal spectrum from being DC-centered to being centered around the optical carrier wave frequency.

2.1.1 Digital Bit-Symbol Mapping

To transmit a sequence of bits, the first step is to add redundant bits using a FEC encoder. However, here we only focus on sending bits and therefore only consider the case of a bit sequence which shall be transmitted over the system, neglecting any detailed discussions on FEC. The interested reader is instead refereed to [48, 49]. Bits are then mapped to symbols, which can carry one or more bits, a process known as mapping. Each symbol $a[n] = a_{\mathrm{I}}[n] + ja_{\mathrm{Q}}[n]$ (n denoting the time index) is a 2D symbol and can have bits mapped onto two quadratures represented by the real and imaginary part of $a[n]$. The interpretation of these two quadratures, can be seen as mapping the bits to symbols belonging to a (sub)-space spanned by both the amplitude and phase of the optical lightwave, resulting in a 2D signal space. Similarly, when exploiting the degeneracy of the fundamental mode in SMF to enable polarization multiplexed (PM) transmission using two quadratures on two polarization (see Section 2.2.5), the signal space is 4D which can be understood by combining two complex symbols $a[n]$ according to

$$\vec{a}_{\mathrm{PM}} = \begin{pmatrix} a_{\mathrm{X}}[n] \\ a_{\mathrm{Y}}[n] \end{pmatrix} = \begin{pmatrix} a_{\mathrm{X_I}}[n] + ja_{\mathrm{X_Q}}[n] \\ a_{\mathrm{Y_I}}[n] + ja_{\mathrm{Y_Q}}[n] \end{pmatrix}. \tag{2.1}$$

While one could think of using a continuous modulation alphabet (and this is shown to be capacity achieving for certain distributions [105]), a finite set of

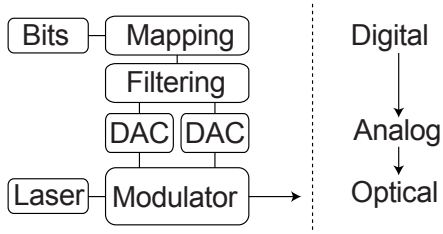

Fig. 2.2. Illustration of the various key blocks building up a digital coherent transmitter. The functionality can be divided into steps performed in the digital, analog electrical and optical domain.

Bit Sequence	Output Symbol	Bit Sequence	Output Symbol
{0,0,1,0}	$(-3+3j)\sqrt{10}$	{0,0,1,1}	$(-3+1j)\sqrt{10}$
{0,0,0,1}	$(-3-1j)\sqrt{10}$	{0,0,0,0}	$(-3-3j)\sqrt{10}$
{0,1,1,0}	$(-1+3j)\sqrt{10}$	{0,1,1,1}	$(-1+1j)\sqrt{10}$
{0,1,0,1}	$(-1-1j)\sqrt{10}$	{0,1,0,0}	$(-1-3j)\sqrt{10}$
{1,1,1,0}	$(1+3j)\sqrt{10}$	{1,1,1,1}	$(1+1j)\sqrt{10}$
{1,1,0,1}	$(1-1j)\sqrt{10}$	{1,1,0,0}	$(1-3j)\sqrt{10}$
{1,0,1,0}	$(3+3j)\sqrt{10}$	{1,0,1,1}	$(3+1j)\sqrt{10}$
{1,0,0,1}	$(3-1j)\sqrt{10}$	{1,0,0,0}	$(3-3j)\sqrt{10}$

Table 2.1. Bit sequence to normalized complex symbol mapping for 16QAM, $N_b = 4$. The selected mapping is of Gray-type (not unique).

"symbols" to represent the bit stream is typically preferred. Considering the above mentioned 4D signal space, optimized modulation which fully exploits the 4 degrees of freedom jointly can maximize performance [106–108]. However, in practice, formats such as PM M-ary quadrature amplitude modulation (PM-MQAM) are most common. These formats map independent QAM symbols on each polarization. The two quadratures of each QAM symbol is furthermore separated into two 1D pulse amplitude modulation (PAM) signals. So to map a bit stream onto PM-MQAM symbols, the bits are divided into 4 sub-streams, each mapping the bits to a 1D PAM constellation. The number of bits N_b encoded in each symbol is directly given by $N_b = \log_2(M)$ with M being the format order. As an example, a PM-64QAM symbol carriers a total of 12 bits, 6 bits on each polarization, corresponding to symbol alphabet of size $2^6 = 64$. Each 64QAM symbol consists furthermore of two independent PAM signals, modulating 3 bits each, corresponding to $2^3 = 8$ levels or equivalent a 8-PAM signal. A PM-64QAM symbol can therefore be decomposed into four individual real-valued 8-PAM signals. However, note that this is only valid

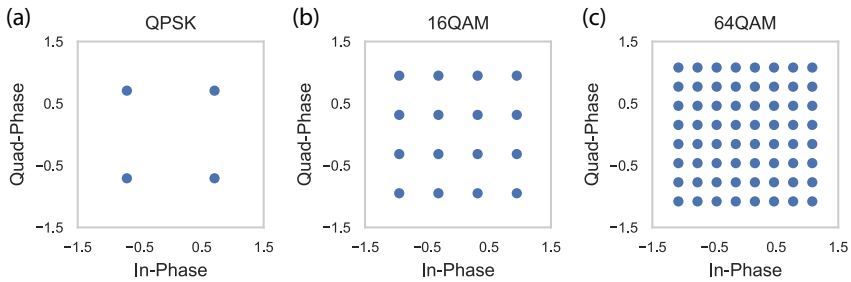

Fig. 2.3. Example of coherent modulation formats used in optical communication. The number of bits encoded in each M-QAM symbol is given by $N_b = \log_2(M)$, corresponding to $N_b = 2$,4 and 6 for the case of QPSK, 16QAM and 64QAM, respectively. Note that average energy for is equivalent for all three constellations, assuming a uniform symbol probability.

for square QAM formats. In the general case of $M = 8$,32,128,..., or non-rectangular formats, a decomposition into two real-valued PAM strings is not possible and the two quadratures have to be mapped jointly.

Focusing on the complex representation of the 2D symbols $a[n]$, Fig. 2.3 shows the resulting constellation diagrams for $M = 4, 16$ and 64, corresponding to QPSK, 16QAM and 64QAM, respectively. To decide on which complex constellation symbol to send, the bit stream is divided into blocks of N_b bits and a look-up-table with a the mapping. An example of such a mapping for 16QAM can be found in Table 2.1.

As a final remark to modulation it is important to point out that when considering an AWGN channel (see Section 2.2.1), the capacity achieving modulation format is a continuous Gaussian distribution [105]. Recently, large research efforts have been focusing on constellation shaping to improve performance. This aims at exploiting the 1.53 dB asymptotic difference between the AWGN capacity (Eq. 2.13) and the use of uniform QAM formats [109]. Shaping can be implemented either by symbols with a non-uniform probability, referred to as probabilistic amplitude shaping (PAS) [58, 59] or by redistributing the constellation symbols spherically in constellation space [62] which is known as geometric shaping. While constellation shaping has been used in several recent record experiments [52, 54, 61, 62], the work in this thesis is focused around standard QAM formats and we therefore do not consider shaping further. However, all presented techniques are fully compatible with constellation shaping and such techniques can hence improve flexibility and efficiency of the proposed systems.

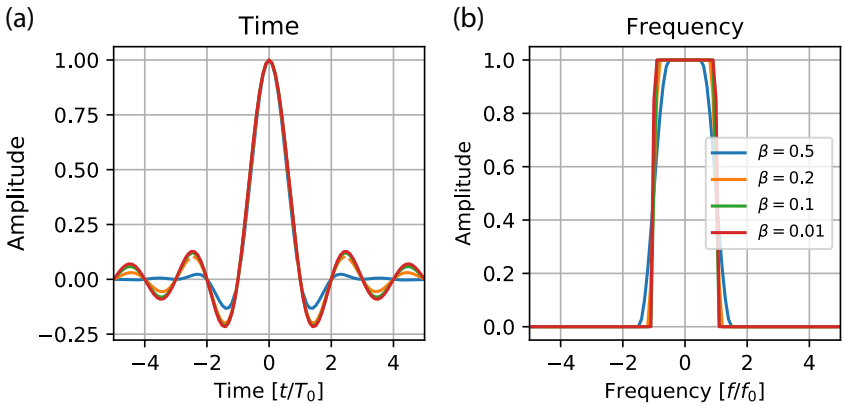

Fig. 2.4. Raised Cosine filtering with varying roll-off factor β. (a) Shows the time-domain impulse response and (b) the equivalent frequency domain transfer function.

2.1.2 Pulse Shaping

After mapping the bit sequence to complex symbols (1 per polarization mode), a pulse shaping filter can shape the signal spectrum to the modulator [110, 111]. This process can be expressed as [105]

$$x[n] = \sum_{k=-\infty}^{\infty} a[n]h(t - kT), \tag{2.2}$$

where $x[n]$ is the output discrete waveform a time instance n, $a[n]$ is the selected complex symbol, h denotes the filter response and T the time interval between pulses. Equation 2.2 represents a discrete convolution between the symbols $a[n]$ and the filter $h(t)$. Several different filters exist but raised-cosine filters (RC) are among the most common. In practice, the RC filter is often further divided and implemented both on the transmitter and receiver side using the square-root of the RC filter response, see Section 3.1. The RC filter can be seen as an approximation to the sinc-pulse, providing a brick-wall filter response in frequency domain. The continuous-time impulse response of the RC filter can be expressed according to [105]

$$h(t) = \begin{cases} \frac{\pi}{4T}\text{sinc}\left(\frac{1}{2\beta}\right), & t = \pm\frac{T}{2\beta} \\ \text{sinc}\left(\frac{t}{T}\right)\frac{\cos\left(\frac{\pi\beta t}{T}\right)}{1-\frac{4\beta^2 t^2}{T^2}}, & \text{otherwise} \end{cases}, \tag{2.3}$$

with T denoting the symbol period and β the roll-off factor. Note that Eq. 2.3 results in a sinc function for the case of $\beta = 0$. The time and frequency response of the RC filter for $\beta \in 0.01,0.1,0.2,0.5$ can be seen in Fig. 2.4. Worth noticing here is that in order to apply a pulse shaping filter, oversampling is needed and the vector with complex symbols is therefore typically up-sampled at this point. Considering systems transmitting data on several wavelengths using WDM (see Section 5.1), RC filters can enable much more effective use of the available signal spectrum as it avoids the typical sinc-spectrum associated with using square time-domain pulses. In addition, we note that pulse-shaping can also be done by exploiting analog filters and components with tailored bandwidth. As a final remark on pulse shaping, we note that digital sub-carrier transmission can increase tolerance towards nonlinearities [112]. While sub-carrier has been implemented in real-time transponders to increase performance[113], every-subcarrier is in-principle equivalent to a single-channel system but the lower symbol rates also challenge the DSP [114].

2.1.3 Digital-to-Analog Conversion

After modulation and pulse-shaping, which both take place in the digital domain, it is necessary to convert the digital signal representation into a continuous analog signal which can be modulated on the optical carrier. In the ideal case, the digital-to-analog conversion does not add any penalty but all real-life DACs have a limited resolution. In particular for high-speed DACs used in optical communication, the resolution limits the performance for multi-level modulation formats [45].

The limited resolution can be understood by considering that a DAC has N different levels to represent the digital signal with a finite resolution expressed in terms of $\log_2(N)$. In addition, the sampling theorem states that sinc functions are required for an ideal signal reconstruction [115]. This also makes intuitive sense, following the condition of bandwidth limited signal and low-pass filtering used in the sampling theorem. However, implementing such an impulse response is not practically feasible and most DACs use the zero-order hold function to interpolate between consecutive samples [116]. The DAC is then controlled by a sampling clock and each discrete sample is held for a sampling period T_{Fs}. For each sample of the digital input signal, the DAC chooses the closest discrete representation and output the corresponding signal amplitude. Due to the quantization, penalties will arise as the output signal differs from the original signal. This can be seen in Fig. 2.5(a), illustrating the implications of quantization for a sine-wave. How this quantization error is affecting a shaped data signal can be seen in Fig. 2.5(b), showing the frequency response of a $\beta = 10\%$ RC-shaped signal. We observe that the noise-floor is about 1 order of magnitude higher for the quantized signal, compared to the floating-point representation.

In addition to the limited resolution, presence of both noise and bandwidth limitations effectively reduce the output signal quality, which is usually quantified in terms of effective number of bits (ENOBs) which assumes a random approximation

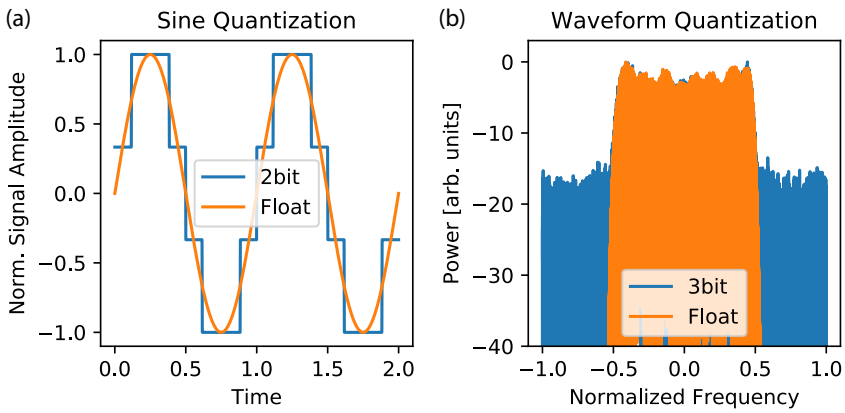

Fig. 2.5. (a) Non-ideal signal reconstruction using the zero-order hold function to interpolate between samples for a 2 bit DAC. The deviation results in a quantization penalty. (b) Shows additional noise added to a shaped waveform as a result of limited DAC resolution for a 3 bit DAC outputing a RC shaped signal with $\beta = 10\%$.

in the quantization error [117]. The combination of DAC resolution, jitter and ENOB can therefore be used to describe the quality of the output signal, including noise from the DAC itself.

2.1.4 Optical Modulation

Information can be modulated onto the light wave using either direct modulation of the laser (switching on-off) or via an external modulator applied after the laser [50]. Until the coherent era, data was modulated using on-off keying (OOK) [118]. Today, direct modulation of integrated lasers is still the base for short-reach optical interconnects [119] but coherent technologies are standard for long haul systems. To enable simultaneous modulation of both the amplitude and the phase of the optical carrier wave, IQ-modulators are used [50, 120]. The IQ-modulator is effectively an optical IQ-mixer, performing equivalent functionality to an RF IQ-mixer in wireless communication systems. Focusing on QAM formats, encoding information on both the amplitude and the phase, the process of modulation can be described as encoding an amplitude envelope $x_0(t)$ and a phase $\phi(t)$ onto a wave oscillating with frequency ω_0. The resulting electric field $E(t)$ can then be expressed as

$$E(t) = x_0(t)\cos(\omega_0 t + \phi(t)). \tag{2.4}$$

Note that the resulting electric field $E(t)$ is real-valued, representing a physical signal that can directly be measured. However, for mathematical convenience, representing amplitude and phase using complex numbers is typically preferred. Denoting the complex envelope $x(t)$, Eq. 2.4 can be re-written as

$$E(t) = \mathrm{Re}\left[x(t)\exp(j\omega_o t)\right] = \mathrm{Re}\left[(x_r(t) + jx_i(t))\exp(j\omega_o t)\right], \tag{2.5}$$

with $x_r(t)$ and $x_i(t)$ denoting the "real" and the "imaginary" part of the complex envelope signal. These are related to the complex envelope $x(t)$ according to

$$\begin{aligned} x_r(t) &= x_0(t)\cos(\phi(t)) \\ x_i(t) &= x_0(t)\sin(\phi(t)). \end{aligned} \tag{2.6}$$

In order to realize a practical IQ-mixer, we make one more algebraic manipulation of Eq. 2.4 using the trigonometric identity $\cos(a+b) = \cos(a)\cos(b) - \sin(a)\sin(b)$ and Eq. 2.6 according to

$$\begin{aligned} E(t) &= x_0(t)\cos(\phi(t))\cos(\omega_0 t) - x_0(t)\sin(\phi(t))\sin(\omega_0 t) \\ &= x_r(t)\cos(\omega_0 t) - x_i(t)\sin(\omega_0 t). \end{aligned} \tag{2.7}$$

Equation 2.7 shows that IQ-modulation can be performed by combining two single-dimensions modulators with real-valued input signals with a $\pi/2$ phase-shift between the two.

The Mach-Zehnder Modulator

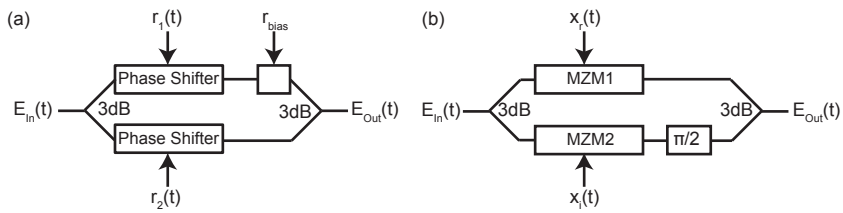

Fig. 2.6. Principle of modulation using Mach-Zehnder modulators. (a) A Mach-Zehnder interferometer. (b) A dual-nested Mach-Zehnder-based IQ-modulator using two parallel interferometers to modulate I and Q independently before rotating one with $\pi/2$ and recombining the signals using a directional coupler.

There are many structures that can be used to preform optical modulation. Many are based on interferometers with the most famous and common one being the Mach-Zehnder modulator (MZM), illustrated in Fig. 2.6(a). By applying different RF-signals, $r_1(t)$ and $r_2(t)$ onto the two phase shifters and controlling the bias,

the modulation of the output electrical field E_{Out} can be controlled. The transfer function of the MZM can be expressed in a simplified manner according to

$$\frac{E_{\mathrm{Out}}}{E_{\mathrm{In}}} = \frac{1}{2}\left[\exp(j(r_1(t) + r_{\mathrm{bias}})) + \exp(jr_2(t))\right], \tag{2.8}$$

where we neglected the inherent $\pi/2$ phase shift between the two output ports of a 3 dB coupler (this is further discussed in Section 2.1.4). Equation 2.8 can be re-written according to

$$\frac{E_{\mathrm{Out}}}{E_{\mathrm{In}}} = \exp\left(j\frac{r_1(t) + r_2(t)}{2} + j\frac{r_{\mathrm{bias}}}{2}\right)\cos\left(\frac{r_1(t) - r_2(t)}{2} + \frac{r_{\mathrm{bias}}}{2}\right). \tag{2.9}$$

Equation 2.9 reveals a crucial insight to the two most common operating modes of a MZM, the push-push and the push-pull mode. If $r_1(t) = r_2(t)$, the cos-term in Eq. 2.9 cancel out and we have a pure phase modulator, the push-push mode. If instead, $r_1(t) = -r_2(t)$ and the modulator is operated in push-pull mode and acts as a pure intensity modulator. In both cases, the bias point is determined by changing r_{bias}.

Realizing the Optical IQ-Modulator

Using the derived transfer function for a MZM and the results from Eq. 2.7, an optical IQ-modulator can be designed by using two parallel MZMs as illustrated in Fig. 2.6(b). This is referred to as a dual-nested MZM-based IQ-modulator. Each MZM is operated as a pure intensity modulator and fed with the RF signals x_r and x_i, respectively. In one of the arms, a $\pi/2$ phase shift is added so that a practical IQ-mixer is realized.

Today, IQ-modulators based on the dual-nested MZM structure is a mature technology that is essential in modern coherent transponders. It allows for encoding an arbitrary complex modulation format and avoids the issues with chirp that are present when using pure phase modulators. A variety of material platforms can be used, with the most common being $LiNbO_3$. Recent work on integrated $LiNbO_3$ has showed bandwidths of 100 GHz [121]. Beyond $LiNbO_3$, other materials considered includes silicon [122], InP [123] and plasmonic modulators [124, 125].

The important part of this is that the principle of building an IQ-modulator from two nested MZMs can be further expanded. Combining two IQ-modulators with a polarization beam combiner (PBC) realizing a 90-degree polarization rotation between the two arms, a dual-polarization modulator can be built. Expanding this with mode-multiplexers for higher-order spatial modes and/or wavelength multiplexers for multiple spectral modes, a multi-channel device is quickly realized.

Challenges with Traditional MZM-based IQ-modulators

Although dual-nested MZM-based IQ-modulators are very mature and powerful, they are not ideal and there are several challenges related to their use. First, the

bandwidth of the output signal is directly limited by the optical bandwidth of the device and/or the bandwidth of the electrical drivers, whichever being lowest. Even though novel techniques such as plasmonics can enable ultra-high optical bandwidths reaching far beyond 100 GHz [126], realizing high performance electrical DACs with equivalent bandwidths is very challenging. As an alternative to increasing the electrical bandwidth, multiple optical carriers can be used (see Section 5.1). While we note that a single MZM-based IQ-modulator can modulate multiple lines simultaneously, each line will be modulated with exactly the same envelope. In some cases, such as multi-casting for passive optical networks or microwave photonics [127], this can be an advantage but for the superchannel focus of this thesis it is inherently a drawback. From this perspective, although this can be very convenient to cope with experimental limitations in multi-channel/superchannel transmission experiments, it does not enable independent control of the individual lines in a single device and can therefore not modulate a superchannel.

In addition, the use of two nested MZM-based intensity modulators makes the IQ-modulator inherently lossy as the waveform is encoded by carving out power from the carrier wave. Furthermore, when modulating multi-level formats such as 64QAM, each MZM is effectively modulating a multi-level PAM signal. In the case of 64QAM, it can be decomposed into two 8-PAM sequences and assuming equal probability, the average voltage swing will be half of the total swing. Moreover, pulse shaping using RC-pulses and pre-compensation (see Section 3.5.2) will furthermore increase the peak-to-average power ratio (PAPR) [128] This reduction in effective swing is further enhanced as the total swing is usually significantly lower than the full π-phase shift, which theoretically is available, in order to avoid nonlinear distortions and constellation squeezing from the cos-term in Eq. 2.9, which 1 dB compression point is about $\pm\pi/4$. While neither of these effects pose any problem for a constant-intensity format such as QPSK, they impose large limitations for transmitters using higher-order formats as the lower PAPR implies a much higher modulation loss. Finally we note that with the recent introduction of probabilistic shaping [58], the probability of transmitting each constellation point is alternated. As a direct result, the modulator loss increase even further. In addition, two different signals cannot be combined in a loss-less way using a directional coupler. As a result, there is a fundamental 3 dB loss from the output combiner in Fig. 2.6(b). In practice, the insertion loss is usually higher, around 10 dB [129].

To overcome these limitations, alternative modulation schemes are necessary. Aiming for a loss-less IQ-modulation, the 3 dB coupler has to be avoided and both the amplitude and phase modulation have to be modulated in a single device. Rather than carving out energy using intensity modulators, the energy has to be temporally redistributed to meet the target waveform. Such a device is, to the best of our knowledge, realized for the first time as part of this thesis and described in Paper I. In addition to enabling loss-less modulation, it enables simultaneous encoding of independent waveforms on multiple spectrally separated lines.

2.2 The Optical Fiber Channel

The point-to-point optical fiber channel consists of the optical fiber waveguide and the amplifiers used to periodically amplify the signal in multi-span links. While optical networks can be formed by inserting reconfigurable optical add-drop multiplexers (ROADMs) [130] built from multiple wavelength selective switches (WSSs) [131], we here focus on the point-to-point case. Several different kinds of fibers can be used for data transmission, depending on operating wavelength and practical demands. While short-reach optical interconnects typically use a graded-index MMF, high-throughput communication systems normally rely on the use of SMF and operation in the C-band (around 1550 nm). Important to note here is still that longer wavelengths are becoming increasingly important also for short-reach communications [132].

Focusing on the fiber channel, signal distortions arise from propagation in the waveguide as well as from optical amplifiers along the link. Several amplification schemes exists such as EDFAs, distributed Raman amplification [133], parametric amplifiers [134] and semiconductor optical amplifiers [135]. In addition, hybrid schemes such as combination of Raman and EDFA amplification can be used to reduce the effective span loss [136, 137] and allow for optimization of the amplifier power consumption [138]. Any detailed amplifier comparison is beyond the scope of this thesis and here we solely focus on the use of EDFAs, which is the most used commercially deployed amplifier technology. EDFAs relies on pumping a doped fiber segment at the erbium transition wavelengths of around 980 nm and 1480 nm, based on the principle of stimulated emission [17, 20].

The EDFA noise properties is often characterized by its noise figure (NF), F_{n} which is a measure of the added noise in the amplification process. It is defined as [139]

$$F_{\mathrm{n}} = 2n_{\mathrm{sp}}\frac{G-1}{G}, \tag{2.10}$$

where N_{sp} is the population-inversion factor which is $n_{\mathrm{sp}} \geq 1$ and G denotes the amplifier gain. The implication of $n_{\mathrm{sp}} \geq 1$ is that all EDFAs have a theoretical minimum NF of 3 dB for a quantum limited input signal, being limited by quantum mechanics [140]. Assuming a large gain which do not depend on frequency, the noise figure can be translated into an equivalent power spectral density (PSD) per polarization (Gaussian noise) of

$$P_{\mathrm{ASE}}(\omega) = \frac{F_{\mathrm{n}}}{2}G\hbar\omega \qquad [\mathrm{W/Hz/Pol}], \tag{2.11}$$

with $\hbar$ denoting Planck's constant and ω the angular frequency. Based on the key role of EDFAs together with understanding from Eq. 2.11 it is natural to understand the importance of models which considers additive white Gaussian noise (AWGN) contributions. Such models and their extensions to more complex fiber models are introduced in the upcoming sections.

2.2.1 The AWGN Fiber Channel Model

One of the simplest discrete models available in communication is the AWGN model [105]. The input-output relation is given by

$$y[n] = a[n] + N[n], \tag{2.12}$$

where $y[n]$ denotes the received symbol, $a[n]$ the transmitted one and $N[n]$ is AWGN. We note that although Eq. 2.12 here is expressed in discrete-time representation, it can also be expressed in continuous form by simply replacing n with t. While not representing the full fiber channel, the AWGN fiber channel can still be used as a simple reference when designing DSP and performance is often referenced to the theoretical case of transmission over an AWGN channel. Worth pointing out here is also that the AWGN channel is one of few channels with a known channel capacity given by [47]

$$C = \log_2\left(1 + \frac{P_s}{N_0}\right) \qquad \text{[bits/s/Hz/Pol.]}, \tag{2.13}$$

with C denoting the channel capacity, P_s the signal power and N_0 the noise variance, defined according to

$$P_s = \mathbb{E}\left[|a[n]|^2\right], \tag{2.14}$$

$$N_0 = \mathbb{E}\left[|N[n]|^2\right], \tag{2.15}$$

with $\mathbb{E}$ denoting the expected value operator. The term $\frac{P_s}{N_0}$ is the signal-to-noise ratio (SNR) and Eq. 2.13 is therefore often expressed as $C = \log_2(1 + \text{SNR})$. The channel capacity, C, denotes the highest rate at which information can be communicated over the channel with arbitrary small error probability [47].

2.2.2 The Dispersive Fiber Channel

As discussed in Section 1, dispersion is a key aspect for the fiber channel. While being inherent in waveguide design, the dispersion causes different spectral components of the modulated channel to walk-off with respect to each other. To include dispersion, we move from looking at individual complex symbols $a[n]$ to the continuous temporal envelope $A(z,t)$ of the electrical field. Focusing on a single polarization, the effect of dispersion can then be modelled as [139]

$$\frac{\partial A}{\partial z} + \beta_1 \frac{\partial A}{\partial t} + \frac{j\beta_2}{2}\frac{\partial^2 A}{\partial t^2} + \frac{\alpha}{2}A = 0, \tag{2.16}$$

with z denoting the propagation direction, β_1 denoting the group velocity inside the fiber, β_2 the second order dispersion and α the fiber loss. Since we are typically not interested in propagation with respect to a fixed point in space, we can reformulate Eq. 2.16 by considering a co-moving reference system (a reference system in which

the observer is sitting centralized on the pulse A and follows it during propagation) according to

$$\frac{\partial A}{\partial z} + \frac{j\beta_2}{2}\frac{\partial^2 A}{\partial t^2} + \frac{\alpha}{2}A = 0. \tag{2.17}$$

Solving Eq. 2.17 is usually done in the frequency domain and since the loss term only reduces the amplitude of the pulse, we make a variable substitution according to $U(z,t) = \frac{A(z,t)}{\exp(-\alpha z/2)}$ and insert it into Eq. 2.17 which reduces to

$$\frac{\partial U}{\partial z} + \frac{j\beta_2}{2}\frac{\partial^2 U}{\partial t^2} = 0. \tag{2.18}$$

Taking the Fourier transform of Eq 2.18 then results in

$$\frac{\partial U(z,\omega)}{\partial z} = j\frac{\beta_2\omega^2}{2}U(z,\omega). \tag{2.19}$$

Equation 2.19 is a first order ordinary differential equation in z and can be solved according to

$$U(z,\omega) = \exp\left(j\frac{\beta_2\omega^2 z}{2}\right)U(0,\omega). \tag{2.20}$$

From Eq. 2.20, the effect of dispersion can be understood as a parabolic phase shift in frequency domain. Given that the inverse Fourier transform of a linear phase shift is a time delay, dispersion simply induce a wavelength-dependent time delay of the pulse as it propagates along the fiber.

2.2.3 The Nonlinear Fiber Channel

In addition to the linear channel response described by Eq. 2.17, the optical fiber also has a nonlinear response originating from the silica glass. The implication of this is an intensity dependent refractive index which can be written as [139]

$$n_{\text{Eff}} = n_0 + n_2 I, \tag{2.21}$$

with n_{Eff} being the resulting, n_0 the linear, and n_2 the nonlinear refractive index coefficients, respectively. In Eq. 2.21, I denotes the intensity of the electric field which gives raise to the nonlinear interaction. The effect of a nonlinear refractive index can then be viewed as a power-dependent modulation of the refractive index in the fiber. Incorporating such effects in our channel model relies on considering the nonlinear polarization response of the electrical displacement field and solving Maxwell's equations for fiber propagation. A more detailed derivation is beyond the scope of this thesis, but can be found in [139].

Including the nonlinear effect, known as Kerr nonlinearity, into Eq. 2.18, results in the famous nonlinear Schrödinger equation for fiber optics, according to [139]

$$\frac{\partial A}{\partial z} + \frac{j\beta_2}{2}\frac{\partial^2 A}{\partial t^2} + \frac{\alpha}{2}A = j\gamma|A|^2 A, \tag{2.22}$$

with γ being the nonlinear coefficient of the optical fiber. Equation 2.22 has no analytical solution and numerical methods are required to approximate the solution in the general case. However, important insights to the implications of fiber nonlinearities can be found by considering the case of a channel without dispersion, i.e. $\beta_2 = 0$. Substituting $U(z,t) = \frac{A(z,t)}{\sqrt{P_0}\exp(-\alpha z/2)}$, with P_0 denoting the pulse peak power, an analytical solution in this case can be found according to

$$U(z,t) = U(0,t)\exp(j\phi_{\mathrm{NL}}(z,t)). \tag{2.23}$$

The term ϕ_{NL} is often refereed to as the nonlinear phase shift given by

$$\phi_{\mathrm{NL}} = |U(0,t)|^2 \gamma P_0 \int_0^z \exp(-\alpha z')dz'. \tag{2.24}$$

At first glimpse, Eq. 2.24 can look a bit confusing and to ease the understanding it is convenient to introduce two additional length scales known as the nonlinear length L_{NL} and the effective length L_{Eff}, defined according to

$$L_{\mathrm{NL}} = \frac{1}{P_0\gamma} \tag{2.25}$$

$$L_{\mathrm{Eff}} = \int_0^z \exp(-\alpha z')dz' = \frac{1-\exp(\alpha z)}{\alpha} \tag{2.26}$$

Introducing L_{NL},L_{Eff}, Eq. 2.24 changes to

$$\phi_{\mathrm{NL}}(z,t) = |U(0,t)|^2 \frac{L_{\mathrm{Eff}}}{L_{\mathrm{NL}}}, \tag{2.27}$$

and we can understand the Kerr nonlinearity as a phase-shift in the time domain which depends on the pulse shape as well as the relation between the nonlinear and the effective length. Note that $\phi_{\mathrm{NL}}(z,t)$ is directly proportional to the optical power and a way of increasing or decreasing the amount of nonlinearities is therefore simply to adjust the optical power. A final important remark on fiber nonlinearities is that while both nonlinear and dispersive effects give rise to a phase shift, the implications are very different. Dispersion is an inherently linear effect in which the phase shift is dependent on the frequency content. In contrast, nonlinearities depend on the profile in time and the phase shift there causes spectral broadening and transfer of energy among different spectral components within the pulse.

2.2.4 The Gaussian Noise Model

While numerical solution of the nonlinear Schrödinger equation provides a way of estimating system performance using simulations, brute force solutions is computationally heavy. As a result of this, large efforts have been devoted to developing simpler models with the most famous one being the Gaussian noise model (GN-model) [141–143].

The GN-model focus on dispersion uncompensated transmission systems in which the signal can be assumed to be highly dispersed. As given away by the name, the model therefore assumes that the signal can be approximated with a Gaussian distribution and that the nonlinear penalty can be approximated with an extra noise term so that the SNR is expanded according to [142]

$$\mathrm{SNR} = \frac{P_S}{\sigma^2_{\mathrm{ASE}} + \sigma^2_{\mathrm{NL}}}, \tag{2.28}$$

with $\sigma^2_{\mathrm{ASE}}, \sigma^2_{\mathrm{NL}}$ being the variance of the amplifier noise and the nonlinear noise-like distortions, respectively. For uncompensated transmission, the model has proven accurate over a broad range of fiber types and transmission distances [144]. Worth emphasizing though is that the GN-model assumes that the signal is a Gaussian process and is hence modulation format independent. However, an extended version, the extended GN-model (EGN-model) accounts for this at the expense of being a more complicated [145].

2.2.5 Polarization-Dependent Channel Models

As discussed before, the fundamental mode in a SMF is polarization degenerate. However, the circular symmetry of a transmission fiber is non-ideal in practice and small fiber birefringence causes polarization rotations as well as give raise to effects such as polarization mode dispersion (PMD) and polarization dependent loss (PDL) [146]. Lots of work have been focused on understanding the effect of mainly PMD which, before the introduction of coherent receiver DSP, limited system reach [147–149]. Without going into detail, we only focus on two separate models for dual-polarization transmission. The first is an extension from the classical AWGN channel by including a polarization scattering matrix H. Equation 2.12 can then be expanded according to

$$y[n] = Ha[n] + N[n], \tag{2.29}$$

with H being a 2×2 complex value unitary matrix in the case of no PDL . If PMD is present H is frequency dependent and the matrix product in Eq. 2.29 will be a convolution with $a[n]$.

Several ways exists for including polarization dependence along the propagation, depending on how the polarization is treated. Focusing on communication over longer distances of fiber (spanning kilometers), the Manakov model is commonly used [34]. In the Manakov model, the state-of-polarization is averaged over the Poincare sphere (Stokes representation [150]), leading to a famous extension of Eq. 2.22 according to [151]

$$\begin{aligned} \frac{\partial A_x}{\partial z} + \frac{j\beta_2}{2}\frac{\partial^2 A_x}{\partial t^2} + \frac{\alpha}{2}A_x &= j\gamma\frac{8}{9}\left(|A_x|^2 + |A_y|^2\right)A_x, \\ \frac{\partial A_y}{\partial z} + \frac{j\beta_2}{2}\frac{\partial^2 A_y}{\partial t^2} + \frac{\alpha}{2}A_y &= j\gamma\frac{8}{9}\left(|A_x|^2 + |A_y|^2\right)A_y. \end{aligned} \tag{2.30}$$

2.3 Optical Receiver

The role of the optical receiver is to extract the information carried by the optical carrier and to retrieve the encoded information. For coherent receivers, this process involves several steps including down-conversion, detection, digitizing and DSP.

As outlined in Fig. 2.1, the incoming signal is mixed with a second laser, the LO, in a coherent optical receiver. Coherent detection is nothing new and has been used for decades within the wireless community. Within the field of optical communication, the lack of high speed ADCs and powerful DSP ASICs meant that it took more than 20 years after the introduction of optical communication systems until the coherent era started, marked by the first development of a real-time coherent transponder in 2007 [43].

2.3.1 Optical Receiver Front-End

Coherent detection refers to the process of detecting both the amplitude and phase of the light wave envelope. In this, the optical phase is extracted with an LO as reference by mixing it using an optical hybrid in which one arm is delayed $\pi/2$ with respect to the other one. The result is two output signals, which can be combined two by two using balanced photo detectors to produce output photo-currents according to [152]

$$\begin{bmatrix} i_{\mathrm{I}}(t) \\ i_{\mathrm{Q}}(t) \end{bmatrix} \propto \begin{bmatrix} \mathrm{Re}\left(E_{\mathrm{Sig}}(t)E_{\mathrm{Lo}}(t)\right) \\ \mathrm{Im}\left(E_{\mathrm{Sig}}(t)E_{\mathrm{Lo}}(t)\right) \end{bmatrix}, \tag{2.31}$$

with $i_{\mathrm{I,Q}}$ denoting the resulting electrical currents representing the in-phase and the quadrature-phase of the modulated envelope, $E_{\mathrm{Sig}}(t)$ denoting the input signal field and E_{Lo} denoting the LO field.

Similarly to how two separate IQ-modulators can be used to built up a polarization multiplexed modulator, two separate optical hybrids combined with a polarization beam splitter can be used to create a dual-polarization receiver. In such, Eq. 2.31, is expanded with indices to denote the X,Y polarization components and the hybrid has thus four outputs.

2.3.2 Analog to Digital Conversion

After coherent detection using the optical hybrid, the resulting photo-currents needs to be sampled in order to produce a received signal in the digital domain. This is done by a set of high-speed ADCs, converting the photo-current into a sampled digital signal. As previously mentioned, optical systems are to a large degree limited by the performance of the DACs and ADCs used in the transceivers [45].

Important aspects when characterizing an ADC is the number of bits, or equivalently, the resolution of the ADC, similarly to the DAC. While DAC and ADC design differ significantly, the metrics used to characterize them as well as the implications of limited resolution on optical communication are very similar. The

sample principles as outlined for the DACs in Section 2.1.3 can therefore be applied to the case of ADCs as well.

2.3.3 Receiver-Side Digital Signal Processing

Following the digitization using the ADCs, advanced DSP and strong FEC is used to recovery the transmitted bits. The DSP-chain typically contains a large set of algorithms to mitigate various impairments present in the fiber channel. Separating DSP and FEC, the role of the DSP is to mitigate any impairments and to maximize the receiver performance. The FEC then handles error induced by the noise. The functionality of the various algorithms used to build up such a DSP chain is discussed in Chapter 3.

2.4 Signal-to-Noise Ratio and System Reach

Considering a system from transmitter to receiver as the one outlined in Fig. 2.1, virtually every component present can and will attenuate and add distortions to the signal [153]. Similar to how an optical transceiver can have its functionality divided into operations performed in the digital, analog electrical and optical domain, the noise added in each of these domains (either from a single component or a combination thereof) can have very different implications in terms of affecting the overall system performance. From a practical viewpoint it also differs significantly in terms of how the SNR is measured. To make it clear throughput this thesis, we will consider the term SNR for use in the digital domain applying the definition from Section 2.2.1. Important from a practical perspective is that with this definition the SNR can be effectively estimated from a received constellation diagram at 1 sample per symbol (SPS). Such estimation methods are covered more in detail in Paper II.

The other measurement of signal quality we will consider is the optical-SNR (OSNR). As indicated by the name, OSNR referees to SNR in the optical domain and OSNR measurements is an essential part of any system evaluation. As an example, dedicated pilot tones (PTs) have been studied to simplify OSNR monitoring in WDM systems [154]. However there are practical challenges with this. OSNR is still, by definition, the ratio between the signal power and the noise power. While at 1SPS in the digital domain, the definition of this is clear, it is not in the optical domain simply from the implication of bandwidth. To avoid this issue, a well-defined referenced bandwidth is used and we define the OSNR according to

$$\mathrm{OSNR} = \frac{P_s}{P_{\mathrm{Noise}}(\omega) B_{\mathrm{Ref}}}, \tag{2.32}$$

with $P_{\mathrm{Noise}}(\omega)$ is the noise power spectral density and B_{Ref} the references bandwidth of 0.1 nm (12.5 GHz@1550 nm). The benefit of Eq. 2.32 is that the OSNR can easily be measured using an optical spectrum analyzer (OSA). Using a for example a 1/99

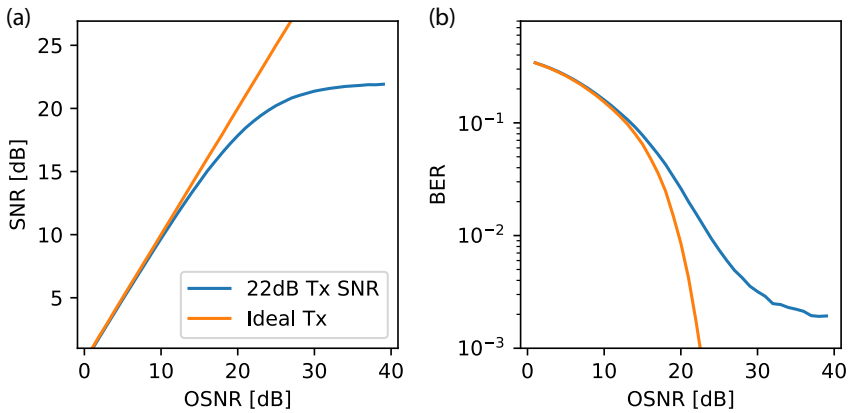

Fig. 2.7. (a) Estimated digital SNR and (b) BER as a function of measured OSNR for a PM-64QAM signal with $B_{\mathrm{Sig}} = B_{\mathrm{Ref}}$. Linear relationship corresponds to a system limited by noise added in the optical domain (link noise). The limited transmitter SNR of 22 dB implies a maximum reachable SNR independent of the measured OSNR, resulting in a BER floor.

coupler/beam splitter, the OSNR can be monitored along the link without requiring any electrical/digital processing. For PM signals, the OSNR can be extracted directly from the measurement. In contrast, the noise power needs to be divided by a factor of 2 if a single polarization signal is considered.

This definition can be used to evaluate OSNR and noise figure from an EDFA. Considering an optical signal into an EDFA of P_{In} and replacing P_{Noise} with P_{ASE} from Eq. 2.11, the OSNR out of the amplifier can be expressed as

$$\mathrm{OSNR} = \frac{P_{\mathrm{Out}}}{P_{\mathrm{ASE}}} = \frac{GP_{\mathrm{In}}}{F_n \hbar\omega B_{\mathrm{Ref}}}, \tag{2.33}$$

with P_{Out} denoting the power out of the amplifier. The power of Eq. 2.33 is that for a multi-span link, consisting of N spans each with a loss L, the OSNR at the receiver can be expressed as [4]

$$\mathrm{OSNR} = \frac{P_{\mathrm{Out}}}{NLF_n \hbar\omega B_{\mathrm{Ref}}}. \tag{2.34}$$

Using the laws for logarithms, this can be written into the famous formula [4]

$$\mathrm{OSNR}_{\mathrm{dB}} = P_{\mathrm{Out}}[\mathrm{dBm}] - F_n[\mathrm{dB}] - 10\ \log_{10}(N) - L[\mathrm{dB}] + 58[\mathrm{dBm}], \tag{2.35}$$

with -58 dBm being the equivalent vacuum fluctuation noise power over the reference bandwidth of 0.1 nm. Equation 2.35 can be used to directly estimate the number

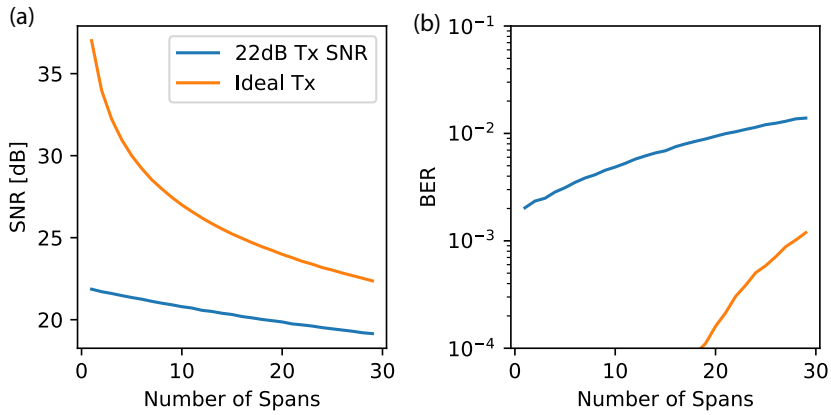

Fig. 2.8. (a) Estimated digital SNR and (b) corresponding BER as a function of number of spans ($\alpha = 0.2\,\text{dB/km}$, $F_n = 5\,\text{dB}$ and $L = 80\,\text{km}$) for a PM-64QAM signal with $B_{\text{Sig}} = B_{\text{Ref}}$. Linear relationship corresponds to a system limited by noise added in the optical domain (link noise). The limited transceiver SNR implies a maximum reachable SNR independent of the measured OSNR, resulting in a BER floor.

of spans over which a signal can be transmitted given a required receiver OSNR. Assuming perfect DSP to mitigate all impairments and implement matched filtering (see Chapter 3), the OSNR can be related to the digital SNR according to

$$\text{OSNR} = \frac{B_{\text{Sig}}}{B_{\text{Ref}}}\text{SNR}, \tag{2.36}$$

with B_{Sig} denoting the ideal Nyquist bandwidth for a signal (e.g. 25 GHz for 25 Gbaud).

However, in taking a measured OSNR and converting it to a corresponding digital SNR for performance estimation, there is a very important assumption that the signal is limited by noise added from optical amplifiers and not by transceiver noise. This can be understood from Eq. 2.33 which assumes that the noise power is from ASE noise only. If transceiver noise, digital and/or electrical is present, this extra noise has to be accounted for in Eq. 2.33, similar to how nonlinear distortions were accounted for using an extra noise term in Eq. 2.28. The implication of this is that Eq. 2.36 and the linear relationship is no longer valid.

This is illustrated in Fig. 2.7, which shows the estimated SNR (see Paper II) and the simulated BER (see Section 3) vs estimated OSNR for a signal with $B_{\text{Sig}} = B_{\text{Ref}}$. Similar results are also observed experimentally, especially for systems focusing on

maximizing SE [137]. The linear relationship observed for low SNR shows a region in which the system is link limited. Deviation from this linear relationship shows a transceiver-limited system resulting in a performance floor, independent of receiver OSNR. In experiments, this deviation is typically quantified by an implementation penalty at a given BER. This difference corresponds to the difference in dB between the ideal case and the real transceiver in Fig. 2.7(a). Important to note here is that the penalty depends strongly on the selected reference point. In this case, the system will have an infinite penalty at BER=10^{-3}, a negligible penalty at BER=$4 \cdot 10^{-1}$ and about 5 dB at BER=10^{-2}. This penalty has to be included in the link budget from Eq. 2.35 in order to accurately estimate the required receiver OSNR.

Considering the example illustrated in Fig. 2.7 and assuming a target BER=10^{-2}, the number of spans can be calculated using Eq. 2.35 according to

$$N[\text{dB}] = P_{\text{Out}}[\text{dBm}] - L[\text{dB}] - F_n[\text{dB}] - 24 + 58. \tag{2.37}$$

Assuming $F_n = 5\,\text{dB}$, $P_{\text{Out}} = 0\,\text{dBm}$ and $L = 20\,\text{dB}$, it is possible to transmit the signal about 20 spans, which would correspond to 1200 km assuming a loss coefficient of $\alpha = 0.2\,\text{dB/km}$. However, the calculation in Eq. 2.37 neglect any nonlinear contributions, which will degrade the signal quality further. However, at the expense of more complex computations, the GN-model (see Section 2.2.4) could be used to add an additional nonlinear contribution to Eq. 2.37.

By using Eq. 2.35, the interplay between transceiver and optical noise can be studied as a function of number of spans. This is shown in Fig. 2.8. Here we observe a very different behavior between the two studied cases, as a result of the significant noise limitation in combination with the use of 64QAM. Finally, we note that similar care is needed when evaluating SNR using an electrical spectrum analyzer (ESA). In that case, special care is needed to ensure that the measured electrical SNR match the digital and optical measurements.

Chapter 3

Digital Signal Processing

After transmission through the optical channel, coherent optical receivers use advanced DSP and powerful FEC to ensure reliable communication. The role of the DSP is to compensate for various signal impairments such as bandwidth limitations and polarization effects. In addition, the receiver implements a matched filter to maximize the probability of correct detection, or equivalently maximize the receiver SNR. Following this, FEC (or transmission of redundant data in clever ways) is used to ensure that the resulting error probability is below a selected threshold, often taken to be a BER of $< 10^{-15}$.

In the following descriptions of all algorithms we consider a received signal $r'[n] = I'[n] + jQ'[n]$, denoting the received signal with the impairment(s) under consideration. The corresponding output signal after processing is denoted $r[n] = I[n] + jQ[n]$. While there exist default schemes outlining the order in which the signal should be processed (see for example [111]), this is not necessarily fixed and some stages can be moved around to gain performance or ease the processing requirements. For example, steps done in the frequency domain can be grouped and performed in cascade to minimize the number of Fourier transforms needed in a hardware implementation. The following sections describe typical DSP algorithms without strictly enforcing an order.

3.1 Matched Filtering

Matched filtering is the processes of maximizing the chances of detecting the signal correctly in the presence of AWGN by filtering it with a filter resulting in the minimum-mean-square error between the transmitted and received signals [105]. As such, considering a pure AWGN channel, this is the only DSP-step needed. If a transmitter signal is shaped with a filter $h(t)$, the matched filter corresponds to

the time-reversed complex-conjugate $h^*(-t)$ [155]. Matched filtering is a core part of communication theory and detailed derivations can be found in [105]. For the purpose of this thesis we only focus on the matched filtering criterion when using raised cosine (RC) pulse shaping from Eq. 2.3 for improving the spectral efficiency, as discussed in Section 2.1.2. When using a RC filter it is common to split the filtering between the transmitter and the receiver. The transmitter spectrally shapes the signal according to

$$s[n] = a[n] * h[n], \tag{3.1}$$

with $s[n]$ denoting the output discrete transmitted signal, $h[n]$ the transmitter pulse shaping filter and $*$ the convolution operator (Eq. 2.2). Assuming the AWGN channel, the received signal $r[n]$ can be written as (see Eq. 2.12 for a description of the AWGN channel model),

$$r'[n] = s[n] + N[n]. \tag{3.2}$$

To maximize the probability of correct detection, the receiver now uses the matched filter according to

$$r[n] = r'[n] * h^*[-n], \tag{3.3}$$

resulting in $r[n]$ being the least-mean-square estimate of the transmitted symbols $a[n]$. Important here is that when using RC pulses, is it often implemented by performing one filtering step at the transmitter and one at the receiver according to [105]

$$h_{\mathrm{RC}} = h_{\mathrm{Tx}} * h_{\mathrm{Rx}}. \tag{3.4}$$

In this case, the proper filter can be found by Fourier-transform Eq. 3.4 according to

$$H_{\mathrm{RC}}(\omega) = H_{\mathrm{Tx}}(\omega)H_{\mathrm{Rx}}(\omega) = |H_{\mathrm{RRC}}(\omega)|^2, \tag{3.5}$$

which shows that the proper transmitter and receiver filters are the square-root of the overall desired response denoted $H_{\mathrm{RRC}}(\omega)$. Also note that while the key aspect of a RC filter is to shape the signal spectrum and ensure ISI-free operation, the ISI criterion is not full-filled by the square root RC filter (RRC) itself. Instead, ISI-free signaling is ensured by applying the matched receiver filter being implemented either by using the known filter response or via the use of a dynamic equalizer. Finally it is important to note that while being straight forward for the AWGN channel, or a set of known filter responses, matched filtering is more tricky for a more general fiber-optic channel containing a number of unknown filter shapes. In practice, dynamic updating of the filtering taps is therefore required to fulfill the matched filtering condition and minimize the ISI, even under presence of impairments unknown to the receiver.

3.2 Static Equalization

Static equalization aims at mitigating static channel impairments. In general, static equalization is cumbersome as compensation as the channel response might not be

accurately described by an all-pass filter, which can be reverted by applying its inverse filter response. The reason is that the matched filter condition presented above only considers at a single symbol $s[n]$, working under the assumption that pulses separated by the duration T are orthogonal. This condition is also refereed to as the Nyquist criterion or ISI criterion. For a given pulse shape $h(t)$, this implies that [105]

$$\int_{-\infty}^{\infty} h(t-kT)h^*(t-k'T)dt = \delta(k-k'), \tag{3.6}$$

where k,k' are two time indices. The implication of the ISI criterion is that pulses time shifted by T will not overlap. Thus if a given filter fulfills the matched filtering criterion for an individual pulse, it also does so for a sequence of pulses. Example of filtering shapes fulfilling this condition are ideal rectangular pulses in time or frequency and RC pulses (as mentioned in Section 2.1.2). However, while the theory literature is largely based on sequences of ISI-free pulses, this is a theoretical assumption that is seldom fulfilled in practical systems for reasons such as components with limited bandwidth, sampling, and windowing to mention a few, there will be residual ISI. As a result, when looking at a sequence of sent symbols, it is not sufficient to consider the matched filtering condition for an individual symbol as done in Section 3.1. Instead, the matched filter for a sequence of pulses is a filter that maximize the sequence SNR, corresponding to finding the optimal trade-off between mitigating ISI and avoiding excessive noise enhancement. While the shape of such a matched filter could be derived, it requires full knowledge of the system, making such derivations cumbersome in practice.

As a key example, and maybe the most used static filter in optical communication, we consider transmission through the dispersive channel described in Section 2.2.2. In this case, the signal reaching the receiver can be expressed as combination of the Tx pulse shaping filter and the channel response $H_{\mathrm{Ch}}(\omega)$ according to

$$H_{\mathrm{Ch}}(\omega) = H_{\mathrm{Tx}}(\omega)H_{\mathrm{Disp}}(\omega), \tag{3.7}$$

with $H_{\mathrm{Disp}}(\omega)$ denoting the dispersive response. From Eq. 3.4, it can directly be seen that the Rx filter needs to contain $H^*_{\mathrm{Disp}}(\omega)$ in order to undo the effect of dispersion, which is called the dispersion compensating filter. This static filter can be implemented by directly considering the frequency domain solution, Eq. 2.20, to the dispersive channel model (Eq. 2.17). A static frequency domain dispersion compensating filtering can be implemented according to

$$r(t) = \mathscr{F}^{-1}\left(U(-z,\omega)\mathscr{F}\left(r'\right)\right), \tag{3.8}$$

with $\mathscr{F}$ denoting the Fourier transform operator and $U(z,\omega)$ is the dispersive phase response from Eq. 2.20. However, for real-time sequential processing it is necessary to apply the filter in a continuous manner. This is done by dividing the signal into processing blocks and each block is independently compensated by using a discrete Fourier transform implementation. To avoid issues from discontinuities and the

periodic boundary conditions imposed by the block-wise Fourier transform [115], the blocks are selected with a certain overlap which is then removed after processing, a process known as overlap-and-save [111, 156]. Finally, we note that that when using a fixed static filter, its exact shape has to be known. For dispersion compensation of a point-to-point link, this is straight-forward, however, in dynamic network scenarios where optical signals are re-routed along the path, this might not be true and dispersion estimation is required to resolve the propagated distance [157]. In this case, dispersion estimation can be used prior to applying the static filter [158–160].

3.3 Dynamic Equalization

While static equalization is very powerful, the key drawback is that it requires exact knowledge of the system in order to find the receiver filter that minimize the difference between the transmitted symbol and the detected symbols. This might be straightforward in the case of dispersion but implies knowing the exact response for every transceiver component and the complete fiber link. In addition, some effects present in optical communication systems, such as polarization effects, are not static and the filter response therefore changes with time. To cope with these challenges, dynamic filtering is needed. Dynamic filtering can be understood as a receiver filter that is continuously tuned to minimize an error function. The dynamic equalizer therefore aims at suppressing penalties from the combination of unknown noise sources present in the systems and distortions not compensated by the static filtering stage.

Due to its dynamic nature this equalizer is inherently more challenging to implement than its static counterpart. Filtering can be implemented in either the time or frequency domain and which one to choose depends largely on the memory length of the filter. While computations of long responses can be done more effectively in frequency domain, something of key importance for SDM systems with long impulse responses such as mode-division multiplexing systems [161, 162], short filters are computed more effectively in time domain [163]. This is important as the DSP can be done more effectively by compensating large memory effects such as dispersion using static filters implemented in the frequency domain and then use a time-domain implementation of the dynamic equalizer to compensate residual distortions. This is the implementation we focus on in this work.

Time-domain filtering using finite impulse response (FIR) filters can be described as [155]

$$r[n] = \vec{w}^{H}[n] \cdot \vec{r'}[n], \tag{3.9}$$

with $\vec{w} = [w(n),w(n-1),...,w(n-N)]^{T}$ denoting the N filter taps, superscript H the Hermitian transpose and $\vec{}$ denotes a time vector. The filter weights can be real or complex valued. As given by Eq. 3.9, these filter taps are weights used in the summation of the N input samples. Also note that the filter can be shifted to have memory both forward and backwards in time which is required for matched filtering

of, for example, RC pulses. However, doing so always introduces a fundamental delay, to maintain causality.

In the case of dual-polarization transmission, the equalizer can undo polarization rotations and compensate for PMD. This is typically done by multiple-input-multiple-output (MIMO) processing with a 2×2-butterfly configuration of the equalizer according to [111]

$$\begin{pmatrix} r_{\mathrm{X}}[n] \\ r_{\mathrm{Y}}[n] \end{pmatrix} = \begin{pmatrix} w_{\mathrm{XX}}^{H}[n] & w_{\mathrm{XY}}^{H}[n] \\ w_{\mathrm{YX}}^{H}[n] & w_{\mathrm{YY}}^{H}[n] \end{pmatrix} \begin{pmatrix} r'_{\mathrm{X}}[n] \\ r'_{\mathrm{Y}}[n] \end{pmatrix}. \tag{3.10}$$

Equation 3.10 implements the polarization de-multiplexing required in dual- polarization systems. Importantly, a pure polarization rotation can be undone using a 2×2 complex unitary matrix and no time memory is needed. Instead, the memory requirement in the polarization de-multiplexing process arises due to the PMD present in optical fibers and the requirement of ensuring match filtering. To track time-varying impairments, the filtering weights in Eq. 3.10 have to continuously be re-optimized. Considering an error signal according to $e[n]$ the mean squared error criterion aims at minimizing the cost function $J[n] = \mathbb{E}[e[n]e^*[n]] = \mathbb{E}[|e[n]|^2]$. The gradient of the cost function with respect to the applied filter $\vec{w}$ can be defined according to

$$\nabla J_k[n] = \frac{\partial J[n]}{\partial w_k^*[n]}, \tag{3.11}$$

where $k = 0, 1, ..., N-1$ and ∇ is the vector differential operator. This can be minimized using an iterative approach based on the steepest decent method according to according [155]

$$w_k[n+1] = w_k[n] - \mu \frac{\partial J[n]}{\partial w_k^*[n]}. \tag{3.12}$$

If we now focus on minimization of an error $e[n] = d[n] - r[n]$ being the difference between a target signal $d[n]$ (different ways of defining the error signal are covered later) and the filter output $r[n]$. From a constellation diagram, the desired signal corresponds to the transmitted constellation point and a least mean squared (LMS) equalizer therefore aims at minimizing the distance between transmitted and received constellation points. The challenge with applying LMS-based equalization is that $d[n]$ is typically no known to the receiver (see below). The iterative LMS solution to Eq. 3.12 is given by [155]

$$\vec{w}[n+1] = \vec{w}[n] + \mu \vec{r'}[n] e^*[n]. \tag{3.13}$$

Updating the filter taps using Eq. 3.13 is valid for all LMS-based error functions. Expanding this to the case of dual-polarization MIMO equalizer, the update is done

according to

$$\begin{aligned}\vec{w}_{\mathrm{XX}}[n+1] &= \vec{w}_{\mathrm{XX}} + \mu\vec{r'}_{\mathrm{X}}[n]\epsilon^*_{\mathrm{X}}[n] \\ \vec{w}_{\mathrm{XY}}[n+1] &= \vec{w}_{\mathrm{XY}} + \mu\vec{r'}_{\mathrm{Y}}[n]\epsilon^*_{\mathrm{X}}[n] \\ \vec{w}_{\mathrm{YX}}[n+1] &= \vec{w}_{\mathrm{YX}} + \mu\vec{r'}_{\mathrm{X}}[n]\epsilon^*_{\mathrm{Y}}[n] \\ \vec{w}_{\mathrm{YY}}[n+1] &= \vec{w}_{\mathrm{YY}} + \mu\vec{r'}_{\mathrm{Y}}[n]\epsilon^*_{\mathrm{Y}}[n]\end{aligned}, \tag{3.14}$$

with $\epsilon_{\mathrm{X/Y}}$ denoting the error function and μ a constant (error scaling factor) known as the step length. The error function is essential for the performance of the dynamic equalizer and choosing the most suitable error function is critical to maximize the equalizer performance. Several different error functions exists of which some are covered in the following sections. A more detailed overview over different algorithms can be found in [111, 164]. The power of dynamic equalization can be seen in Fig. 3.1, in which the dynamic equalizer performs polarization de-multiplexing and matched filtering on the receiver side. Here we also emphasize that the signal in Fig. 3.1(a) is shaped with an RRC filter and the apparent SNR improvement seen when comparing Fig. 3.1(a) and (c) is attributed to the equalizer finding a filter that to minimize both effect of ISI (as RRC pulses do no fulfill the Nyquist criterion from Eq. 3.6) and out-of-band noise.

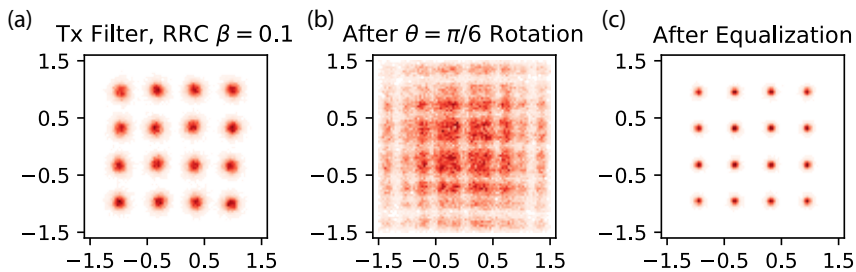

Fig. 3.1. Effect of dynamic equalization. (a) Transmitted signal shaped with a root-raised cosine filter with $\beta = 0.1$. (b) resulting constellation after a small polarization rotation. (c) Constellation after dynamic equalization using a LMS-based equalizer. The constellation diagram shows is the equalizer has converged to steady-state performance.

3.3.1 Constant Modulus Algorithm

The constant modulus algorithm (CMA) is one of the key algorithms in dynamic equalization [165]. The CMA is based on minimizing the mean squared error of the

signal, with respect to a given reference level, R_{Ref}, according to [165, 166]

$$\begin{aligned}\epsilon_{\mathrm{X}}[n] &= R_{\mathrm{Ref}} - |r_{\mathrm{X}}[n]|^2 \\ \epsilon_{\mathrm{Y}}[n] &= R_{\mathrm{Ref}} - |r_{\mathrm{Y}}[n]|^2\end{aligned}. \tag{3.15}$$

The CMA is a simple, frequently used, very powerful error function. However, as seen in Eq. 3.15, the average power is always referenced with respect to a fixed value. For constant power constellations such as QPSK this works well but for multi-level modulation formats such as general M-QAM this is not true. Still, by choosing R_{Ref} according to [167]

$$R_{\mathrm{Ref}} = \frac{\mathbb{E}\left[|a[n]|^4\right]}{\mathbb{E}\left[|a[n]|^2\right]}, \tag{3.16}$$

the standard CMA can be used for multi-level modulation formats at the expense of a penalty, which becomes larger when increasing the modulation order. Importantly, CMA is one of the most used algorithms but it is not an LMS algorithm. The update scheme from Eq. 3.13 should therefore be changed according to [168]

$$\vec{w}[n+1] = \vec{w}[n] + \mu\vec{r'}[n]e[n]r^*[n], \tag{3.17}$$

which can be extended to MIMO operation using the same structure as in Eq. 3.14. However, to simplify implementation and direct comparison of algorithms, the CMA error function can be re-written according to

$$\epsilon[n] = r[n]\left(R_{\mathrm{Ref}} - |r[n]|^2\right), \tag{3.18}$$

for a single polarization signal. This convenient modification makes the CMA update function equivalent to that of an LMS equalizer given by Eq. 3.13.

3.3.2 Radius-Directed Equalization

One way of extending the CMA to cope with multi-level modulation format is the radius-directed equalizer (RDE) [169]. As given away by the name, this equalizer relies on estimating the radius of the equalizer output and compare it to a set of reference levels (in contrast to CMA which only has one fixed level). This is done by adapting Eq. 3.15 according to [169]

$$\begin{aligned}\epsilon_{\mathrm{X}}[n] &= \mathbb{D}_{\mathrm{R}}\left[|r_{\mathrm{X}}[n]|^2\right] - |r_{\mathrm{X}}[n]|^2 \\ \epsilon_{\mathrm{Y}}[n] &= \mathbb{D}_{\mathrm{R}}\left[|r_{\mathrm{Y}}[n]|^2\right] - |r_{\mathrm{Y}}[n]|^2\end{aligned}, \tag{3.19}$$

with $\mathbb{D}_{\mathrm{R}}$ denoting a radius decision operator which selects the maximum-likely-hood radius of the received constellation point given a set of reference radii. As such, the use of RDE requires knowledge of the constellation. Moreover, the performance depends on the probability of correctly estimating the signal radius, which is particularly challenging during the initial convergence phase in which symbol errors

are frequent. To overcome this, a RDE is often used in cascade with an initial CMA equalizer to pre-converge the taps. After the CMA has converged to the best average error, the RDE is used to account for the multi-level constellation. The tap update using RDE can be done either using a corresponding update scheme to that of the CMA given by Eq. 3.17 or by multiplying the error function with the output $r[n]$ and use the LMS update scheme from Eq. 3.13.

3.3.3 Decision-Directed Least Mean Square

The RDE can be seen as an extended CMA which uses a decision-directed (DD) circuit to choose the most proper reference level from a given reference set, resulting in a real-valued error signal. Another option is to use the LMS-based error function introduced before but it knowledge of the desired output signal, which is equivalent to the transmitted constellation point and this information is not known to the receiver. However, a decision on the most likely received symbol can be used and the error taken as the distance between the received symbol according to [170, 171]

$$\begin{aligned} \epsilon_{\mathrm{X}}[n] &= \mathbb{D}_{\mathrm{S}}\left[r_{\mathrm{X}}[n]\right] - r_{\mathrm{X}}[n] \\ \epsilon_{\mathrm{Y}}[n] &= \mathbb{D}_{\mathrm{S}}\left[r_{\mathrm{Y}}[n]\right] - r_{\mathrm{Y}}[n] \end{aligned}, \tag{3.20}$$

refereed to as DD least mean square (DD-LMS) equalizer with $\mathbb{D}_{\mathrm{S}}$ denoting the symbol decision operator. The decision operator $\mathbb{D}_{\mathrm{S}}$ returns the most likely transmitted symbol conditioned on the received sample and the error is then calculated as the distance in constellation space between the received symbol and the estimate of the transmitted one. The DD-LMS algorithm therefore tries to minimize the variance of the distance between detected symbol and decided symbol. The convergence rate and performance for DD-LMS depends strongly on the probability of making a symbol error in the detection, quantified by the symbol error ratio (SER), due to the dependence on the symbol decision operator $\mathbb{D}_{\mathrm{S}}$. While DD-LMS is very powerful at higher SNRs, strong performance fluctuations can be present at lower SNRs.

The use of a DD-LMS is suitable for complex multi-level constellations such as higher-order M-QAM. In contrast to CMA and RDE, the DD error function uses both the real and imaginary part of the signal error. If carrier offsets (see Section 3.4) are present on the signal, these have to be compensated in order to make accurate symbol-based decision which causes delays in feedback when considering real-time processing. Moreover, similar to RDE, the DD-LMS is sensitive to symbol decision errors and initial pre-convergence with a CMA-like algorithm is normally required to ensure stable performance.

3.3.4 Data-Aided Least Mean Square

Data-aided LMS (DA-LMS), or simply LMS, is very similar to DD-LMS with a small but crucial difference. For DD-LMS, the decision operator $\mathbb{D}_{\mathrm{S}}$ is needed as

the transmitted symbol, being the desired signal $d[n]$, is not known to the receiver. However, for DA-LMS the receiver has access to the transmitted symbol $a_{\mathrm{X/Y}}[n]$ and pure LMS-based optimization can therefore be performed. The error functions then change from Eq. 3.20 to

$$\begin{aligned} \epsilon_{\mathrm{X}}[n] &= a_{\mathrm{X}}[n] - r_{\mathrm{X}}[n] \\ \epsilon_{\mathrm{Y}}[n] &= a_{\mathrm{Y}}[n] - r_{\mathrm{Y}}[n] \end{aligned}. \tag{3.21}$$

The performance of DA-LMS is therefore equivalent to that of DD-LMS when the symbol error probability $\rightarrow 0$. The problem with DA-aided processing is that the information rate drops to zero once the transmitted information is known to the receiver. If a few symbols are known, these are refereed to as pilots and this can be exploited to realize very powerful dynamic equalization (see Paper II). However, mentioning DA-LMS is important aside pilot-based processing too, as it is frequently being used in transmission experiments. The used of DA-LMS provides an upper benchmark of what can be achieved using LMS-based equalization and therefore serves as a suitable benchmark when comparing other error functions or decision operators. However, it is worth emphasizing that this is a non-practical approach requiring full knowledge of the transmitted pattern and the information rate of such a system drops to zero.

3.4 Carrier Recovery

The carrier recovery is a special part of the DSP designed to cope with distortions originating from the transmitter and receiver laser. As these impairments differ significantly from other effects such as polarization rotations both in terms of the speed of the dynamics and how the impairment is manifested, they are preferable treated using tailored algorithms. The transmitter laser and the local oscillator (LO) should ideally be the "same" laser but in practice, unless homodyne schemes (see Section 5.3) or external stabilization is used, this is not the case. Any mismatch between the lasers will give raise to carrier offsets [172, 173]. This can be qualitatively understood by considering the up-down conversion process in the transmitter and receiver according to

$$r[n] = a[n] \exp\left(j\left(2\pi n f_0 T + \phi_0[n]\right)\right) \cdot \exp\left(-j\left(2\pi n f_1 T + \phi_1[n]\right)\right) + N[n], \tag{3.22}$$

with f_0,f_1 and ϕ_0,ϕ_1 denoting frequencies and phase fluctuations of the transmitter and receiver lasers, respectively. Ideally, the transmitter and receiver laser are perfectly synchronized and without any phase noise. However, in practice the lasers drift and have a non-zero linewidth (the ideal laser is monochromatic). How much and to what extent depends on the laser type but for standard external cavity lasers (ECLs) used in the majority of this work, frequency drifts up to a few GHz [174, 175] together with linewidths around 10-100 kHz are common. While the dynamics

underlying the linewidth of a laser can be complex, a simple system model can be built up under the assumption of a perfectly Lorentzian linewidth. In such case, the phase noise can be approximated as a Brownian motion according to [172]

$$\phi[n] = \sum_{k=-\infty}^{n} \nu[k], \tag{3.23}$$

with $\nu[k]$ being *i.i.d.* Gaussian random variables with zero mean and variance $\sigma_\nu^2 = 2\pi\Delta\nu T$, with $\Delta\nu$ being the laser linewidth (often combined for both the transmitter and the receiver laser). In contrast to frequency offset which corresponds to a linear phase walk, phase noise is a random process. Moreover, the frequency offset is a slowly varying process in contrast to phase-noise compensation which is required on symbol level to ensure high performance. Worth emphasizing here is that most lasers does not have a perfect Lorentzian linewidth. In such cases, measuring the laser linewidth by performing a Lorentzian fit to a spectrum measured by beating the laser with a delayed copy of itself, tends to overestimate the Lorentzian component [176]. This is a common source of deviation between performance estimated using numerical simulations based on Eq. 3.23 and experimental measurements. To avoid this, phase noise should be characterized by measuring the FM noise spectrum, which can easily be done using a standard coherent receiver [177].

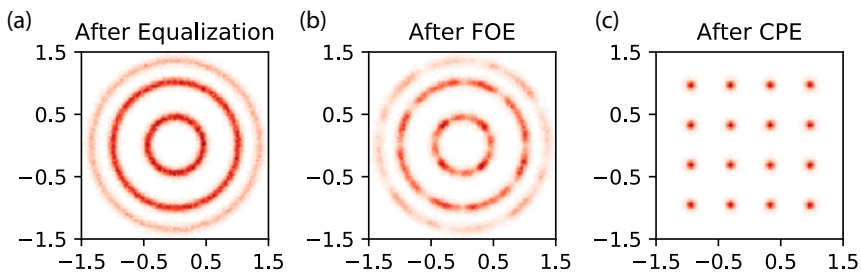

Fig. 3.2. Impact of DSP-based carrier recovery. (a) Signal before compensation with $\Delta f = 500$MHz and $\Delta\nu = 100\,$kHz. (b) Constellation after FOE and (c) constellation after FOE and CPE (BPS with $M = 64$ and $N = 20$).

3.4.1 Frequency Offset Estimation

DSP-based frequency offset estimation (FOE) can be done in several ways [178–183]. While most published studies have been considering offline processing, some recent work has focused on hardware implementations of FOE [175]. One common approach is based on removing the data modulation and estimating the frequency offset by

finding the linear component of the signal phase drift. This can be understood by considering QPSK modulation for with the symbols $a[n] \in \frac{1}{\sqrt{2}}(\pm 1 \pm j)$. QPSK is equivalent to 4-phase shift keying (PSK) and for M-PSK formats, data modulation can be removed by raising the constellation to the M:th power [172]. In the case of QPSK, this translates to

$$(a[n])^4 = -1, \forall n. \tag{3.24}$$

After this process, the frequency offset is found using a linear fit of the phase trace in the time domain, or by Fourier transforming the signal and search for the maximum peak in the resulting spectrum (which is intuitive since the Fourier-transform is nothing else than a change of basis to a set of linear orthogonal frequency components) [183].

While proven powerful for M-PSK, the expression in Eq. 3.24 cannot be generalized to an arbitrary QAM format and there is no trivial operation to remove the data modulation (which follows from the fact that in contrast to PSK, both the amplitude and phase are used for encoding information). However, for M-QAM, this can usually be circumvented by realizing that M-QAM constellation can be decomposed to rings of PSK. For example, a 16-QAM can be decomposed into an inner and an outer ring with QPSK and an intermediate with eight constellation points. Since they have different power, applying Eq. 3.24 to such a constellation will map to 4 points, from which 2 are mapped to the real axis (but with different amplitude). Doing so, the same algorithm can be used even for higher order M-QAM at the expense of requiring more symbols as only a fraction of the symbols actually directly are used to estimate the frequency offset. This can be seen in Fig. 3.2 for the case of 16QAM.

As a final remark, while long averaging filters are not an issue in offline processing, they are for real-time implementations. Moreover, the accuracy of the estimation depends on the number of symbols. As a result, the complexity of frequency offset estimation grows when considering systems operating at low received SNR with a strong presence of symbol errors.

3.4.2 Carrier Phase Estimation

The role of the carrier phase estimation (CPE) is to compensate the random walk caused by the phase-noise. In addition, it also compensates for any residual frequency offset due to limited resolution of the frequency offset estimation, a very important aspect which is often overlooked in simulation work. For PSK-signals, the carrier phase recovery can be implemented the same way as the frequency offset estimation by raising the signal to the M:th power, in line with Eq. 3.24. However, instead of doing a linear fit over a large set of symbols, a sliding average window is used to track and follow the phase fluctuations [184]. This is referred to as Viterbi-Viterbi (VV) phase estimation [185]. In such case, the relation between the amount of phase noise and AWGN decides the optimal block length.

As pointed out in Section 3.4.1, the data modulation can be removed in an optimal way for M-PSK but modifications are required to allow processing of arbitrary M-QAM. Similarly to the case of FOE, partitioning the signal into several PSK rings can be overcome this issue [184, 186–188]. Another frequently used alternative to Viterbi-based CPE for arbitrary M-QAM is the blind phase search (BPS). In contrast to Viterbi-based CPE which relies on a nonlinear operator to remove data modulation, BPS relies on parallel processing using a brute-force scheme in which a set of M test angles are selected according to [189]

$$\phi_m = \frac{m}{M}\frac{\pi}{2}. \tag{3.25}$$

The received symbols are then rotated with every test phase before the symbol decision operator is used to calculate the distance error according to

$$|d_{n,m}|^2 = \left|r'[n]\exp(j\phi_m) - \mathbb{D}_{\mathrm{S}}\left(r'[n]\exp(j\phi_m)\right)\right|^2, \tag{3.26}$$

before a sliding average window of length $2N+1$ is used to suppress noise according to

$$s_{n,m} = \sum_{k=-N}^{N} |d_{k,m}|^2, \tag{3.27}$$

and the output symbol is then selected by minimizing $s_{n,m}$ over the M test angles according to

$$r[n] = \arg\min_m s_{n,m}. \tag{3.28}$$

Following its parallel nature and compatibility with arbitrary M-QAM modulation formats (due to the symbol-based decision in Eq. 3.27), BPS is often used for processing higher-order M-QAM formats. Extensions with maximum-likelihood estimators to improve robustness have also been studied using a two-stage approach [190]. Worth noting here is that the needed number of test angles, M, and averaging block length, N, depends on the modulation order and amount of AWGN present. As a result, processing of higher-order formats in a regime with low SNR can be challenging. Since the CPE also has to cover any remaining frequency offset, which also is more likely in this regime of interest, extra care is required when designing carrier recovery for high spectral efficiency systems using strong FEC. This issue is discussed in Paper V.

3.5 Transceiver Distortions

Transceiver distortions is a global term describing essentially any impairment that is not originating from sending the light through optical fibers. Part of these impairments are limited component bandwidth, which is modelled well using an FIR filter, and carrier offsets. These impairments are handled well by using the

combination of a dynamic equalizer and carrier recovery, as previously discussed. These impairments are typically related to the modulator and optical front-end, as well as the electrical amplifiers and DACs/ADCs used to convert between analog and digital signals.

Before covering key impairments of this kind, it is important to emphasize that FIR filters are linear filters. As a direct result of this, the order does not matter and they can be moved around, as long as the signal is completely linear. So in a linear system, the receiver side effects can be pre-compensated at the transmitter, to give one example. However, in the case of nonlinear responses, this is not true. This is particularly important in fiber-optics as we are working with a nonlinear channel, preventing a direct interchange between receiver and transmitter side functionality. As the role of the receiver side DSP in a way is to go backwards through the system and remove all impairments to recover the information from the transmitter, this has to be accounted for. This implies first compensating receiver distortions, then the channel distortions and as a final step try to mitigate any transmitter distortions. However, even better is of course to pre-compensate the transmitter distortions at the transmitter.

3.5.1 Front-End Imbalance and Skew Compensation

While the ideal optical front-end and IQ-modulator has a perfect $\pi/2$ phase shift between the two arms, which also are identical, practical devices usually deviates from their ideal counterpart. As a result, both the optical hybrid and the transmitter modulator can cause skew and imbalance between the I and Q components of the modulated and/or detected signal, causing distortions which leads to reduced performance [191, 192]. Skew and imbalance can be modeled according to [193],

$$\begin{aligned} r'[n] &= \left(g_{\mathrm{I}} I\left[n - \frac{\tau_{\mathrm{IQ}}}{2}\right] + o_{\mathrm{I}}\right) + \left(g_{\mathrm{Q}} Q\left[n + \frac{\tau_{\mathrm{IQ}}}{2}\right] + o_{\mathrm{Q}}\right) \exp\left(j\left(\frac{\pi}{2} + \phi_{\mathrm{IQ}}\right)\right) \\ &= I'[n] + jQ'[n], \end{aligned} \tag{3.29}$$

with $r'[n]$ denoting the received complex signal with, τ_{IQ} denoting the timing skew, ϕ_{IQ} the phase error, $g_{\mathrm{I,Q}}$ and $o_{\mathrm{I,Q}}$ the gain and DC offset of the I and Q components, respectively. Equation 3.29 gives important insights to how the signal is affected by such impairments. The effect of various imbalance impairments can be seen in Fig. 3.3 for the unimpaired of 16QAM shown in Fig. 3.3(a). In Fig. 3.3(b), the effect of varying gain between $I'(t)$ and $Q'(t)$ is illustrated, which result in signal compression of one of the axis relative to the other one. As a result, the realtive power per dimension (considering constant average power) will vary, resulting in a performance differences between I' and Q'. The effect of offsets (o_{I},o_{Q}) is visualized Fig. 3.3(c) and we observe that while the constellation looks identical to the reference case in Fig. 3.3(a), the center of the constellation is shifted. Finally, a mismatch in

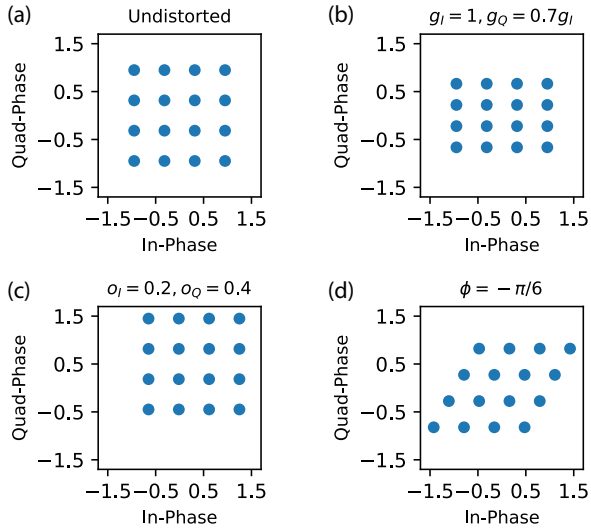

Fig. 3.3. Effect of IQ-imbalance on a signal constellation. (a) Unimpaired 16QAM constellation, (b) different gain of the I and Q component, (c) non-zero centered constellation in I and Q and (d) a $\phi = -\pi/6$ offset from the ideal case of a $\pi/2$ angular difference between I and Q component.

the $\pi/2$ phase-shift between the two components cause I and Q to be non-orthogonal, which skews the constellation along the axis, as seen in Fig. 3.3(d).

Depending on the impairment, these imbalances can be compensated in different ways. Non-zero offsets can be compensated by re-centering the signal according to

$$r[n] = r'[n] - \mathbb{E}\left[r'[n]\right]. \tag{3.30}$$

Similarly, non-equal gain factors can be compensated for by scaling the signal according to

$$r[n] = c\left(\frac{I'[n]}{\mathbb{E}\left[|I'[n]|^2\right]} + j\frac{Q'[n]}{\mathbb{E}\left[|Q'[n]|^2\right]}\right), \tag{3.31}$$

with c being an arbitrary scaling constant. While gain variations and offsets are straightforward to account for, the case of $\phi \neq 0$ causes the received in-phase and quadrature-phase components to be non-orthogonal. Several algorithms can be used to orthogonalize I and Q, including the commonly used Gram-Schmidt (GS) algorithm [194]. Using the GS scheme, one vector is selected as the reference and the second vector is then being orthonormalized with respect to the chosen initial

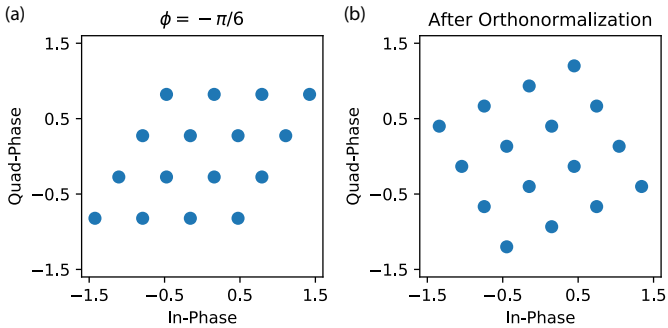

Fig. 3.4. Effect of orthonormalization to compensate for an IQ-skew ($\phi \neq 0$). (a) before orthonormalization, $\phi = -\pi/6$. (b) after orthonormalization.

vector according to

$$\begin{aligned} \vec{I}[n] &= \vec{I}'[n] \\ \vec{Q}[n] &= \vec{Q}'[n] - \frac{\left\langle \vec{I}'[n], \vec{Q}'[n] \right\rangle}{\left\langle \vec{I}'[n], \vec{I}'[n] \right\rangle} \vec{I}'[n], \end{aligned} \tag{3.32}$$

with $\vec{I}[n], \vec{Q}[n]$ being vectors in time and <> denoting the dot product. The effect of using the GS orthogonalization is depicted in Fig. 3.4. Moreover, Eq. 3.32 performs an orthonormalization and will thus also compensate for any gain and offset variations. Complete compensation of the receiver IQ-imbalance can therefore be done in a single step.

As a final remark to the effect of skew and imbalances, it is important to note that while these algorithms work very well in the ideal case, any noise on the constellations will be re-scaled when re-scaling the signal. Performance will therefore be limited in systems suffering from large imbalance. For the orthonormalization, several other methods exists which instead of normalizing one vector with respect to the other perform the orthogonalization symmetrically. In severe cases, such approaches can improve performance over the simple GS scheme.

3.5.2 Compensation of Transmitter Distortions

As previously mentioned, transmitter distortions should preferably be compensated at the transmitter side. The signal at the transmitter side has higher SNR and, if DSP-based compensation is being used, it is most effective if it is close to the source of the impairments. Multiple schemes to mitigate transmitter distortions have been developed, including Volterra-like equalizers or look-up tables [195–197].

For generating QAM-formats with $M > 64$ in Paper V and VII, such pattern-based pre-compensation scheme was used. In addition, the nonlinear response of the modulator can be compensated by applying the inverse to the cosine response given by Eq. 2.9. However, important here is that such pre-compensation will compress the lower amplitude part of the signal, causing SNR degradations when using DACs and ADCs with a limited resolution. As a result, modulator swing need to be jointly optimized with modulator pre-compensation, patter-based pre-compensation and signal clipping to maximize the signal SNR.

Distortions not compensated at the transmitter will nevertheless remain at the receiver. Following the CPE, the output symbols are usually fed to a de-mapper followed by a decoder to recover the bits. However, similar to how an initial IQ-imbalance compensation stage can be used to compensate for receiver IQ-imbalance, additional compensation can be used to compensate for transmitter distortions [160]. As the modulator skew and imbalance problems are equivalent to the ones arising from the optical front-end, these distortions are the same as the once outlined in Sec. 3.5.1 for the case of the receiver and can be compensated in the same way. For a well-balanced transmitter, this stage is usually not needed and in the case of minor distortions a single orthogonalization stage is usually sufficient. However, for completeness, it is important to point out that real-valued equalization can be used to combat more severe distortions and improve performance. This is typically needed in systems with subcarrier-modulation [191]. The key difference is while a complex modulation assume orthogonality between I and Q, a real-valued can be used to compensate for scenarios when this is not the case [160, 192, 198].

3.6 De-Mapping and System Performance Evaluation

After carrier recovery and compensation of transmitter distortions, the next step is to de-map the transmitted symbols to a bit stream which then is forwarded to the FEC decoder used to recover the transmitted bits. Important to note here (and all to often overlooked in the experimental literature) is that several types of codes exist and depending on the chosen type, the output from the de-mapper can be either soft or hard information. Hard information corresponds to the de-mapper outputting a bit sequence and soft corresponds to the de-mapper outputting the probability that each bit is a 1 or a 0. While coding is seldom implemented in transmission experiments and other performance metrics are used instead, distinction between hard and soft codes is necessary as they require different metrics to accurately predict the performance after decoding.

3.6.1 Hard-Decision De-mapping

The classical de-mapper is a hard decision (HD) de-mapper, which outputs the maximum likelihood bit sequence given the received symbols. Assuming the AWGN channel (this assumption is most often used when designing de-mappers), this corresponds to selecting the closest constellation symbol to the transmitted ones. The implication of the assumption of a HD-FEC is that measured BER after the de-mapper can be used to verify that the system performs within the target limit of a code assumption which usually is around BER $\approx 1 - 5 \cdot 10^{-3}$ with corresponding coding overheads of around 7% .

3.6.2 Soft-Decision De-mapping

Recently, more and more research has turned towards studying the use of soft-decision (SD) FEC which is capable of improved coding gain at the expense of increased complexity of the de-mapper and the de-coder. Code-design and structures are far beyond the scope of this thesis, and we therefore only focus on performance metrics used to estimate the performance. The first key difference between HD- and SD-decoding is that instead of forwarding de-mapped bits, a SD-demapper outputs log-likelihood ratios (LLRs) which can be understood as the probability of a specific bit being a 1 or a 0. The corresponding case of HD would be to simply output the most likely outcome of the corresponding bit. For a complex symbol there are $k = \log_2 M$ LLRs as [199]

$$L[k] = \log \frac{\sum_{x \in \chi_k^1} P_{X|C_k}(x|1) f_{Y|X}(y|x)}{\sum_{x \in \chi_k^0} P_{X|C_k}(x|0) f_{Y|X}(y|x)}, \tag{3.33}$$

where χ_b^b is the set of constellation symbols with $b \in 0{,}1$ at bit position $k \in 1,..., \log_2 M$ and $f_{Y|X}(y|x)$ is the probability of a received symbol Y conditioned on a transmitted symbol X. After calculating the LLRs, these values are forwarded to the FEC decoder. The improvement of using LLRs can easily be understood by considering a sequence of bits in which one is wrong (as detected by the parity check in the decoder). If only the bits are present, all bits are equally likely to be the one being wrong (even though clever encoding and decoding algorithms allows for educated guesses) but if the LLRs are present, statistical knowledge of the probabilities of each bit being wrong are available and the most uncertain one can be changed. However, SD comes at the price of higher computational complexity in both the de-mapper and the decoder.

Estimating the performance of a system with soft-decision is more cumbersome and requires assumptions on which SD code is being used. Assuming a memory-less channel and the use of bit-interleaved coded modulation (BICM), the proper metric to use is the generalized mutual information (GMI) [199]. If one instead allows for the use of non-binary codes or iterative de-mapping, the proper metric is the

mutual information (MI) [199]. The GMI is upper bounded by the MI. Assuming a memory-less AWGN channel, the GMI can be estimated according to [199, 200]

$$\mathrm{GMI} \approx M - \frac{1}{n_s} \sum_{k=1}^{M} \sum_{l=1}^{n_s} \log_2 \left(1 + \exp\left((-1)^{c_{k,l}} \lambda_{k,l}\right)\right), \tag{3.34}$$

using a sequence of $M \cdot n_s$ transmitted bits denoted by $c_{k,l}$ and the corresponding L-values $\lambda_{k,l}$ estimated using Eq. 3.33. A comparison between BER and GMI for standard M-QAM modulation formats in the AWGN channel can be seen in Fig. 3.5.

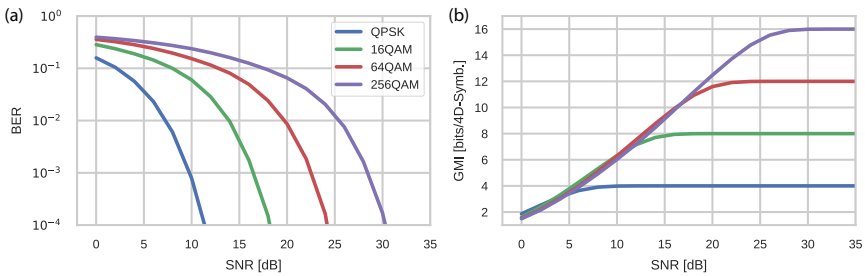

Fig. 3.5. Comparison between BER and GMI for standard M-QAM modulation formats in the AWGN channel. (a) bit to error rate (BER) and (b) generalized mutual information (GMI).

Two additional considerations are important when discussing performance metrics and codes. The first is that good channel models to estimate the statics of a received symbol given a transmitted one are lacking for transmission in the optical fiber. Instead, mapping schemes and codes are often designed under the assumption of a memory-less AWGN channel and deviations from ideal performance can therefore be expected. However, with uncompensated transmission around optimal launch power, the AWGN is in general a good model. Secondly, the purpose of the FEC is to ensure a residual BER below a given level, usually selected as 10^{-15}. The frequently applied low-density parity-check (LDPC) codes have an error floor, which usually is significantly above the target value and also not possible, to date, to predict from analytical estimates. To ensure that the target performance is met, the SD code is usually concatenated with an outer low-overhead HD-FEC. The combination of these two codes ensure target performance. Coding is a research field by itself and from the perspective of this thesis we therefore simply measure use the performance metrics and assume that the code can be implemented. For combinations of SD and HD codes, see [48, 107, 199].

3.7 Compensation of Fiber Nonlinearities

A chapter on DSP would not be complete without discussing and mentioning algorithms tailored to mitigate distortions induced by fiber nonlinearities. Multiple DSP-based methods have been proposed for mitigating penalties [201]. These include digital back propagation (DBP) [202], Volterra-based equalizers [203], digital pre-distortion [204] and the use of tailored modulation formats such as geometric shaping [63] and polarization balanced formats achieving a constant multi-dimensional energy [205]. Out of these, DBP and Volterra-based equalizers are probably the most studied receiver-side DSP techniques.

DBP propagates the signal backwards in DSP through a virtual fiber with opposite signs (dispersion, nonlinear coefficient and loss), typically using the Manakov equations (Eq. 2.30) [202]. DBP is typically performed as one of the first steps in the DSP chain and jointly compensates for both fiber nonlinearities and dispersion. It has been extensively studied but performance ultimately is limited because of stochastic effects in the fiber and interactions with noise together with nonlinear interference from neighboring channels [206]. In addition, DBP is very computationally intense and large research efforts have been devoted to invent simpler algorithms that are more suited for real-time implementation [207]. One such is time-domain DBP (TD-DBP) [208], which relies on time-domain dispersive filtering and simplified implementations of the nonlinear step in the split-step method [208, 209]. DBP accounting for PMD has also been investigated but result in large performance fluctuations arising from the stochastic nature of PMD [210]. As a concluding remark on DBP we note that while multi-channel DBP can be used to jointly back propagate a complete superchannel [211], the gain from adding more channels is limited [212]. Multi-channel DBP performed in the transmitter side have been shown to improve the performance of DBP-like schemes for systems using frequency combs (see Section 5) [213, 214].

Similar to DBP, Volterra equalizers are also hindered by large computational requirements and multi-channel interference. A Volterra equalizer can be seen as an extension of a general dynamic equalizer (see Section 3.3) to account for higher-order terms. Using Volterra series to model and invert the response of a nonlinear system and finding the inverse using such a model dates back long before the introduction of coherent systems [215] and more lately, simplified models describing the fiber has been developed [216]. Still, Volterra equalizers are very powerful and work on reducing the computational burden has nevertheless showed promising results with respect to DBP [216]. In addition, we note that Volterra-based equalizers can be used to compensate transmitter distortions, as further described in Section 3.5.2.

Finally we note that more exotic transmission schemes such as the nonlinear Fourier transform (NFT) [73, 217, 218] and the use of machine learning and the use of deep neural networks [219–221], to mention two, are emerging. Using machine learning to optimize TD-DBP also shows promising results to further improve low-complexity implementation [222].

3.8 Pilot-Based DSP

Finally, we emphasize that the purpose of this chapter is to outline the different key blocks used to built up a complete blind DSP-chain used to recover a data stream after transmission through the optical SMF channel. As hinted when introducing DA-LMS, an alternative to blind processing is to use knowledge of the transmitted information to performance DSP and improve its performance [164]. Pilot DSP is highly flexible, tolerant to large SNR variations and modulation format independent. This makes it very suitable for application in modern state-of-the-art systems [223, 224].

Similar to how there exist a number of different blind algorithms to perform each DSP task, there are pilot-based algorithms counterparts. Example of this includes pilot-based equalization [164, 182, 225–227] and carrier recovery [223, 228–232]. The key design concern is then the required overhead, which will degrade the system information rate and therefore has to be weighted against the performance increase enabled by pilot-based processing. Paper II is dedicated to the design and performance evaluation of pilot-based DSP for high SE transmission. It also contains a comparison with some of the standard algorithms outlined in this chapter and the reader is therefore refereed to Paper II for more information on pilot-based DSP. As a final remark, we note that recent industry products with state-of-the-art capabilities of 69 Gbaud PS-64QAM use one pilot symbol for every 33 transmitted, corresponding to an overhead of 3.1% [153].

Chapter 4

Optical Frequency Combs

This chapter introduces optical frequency combs and the unique properties that separate optical combs from other multi-wavelength light sources such as a laser arrays. Today, frequency combs are extensively researched in a number of areas. These includes spectroscopy [233–237], optical arbitrary waveform generation [238, 239], optical frequency synthesis [240], light detection and ranging (LIDAR) [241–243], microwave photonics [244, 245], astronomy [246] and all-optical signal processing [247, 248]. In addition, as given by the title of this thesis, combs have been studied for applications in optical communications, as further discussed in Chapter 5. In this chapter, frequency combs are introduced and different ways of generating a frequency comb are discussed.

4.1 General Description

An optical frequency comb is a coherent multi-wavelength light-source characterized by its center frequency f_0 and its line spacing Δf, as shown in Fig. 4.1. Following this, any comb lines/mode n is given by

$$f_n = f_0 + n\Delta f. \tag{4.1}$$

In this definition, n is an integer that can be both positive and negative, following the definition in Eq. 4.1 with the comb spectral envelope being centered on f_0. A frequency comb can be understood via Eq. 4.1 as the superposition of multiple phase-locked carrier waves. The amplitude of classical sine-waves with normalized frequency $\in$ [1,2,4,6] are shown in Fig. 4.2(a), with the waveforms vertically separated for illustration purpose. Important here is that all waves are locked together in phase. Figure 4.2(b) shows the superposition of the first 5 sine-waves plotted on top of each other and the summation of the first 5, 10, 20 and 50 waves is shown in

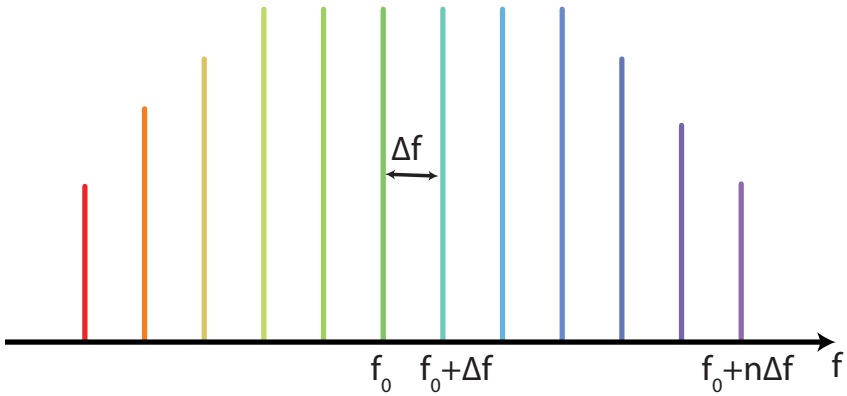

Fig. 4.1. Principle of an optical frequency comb. The comb can be fully characterized by its center frequency f_0 and its line spacing Δf.

Fig. 4.2(c). Here we observe that when more harmonics are combined, the resulting pulse width shrinks. Finally, as shown in Fig. 4.2(d), these pulses are periodic with a periodicity corresponding to the inverse of the separation frequency.

A frequency comb can mathematically be described as a train of pulses with envelope $A(t)$ and a carrier wave $C(t)$ The output electric field is then given by

$$E(t) = \mathrm{Re}\left[A(t)C(t)\right]. \tag{4.2}$$

The periodicity of the time-domain pulses is given by enforcing that $A(t) = A(t-T)$ with $T = 1/(\Delta f)$ denoting the pulse repetition time. The frequency domain representation of this is given by the Fourier transform of Eq. 4.2 according to

$$\tilde{E}(\omega) = \frac{1}{2\pi}\int_{-\infty}^{\infty} \tilde{A}(\omega')\tilde{C}(\omega-\omega')d\omega', \tag{4.3}$$

with $\tilde{E}$ denoting the frequency representation of the time domain field $E(t)$. The individual Fourier transforms of $C(t)$ and $A(t)$ are given by

$$\tilde{A}(\omega) = \sum_{n=-\infty}^{\infty} \delta(\omega - n2\pi\Delta f)\tilde{A}_n \tag{4.4}$$

$$\tilde{C}(\omega) = \int_{-\infty}^{\infty} C(t)\exp(j\omega t)dt, \tag{4.5}$$

with δ denoting Dirac pulses and $\tilde{A}_n$ the spectral shape of the pulse with mode

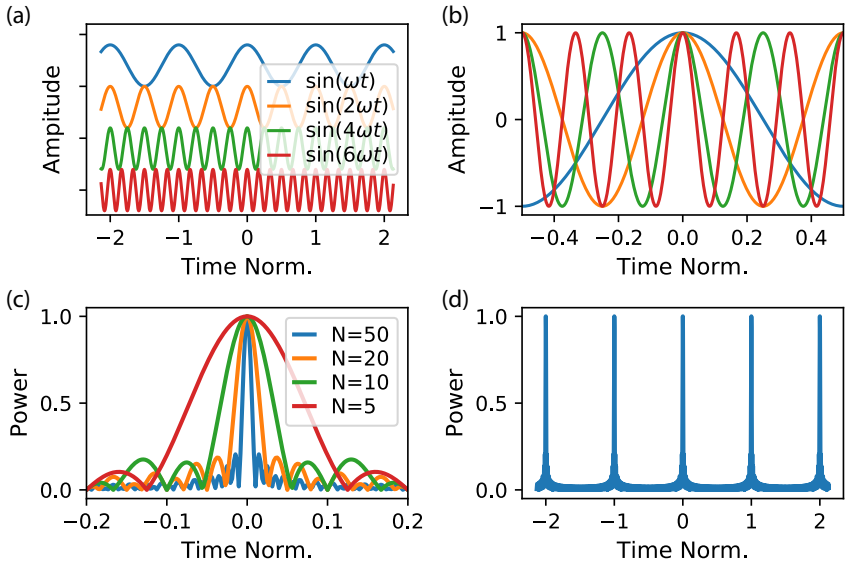

Fig. 4.2. Underlying principle of a frequency comb. (a) Spatially separated sinusoidal waves with harmonic [1,2,4,6]. (b) Zoom-in of the corresponding harmonics overlapped. (c) The resulting summation for N number of harmonics. (d) The resulting pulse-train for $N = 50$ harmonics. The pulse separation follows from $T = \frac{1}{\Delta f}$.

number n. Inserting this into Eq. 4.2 gives

$$\tilde{E}(\omega) = \frac{1}{2\pi} \sum_{n=-\infty}^{\infty} \tilde{A}_n \tilde{C}(\omega - n2\pi\Delta f). \tag{4.6}$$

The resulting sum from Eq. 4.6 corresponds to a periodic frequency spectrum. Conditioned on the fact that the spectral width of the carrier is much smaller than Δf, it represents regularly spaced, well separated spectral tones. A frequency comb can therefore be understood a frequency domain convolution of a carrier $\tilde{C}(\omega)$ with a frequency domain comb $\tilde{A}(\omega)$ with spacing given by the pulse repetition rate. While the description in Eq. 4.6 is very general, for the purpose of this thesis we restrict the carrier wave to being a monochromatic such that

$$C(t) = \exp(j(2\pi f_0 t + \phi)) \tag{4.7}$$

$$\tilde{C}(\omega) = 2\pi\delta(\omega - 2\pi f_0)\exp(j\phi), \tag{4.8}$$

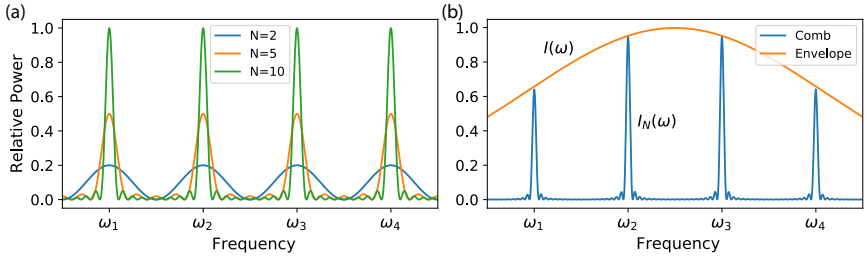

Fig. 4.3. Illustration of frequency comb formation and spectral line width. (a) Second term in Eq. 4.12 for N=[2,5,10] lines. (b) The resulting comb formed together with the envelope function for N=20.

with ϕ being an arbitrary phase offset. Combining this with Eq. 4.6, the convolution operator corresponds to shifting the frequency tones so that the spectral envelope is centered on f_0. The shape and width of the envelope will be dictated by the shape of the time-domain pulses, where the perfectly flat comb would correspond to having δ-like time-domain pulses. However, this case is only of interest for conceptual understanding as we note that such a frequency comb might be perfectly flat but it also spans an infinite bandwidth and have infinite pulse energy.

The phase difference between the different pulses will then be given by $\Delta\phi = \arg(C(t)) - \arg(C(t-T)) = 2\pi f_0 T$. The center frequency f_0 can also be expressed using Eq. 4.1, as $f_0 = m\Delta f + \nu_{\mathrm{CE}}$. The phase shift $\Delta\phi$ can then be expressed as

$$\Delta\phi = 2\pi(\nu_{\mathrm{CE}} + m\Delta f)T = \frac{2\pi\nu_{\mathrm{CE}}}{\Delta f} + 2\pi m. \tag{4.9}$$

From Eq. 4.9 it can be seen that the offset frequency ν_{CE}, also known as the carrier envelope offset, corresponds to taking the phase difference between consecutive pulses modulus 2π. Defining the phase shift as $0 \leq \Delta\phi \leq 2\pi$ then corresponds to locking the carrier envelope offset to $0 \leq \nu_{\mathrm{CE}} \leq \Delta f$. This result is essential to the previously mentioned success of frequency combs, as an optical frequency comb can be fully characterized using two RF-frequencies. In metrology, both degrees of freedom from the comb have to be controlled and referenced to create a frequency ruler. In applications where both these two parameters are controlled (or at least monitored), combs are therefore characterized using ν_{CE} and Δf. However, as no absolute carrier envelope offset stabilization is performed in this work, we use the definition given by Eq. 4.1 and characterize the combs using f_0 and Δf.

In practice, and especially for the focus of this thesis, a comb source does not consist of an infinite set of equidistant frequency tones. To gain insights to the limits of how the shape of both the comb envelope and the individual lines depend on the number of lines, we instead look at a the electric field $E_{\mathrm{F}}(t)$ from a finite

length temporal pulse train with shape $h(t)$ according to

$$E_{\mathrm{F}}(t) = \mathrm{Re}\left[\frac{E_0}{\sqrt{N}}\sum_{k=0}^{N-1} h(t-kT)\exp(jk\Delta\phi)\right]. \tag{4.10}$$

Assuming that $h(t)$ is sufficiently confined so the series in Eq. 4.10 converges, we can Fourier transform and solve Eq. 4.10 according to

$$\tilde{E_{\mathrm{F}}}(\omega) = \frac{E_0\tilde{H}(\omega)}{\sqrt{N}}\sum_{k=0}^{N-1}\exp(-jk(\omega T-\Delta\phi)) = \frac{E_0\tilde{H}(\omega)}{\sqrt{N}}\frac{1-\exp(-jN(\omega T-\Delta\phi))}{1-\exp(-j(\omega T-\Delta\phi))}, \tag{4.11}$$

with $\tilde{H}(\omega)$ denoting the frequency domain representation of $h(t)$. The spectral width and shape of N spectral modes can be calculated via the intensity spectrum of a a single spectral mode $\tilde{I}(\omega) = |\tilde{H}(\omega)|^2$. Calculating the intensity spectrum for N pulses from Eq. 4.11 gives

$$\tilde{I}_N(\omega) = \tilde{I}(\omega)\frac{1-\cos(N(\omega T-\Delta\phi))}{N(1-\cos(\omega T-\Delta\phi))} = \frac{\tilde{I}(\omega)}{N}\frac{\sin^2\left(\frac{N(\omega T-\Delta\phi)}{2}\right)}{\sin^2\left(\frac{(\omega T-\Delta\phi)}{2}\right)}, \tag{4.12}$$

showing that the spectral shape of each frequency tone $\tilde{I}_N(\omega)$ will depend both on the shape of the pulses $\tilde{I}(\omega)$ and on the number of pulses in the pulse train. This extra spectral broadening factor is shown in Fig. 4.3(a), showing that a long pulse train is essential to form a frequency comb with narrow comb lines. The comb envelope shape follow the envelope shape of the time-domain pulses $\tilde{I}(\omega)$, as shown in Fig. 4.3(b). From this, we make some concluding remarks. First, there is an analog between controlling the shape of the temporal pulses from a comb source and controlling its spectral envelope. Second, the limit on the temporal pulse width is given by the spectral width of the comb envelope, which is the effect of time-bandwidth limitations given by the Fourier relations. Note that in the limit when $N \to \infty$, the line shape converges to δ-functions and the whole comb turns into a set of equidistant spaced δ-shaped frequency peaks weighted by $\tilde{I}(\omega)$.

Finally, we note that Fourier limited spectral width of the comb lines presented here is only of practical relevance if a very short pulse train is being used. Beyond this, experimental constraints tend to imply limitations in spectral width rather than the fundamental Fourier relations. In practice, the linewidth of the combs used is more limited by the seed laser linewidth, corresponding to having a finite width of the carrier wave $\tilde{C}(\omega)$. This effect will imply a broadening of the spectral tones during the convolution given by Eq. 4.3.

4.2 Generation Techniques

While the previous description has shown the principle behind frequency combs, it does not explain how to generate them. There are many ways of generating

frequency combs and each technology has its own pros and cons. A detailed review of this is beyond the scope of this work but it is still worth mentioning different technologies. Mode-locked lasers [249] are probably the most classical combs. For a basic mode-locked laser, the frequency comb can directly be understood as the laser cavity supports multiple longitudinal modes and the frequency spacing is therefore dependent on the cavity roundtrip time. Mode-locked lasers based on Ti:Sapphire can have $\Delta f >$ GHz-repetition rate with very low noise [250]. Erbium-doped fiber lasers typically have repetition rates on the order of 100 MHz [251] but this can be extended using filters inside the cavity [252]. Recent advancements with the development of quantum dash mode-locked laser have enabled DC-driven combs [253]. As an alternative to classical mode-locked lasers, laser gain-switching can be used to generate combs with GHz-level frequency spacing [254]. Following advantages in surrounding fields such as the development of highly-nonlinear optical fibers to enabling broadening of the output from a mode-locked laser source, octave-spanning frequency combs became available [255]. This enabled the so called f-2f locking scheme to fully stabilize a comb source [256, 257], creating an optical ruler that would change optics forever. This major accomplishment has resulted in numerous awards, peaking in 2005, John L. Hall and Theodor W. Hänsch were awarded the Nobel prize in physics "for their contributions to the development of laser-based precision spectroscopy, including the optical frequency comb technique", highlighting the impact of comb technology as a scientific tool [255].

An alternative to mode-locked lasers is electro-optic (EO) frequency combs, formed by modulating an input CW laser (see Section 4.3). For EO combs, the center wavelength f_0 can easily be tuned by moving the input laser and the spacing is set by the input RF clock, making the comb source very flexible. Hybrid approaches between mode-locked lasers and EO combs can also be used to tune the line spacing [258]. Starting from lines selected from an EO comb, a parametric mixer exploiting the Kerr-effect (see Section 2.2.3) can be used to form very broad frequency combs [259]. The Kerr-effect inside a cavity can also be used to generate frequency combs starting from an input CW. These combs with micro cavities are further discussed in Section 4.5.

4.3 Electro-Optic Frequency Combs

With one exception, Paper III, EO frequency combs have been used throughout this thesis. EO combs are formed by sinusoidal phase-modulation of a CW carrier $C(t)$ according to [260]

$$\begin{aligned} E_{\mathrm{EO}}(t) &= \mathrm{Re}\left[C(t)\exp\left(j\sin\left(2\pi\Delta f t\frac{V}{V_\pi}\right)\right)\right] \\ &= \mathrm{Re}\left[C(t)\sum_{k=-\infty}^{\infty}J_k\left(\frac{V}{V_\pi}\right)\exp\left(j2\pi k\Delta f t\right)\right], \end{aligned} \tag{4.13}$$

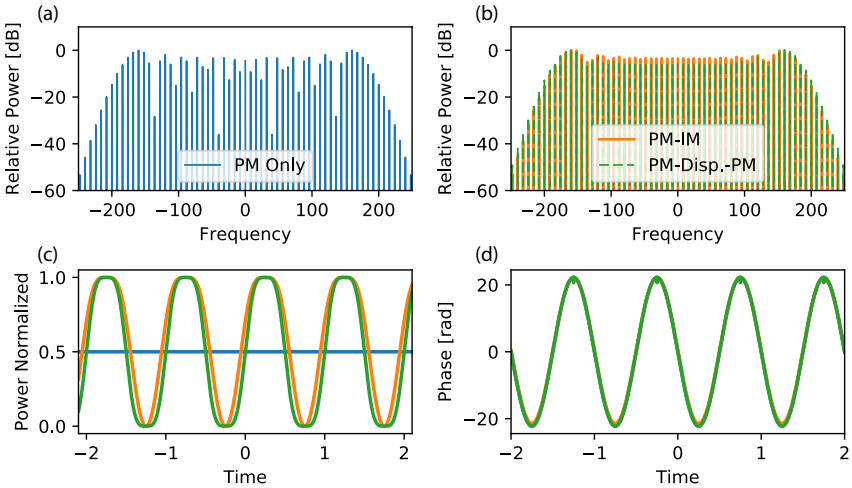

Fig. 4.4. Working principle for realizing a flatter EO comb. (a) EO comb generated using only a PM. (b) EO combs generated using a PM-IM cascade and a PM-Dispersion-PM cascade, both generating very similar output spectral shapes. (c) The resulting amplitude and (d) phase in time-domain for the three presented EO combs.

with V denoting the RF drive signal voltage swing, V_π the swing required for achieving a phase shift of π for the phase modulator and J_k denoting Bessel functions of the first kind [261]. For simplicity, we introduce the normalized driving signal $V_D = \left(\frac{V}{V_\pi}\right)$. From Eq. 4.13 we see that the output waveform is a superposition of weighted Bessel functions of degree k. As a result of this, the output comb is not spectrally flat and the magnitude of the various spectral modes can vary significantly, as showed in Fig. 4.4(a). We observe >35 dB line power variations for the simulated comb and using such a comb for optical communication would require extensive flattening causing significant OSNR degradation (see Section 5.2).

Multiple comb designs and techniques have been developed to overcome this drawback and generate flat EO combs [244]. These include, but is not limited to, using a phase modulator (PM) and an intensity modulator (IM) [262, 263], using a dual-drive MZM [264] and using two cascaded PMs with a dispersive element in between [265]. In addition, flatness can be improved by exploiting the nonlinearity of the IM in the PM-IM configuration [266], using more advanced driving signals containing harmonics of Δf [260] or by combining multiple techniques such as PMs, dispersive elements and an IM [267]. In addition, resonant modulators [268] and external cavities can be used [269, 270].

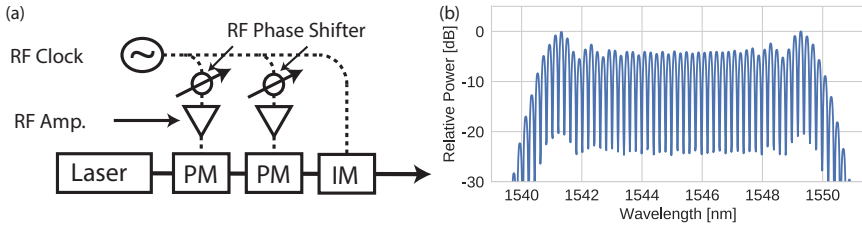

Fig. 4.5. (a) EO comb generation setup consisting of two phase modulators and an intensity modulators. The phase modulator cascade increase the effective modulation depth and the intensity modulator is used to flatten the output spectrum. (b) Resulting measured comb spectrum (0.1 nm resolution).

One of the most used and flexible implementation is to use the PM-IM cascade, as shown in Fig. 4.5(a). The setup shown here has two phase-modulators and is the setup that has been used in most papers of this thesis. However, the use of multiple PMs is just a practical way of extending the number of lines as the available RF power from amplifiers and the practical V_π limits the amount of achievable overdrive in Eq. 4.13. The solution is then to cascade multiple modulators and align the phase between them using phase shifters [271], as shown in Fig. 4.5(a). If the IM is properly biased, so that it carves out pulses when the chirp induced by the PM is almost linear, a much flatter comb is generated [244]. This comb is characterized a famous shape with two "rabbit ears", on each side of a very flat central part. The resulting measured spectrum for such an EO comb is shown in Fig. 4.5(b). A slightly flatter comb can be generated by driving the IM harder and offsetting the bias point [266].

One drawback of the comb design from Fig. 4.5(a) is the loss increase by using the IM. Aside from modulator insertion loss, about 50% of the energy is lost in the pulse carving process. Realizing a theoretically loss-less comb instead requires limiting the operations to only use phase modulation and dispersive all-pass filtering, as discussed in Section 2.1.4. One way of overcoming this is to replace the IM with a dispersive element followed by an additional PM [265]. The comb generator then consists of a cascade built up of a PM, a dispersive element and another PM. The swing of the first modulator is set to $V_{D_1} = \pi/4$ and it is, just as in the case of the design presented in Fig. 4.5(a) driven by a sinusoidal signal with frequency Δf. The output signal is then fed to a dispersive medium with group velocity dispersion ($\beta_2 z$ from Eq. 2.16) given by [265]

$$\beta_2 z = \pm \frac{1}{4\pi \Delta f^2}. \tag{4.14}$$

Following the dispersive medium, the V_{D_2} second PM dictates the number of lines generated and this driving signal should, in contrast to V_{D_1} be larger than V_π.

Worth mentioning here is that the order of the system is not relevant and V_{D_1} and V_{D_2} can hence be interchanged. The resulting comb is shown in Fig. 4.4(b) together with an EO comb flattened using an intensity modulator. Maybe surprisingly, it also has the same shape as the comb produced using the IM shown in Fig. 4.5. This similarity is furthermore confirmed by looking at the corresponding amplitude and phase of the time-domain pulses, as shown in Figs. 4.4(c) and (d), respectively. We observe that in contrast to the case of only using PM (or cascaded PMs), which of course does not produce intensity modulation, both the other presented designs seems to generate a signal with an amplitude modulation looking like flat-top pulses. So how can the comb flatness be explained?

The temporal flat-top pulses generated via the IM can be directly understood from Eq. 2.9, considering an IM based on a MZM in push-pull operation. Driven by the sinusoidal with angular frequency $2\pi\Delta f$, the power will be proportional to the magnitude of the transfer function given by

$$\begin{aligned} P(t) &\propto \left|\cos\left(\sin(2\pi\Delta f t)\frac{V}{V_\pi}+\frac{r_{\text{bias}}}{2}\right)\right|^2 = 1+\cos^2\left(\sin(2\pi\Delta f t)\frac{V}{V_\pi}+\frac{r_{\text{bias}}}{2}\right) \\ &= 1+\cos^2\left(\frac{\pi}{2}\sin(2\pi\Delta f t)\right), \end{aligned} \tag{4.15}$$

where we used the bias tuning in the last step and assume a phase modulator driving signal of $\pi/4$. The importance and presence of the same flat-top pulses was presented in [265]. The reason behind this effect and the formation of combs with this specific shape, using two at first quite different approaches, can be explained via the concept of time lenses [272]. Time lenses are the time-domain equivalent of thin lenses and their relationship follows from the beautiful fact that temporal pulse propagation in waveguides with narrow-band dispersion and propagation of beams in free-space with diffraction are governed by mathematically equivalent equations [273]. This have resulted in a number of impressive demonstrations using concepts such as temporal imaging [274–279]. As the space-time analogy and time lenses are the base for Paper I, we simply conclude here that a time-lens is capable of implementing a temporal Fourier transform. The transform can also be implemented in a simplified version [280]. The output waveform spectrum therefore has the shape of the input temporal pulses. As previously derived, the shape of the comb envelope follows the spectral shape of the temporal pulses and the resulting comb spectral therefore have the flat-top shape. The similarity therefore originates from matching the dispersion following the first PM so that the resulting temporal pulses have the same shape as the pulses carved out by the IM in the PM-IM comb generator. The reason for the formation of the "rabbit ears" is the deviation between an ideal quadratic temporal phase modulation and the modulation realized by a phase modulator. To improve the flatness, this deviation has to be minimized. Examples of this includes either trying to shape the RF signal to compensate this distortion, or reduce the temporal duration of the flat-top pulses prior to the time lens. Finally we note that

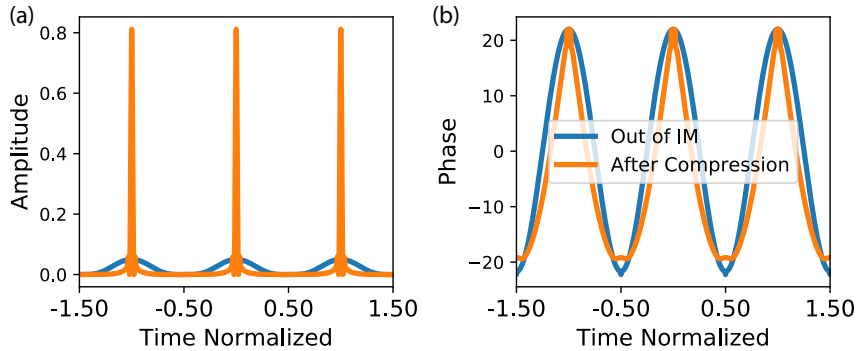

Fig. 4.6. Principle of pulse compression using dispersion. The input EO comb is generated using a PM-IM cascade and shown in Fig. 4.4(b). (a) Amplitude and (b) phase of the time domain pulse train directly out of the comb and after compression using quadratic dispersion.

flat-top pulses can have a very broad application area in all-optical signal processing, performing functionality such as gating and pulse selection [281].

Another very exciting possibility enabled by the space-time analog is the ability to scale the bandwidth and multiply the repetition rate of the comb [282]. In the case of generating a flat comb, the time lens is synchronized and acts on every pulse. In this case, the comb bandwidth can be scaled by increasing the chirping rate of the time lens [272]. However, by tuning the period of the phase modulation from the time lens with respect to the pulse repetition rate, the frequency repetition rate can be scaled similar to dispersive propagation of pulse trains [283]. The new comb spacing is then inversely proportional to the pulse repetition rate out of the time lens as described by the so called temporal self-imaging effect which is also called the (fractional) temporal Talbot effect [284–286]. In a similar fashion, an equivalent to the spatial 4-f system [287] can be designed in time domain [288, 289]. This can be used to build a temporal telescopes, which can scale the temporal duration of pulses [275].

As a final remark on the formation of pulses here, we note that the output of an EO comb is not necessarily the transform-limited pulses previously discussed. Rather than that, dispersive broadening is typically present and dispersion compensation is then necessary to retrieve the pulse train. This is shown in Fig. 4.6 for a simulated EO comb using the PM-IM cascade design. While the output temporal shape is significantly broadened, adding the proper amount of dispersion restores the pulse-train. While this aspect is not of any significant importance for communications, applications such as comb-based LIDAR [241, 242] and spectroscopy [235, 290] can require compressed pulses.

4.4 Electro-Optic Combs with Arbitrary Shapes

As previously discussed, the resulting spectral envelope can be explained using the temporal pulse shape and a time lens. This was presented in [272] as a generalization of the results presented in [265]. One might then ask if this can this be extended (generalized) again to make it possible to generate combs with more arbitrary shapes using the same underlying principle. Of course, an arbitrarily shaped comb can be generated using an IM driven by an arbitrary signal to carve out temporal pulses with the target shape. However, such approaches are limited by the electronics and we here focus on generation using temporal reshaping rather than pulse carving with the aim of generating an arbitrarily shaped comb using a theoretically loss-less scheme.

The answer to this question is provided by the arbitrary temporal transformations introduced in Paper I. Once again, this is all about being able to generate trains of pulses with general shapes. While previously not feasible using pure sinusoidal driving signals, this is possible using the multi-stage reshaping approach introduced in Paper I. Phrased differently, rather than just having the functionality of a time lens, we expand this with the functionality of shaping the pulses into the desired temporal/spectral shape. This provides the most general approach to generating EO combs, overcoming the limitations induced by previous techniques. Compared to the approach using a driving signal composed of multiple harmonics presented in [260], the driving signal is not restricted to being harmonics of the comb line spacing. The reader is referred to Paper I for details on the approach and the computations performed in order to find the phase modulations required to generate a target output pulse shape. In addition, as developing new schemes for generating combs is beyond the scope of this thesis, the following examples are only meant as a first proof-of-principle and to illustrate the true generality of the findings from Paper I.

Using the principle from Paper I, we now consider a comb temporal reshaping comb generator seeded by a CW laser. However, in contrast to the previously used PM-IM cascade, the generator now consists of 11 stages with phase modulation and dispersive all-pass filtering. To illustrate the power of this technique, we simulate two different envelope shapes of the output combs, as shown in Fig. 4.7. Both examples considers generating a comb with 13 lines. The first is an improved flat-top envelope and designed to have a perfectly square envelope in the frequency domain. The temporal intensity of the found pulses together with the resulting spectral shape is shown in Fig. 4.7(a) and (b), respectively. We observe a very good agreement between the simulated output and the design target. The second examples takes inspiration from the famous sech^2-envelope characteristic for microcombs having a soliton propagating in the cavity. However, it is done with a twist of restricting the number of lines to 13 something that naturally cannot be done using a microring resonator. The temporal intensity of the found pulses together with the resulting spectral shape as well as the sech^2-envelope are shown in Figs. 4.7(c) and (d),

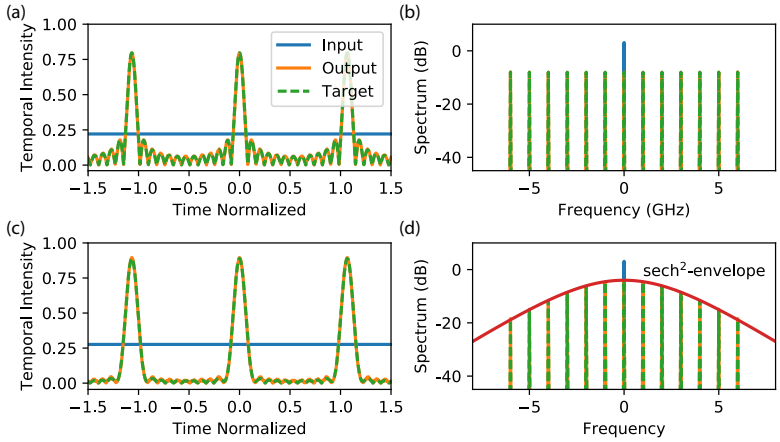

Fig. 4.7. Numerical demonstration of generating EO combs with arbitrary shapes using unitary temporal transformations following the scheme presented in Paper I. For reference, a perfectly square comb and a comb following the famous sech envelope shape (same as Soliton microcombs) but designed to only have 13 lines in total. These designs are not even theoretically possible to realize using neither a traditional EO comb driven by sinusoidal inputs nor a soliton microcomb. (a) Temporal intensity of input and output used to form the comb with a square-shaped envelope. The transformation is implemented using 11 stages. (b) Corresponding spectrum of input CW, output generated comb and the design target. (c) Temporal intensity of input and output used to form the sech-shaped envelope comb restricted to 13 lines. (d) Corresponding spectrum of input CW, output generated comb, the design target and the sech-envelope.

respectively. Similar to the case of a square target shape, we observe a very good agreement between the simulated output and the design target. Finally, we emphasize that neither the number of stages nor the optimization parameters have been thoroughly optimized in Fig. 4.7 and the reader is therefore encouraged not to focus on the numbers but rather on the beauty behind the concept.

Interesting insights can be gained by comparing the results from Fig. 4.7 with the results presented in Paper I. In generating a comb, the focus is to generate a periodic pulse train, something very different from the focus of Paper I, which was to demonstrate encoding of random patterns. In both cases, restrictions were placed to ensure bandwidth-limited phase modulations something that otherwise tend to result in non-implementable solutions using the wavefront-matching algorithm and the maximum allowed swing of each phase modulator is set to V_π. Interestingly

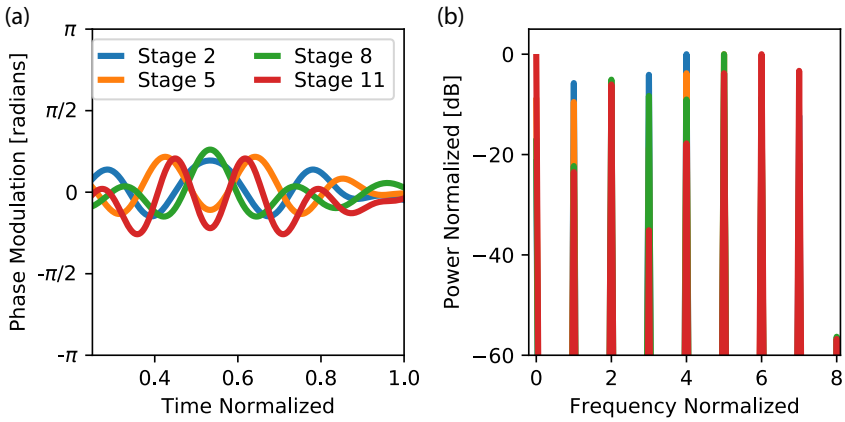

Fig. 4.8. Analysis of phase modulations for the square comb generated using temporal unitary transformations. (a) The applied phase modulations for segment 2,5,8 and 11. (b) The corresponding spectra verifying that the applied phase modulations only consist of harmonics of the fundamental frequency.

enough, while of course the performance depends on any bandwidth restrictions put on the phase modulations, important insights to the problem can be gained by studying these. Figure 4.8(a) shows selected applied modulations for the case of restricting the phase modulations to the total comb bandwidth. The modulations are smooth and looks like typical superposition patterns arising when adding sinusoidal waves together, something which is confirmed by the spectral content shown in Figure 4.8(b). In fact, the found driving signal is consists of weighted harmonics of the comb repetition frequency. This result is perfectly in line with previous approaches on using driving signals consisting of a fundamental frequency Δf and its harmonics to generate a flat frequency comb [260].

As a final note on this we emphasize that interesting combinations between classical EO comb generation and general temporal transformations can be studied. Starting with pulses, such as flat-top pulses from classical EO comb generators, a few segments can be used to tune the envelope to a given target shape. In fact, the possibilities are almost endless and only fantasy limits the number of waveforms that can be generated by combining frequency combs and the newly presented temporal transformations.

4.5 Chip-scale Frequency Combs

As photonics is in general experiencing the era of blooming integration, bringing both benefits and challenges, tremendous research efforts have been devoted to developing chip-scale frequency combs. Similar to the key motivation behind scaling down electronics and transceiver components, micro-scale operation can enable vastly reduced energy consumption and, of course, much smaller device foot-print, to mention two examples. Examples of chip-scale comb sources includes quantum-dash mode-locked lasers [253], integrated EO combs [267, 291, 292] and combs using the nonlinear Kerr effect in micro ring cavities. Kerr combs can have different shapes including so called modulation-instability combs (MI-combs) [293] (with a triangular shape), soliton comb [294] (with a characteristic envelope shape matching a quadratic hyperbolic secant) and so called dark-pulse combs [295].

Soliton microcombs are particularly interesting and represents a novel comb source enabled by nanofabrication. The possibility to realize these frequency combs using microresonators have enabled a compact comb source [294, 296–300]. Using soliton-based microcombs have several advantages as soliton formation enables predictable and reproducible spectral envelopes and stable mode locking [294, 301]. These soliton microcombs have recently enabled major breakthroughs in miniaturizing various comb applications. This includes, but is not limited to, optical frequency synthesis (programmable frequency generator at optical frequencies) [240], ranging using comb-based light detection and ranging (LIDAR) [302, 303], dual-comb spectroscopy [304, 305] and imaging [306, 307], astronomy [308, 309] and building ultra-accurate optical clocks [310]. Importantly for a broad adaptation is power efficiency and the compact form-factor of micro-combs enable low operational power [311–313].

Microcombs have also been used in optical communications, providing a compact multi-wavelength light source for WDM (see Section 5.1). Demonstrations includes the use of combs with line spacing being a multiple of the free spectral range in short-reach [293] and long-haul [314], Soliton combs for short-reach C+L-band transmission [315] and high SE transmission Paper III and dark-pulse combs [316]. There are pros and cons with each of the three technologies and further research is required to understand how these translate to system-level benefits and limitations. These aspects are discussed in more detail in Section 5.2.

Chapter 5

Frequency Combs in Fiber-Optic Communication

This chapter expands single channel systems and focus on high throughput transmission using multichannel multiplexing. The focus is on multiplexing in the wavelength domain, exploiting the broad bandwidth of the SMF and EDFA combination. Following this, we introduce superchannels and compare multiplexing in the spatial and spectral domain. The role of frequency combs and comb-based superchannels in high throughput systems is then explained and different approaches to exploit the unique properties of frequency combs underlying Paper III-VIII are discussed.

5.1 Wavelength-Division Multiplexing

The concept of WDM was introduced in Chapter 1 and it is one of the key enablers behind the multi-Tb/s throughput achieved in today's SMF-based optical transmission systems [62, 97]. The massive scaling in throughput enabled by WDM can be directly understood considering the capacity of the AWGN channel, as previously introduced in Chapter 2, Eq. 2.13. This is plotted together with the GMI of standard square QAM formats in Fig. 5.1(a). As a target channel SE of 5 bits/s/Hz requires a SNR of about 15 dB assuming an ideal constellation (which can be achieved using for example constellation shaping as discussed in Section 2.1.1) and about 17 dB SNR assuming the use of 64QAM or 256QAM. However, to double the channel throughput, the SE also has to be doubled. Targeting 10 bits/s/Hz SE, about 30 dB SNR is needed even with an ideal constellation. Achieving this increase in SNR

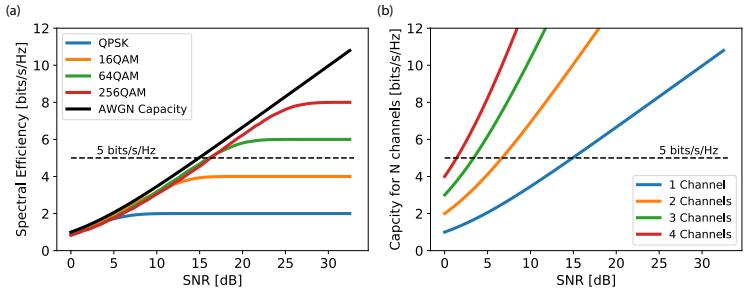

Fig. 5.1. Comparison between scaling the throughput by increasing the SE or increasing the bandwidth. (a) SE versus SNR for standard modulation formats. (b) Channel capacity versus SNR for a N channel system.

would require >20 times more transmitted power. Even if this was feasible, the optical channel can only be approximated with the AWGN channel in the case of a weak nonlinear distortion and at such power levels; severe nonlinear distortions would invalidate the assumption of an AWGN channel.

Nevertheless, if excess bandwidth is available two parallel channels with equal SNR could be used, the throughput could be doubled without requiring an increase in SE. Each channel maintains an SE of 5 bits/s/Hz and only 3 dB more transmitted power is needed, as shown in Fig 5.1(b). This critical distinction originates from the difference between the logarithmic increase in capacity from an increase in SNR compared to the linear scaling from increased bandwidth. This is the key reason behind the use of two orthogonal polarizations in coherent transmission, as this effectively allows for scaling the channel bandwidth by a factor of two using an orthogonal dimension. In this case, it is not wavelength but rather an orthogonal spatial mode and throughout this thesis, we consider a single channel system operating over the 4D signal space spanned by the amplitude and phase on two orthogonal polarizations. Beyond polarization, the bandwidth of a C-band EDFA is about 4 THz and combining C+L-band EDFAs, a total transmission bandwidth of about 10 THz can be realized. This is far beyond the bandwidth of even state-of-the-art electronics, reaching about 100 GHz [64–66, 317]. By combining multiple independent wavelength multiplexed channels to occupy the full EDFA bandwidth, the throughput can be scaled N times. However, the analysis here is for an AWGN channel and nonlinear effects are neglected. Better estimates for broadband transmission can be achieved using the GN-model presented in Section 2.2.4.

Following this, the principle for a WDM system is shown in Fig. 5.2. From a transceiver perspective, each channel is fully independent, transmitting and receiving its own bit stream. However, the channels share the amplifiers and

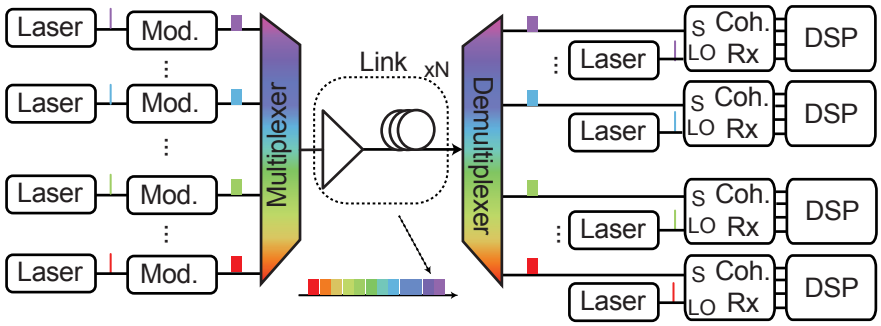

Fig. 5.2. Principle of a standard WDM system. Each channel consists of an optical transceiver, operated independently from all other co-propagating channels.

the optical fiber to reduce both cost and energy consumption. We note that the assumption of independent channels is not perfectly true as nonlinear effects will couple information between channels present in the fiber. This is important for multi-channel nonlinearity compensation, as discussed in Section 3.7.

5.1.1 Superchannels

Superchannels is an important part of the work in this thesis. Superchannels aim to increase the optical network transport throughput [318]. Traditional WDM networks used a fixed ITU-grid with each channel allocated to a separate wavelength slot. These systems are simple and can use fixed components such as WDM couplers to MUX and DEMUX channels. However, their SE is poor as channel BW cannot be tailored [25]. By using WSSs, which can enable flexible filtering and selection of channels, networks can move away from a fixed grid to support flexible bandwidth allocation, so called flex-grid networks [319, 320]. This enables more flexibility and can be used to minimize excessive guard-bands and unused spectrum. This can in theory increase network efficiency with up to 33% but practically cascaded filtering penalties from network ROADMs [321] limits the gain, which can even be negative [322].

One solution to this is to form a flex-grid network using spectral superchannels. A superchannel is a set of tightly spaced WDM channels treated as a unit [323]. As such, narrow-band channel selection filters between every channel is avoided, drastically reducing the overall filtering penalty and increasing performance [97]. Superchannels also provide a path to realize multi-Tb/s throughput, something that is normally not feasible following bandwidth limitations of the electronic, electro-optic and opto-electronic components. As such, state-of-the-art transceivers are

limited to about 1 Tb/s [87]. However, for a superchannel, the total bandwidth is the combined bandwidth of all channels and the bandwidth can therefore be much larger. Superchannels are commercially available [318] and with the progress in integrated photonics, multiple transceivers can be integrated on a single chip [85, 87, 324].

While superchannels are very powerful, their modulation and detection is more cumbersome than traditional WDM channels. First, the guard-bands considered are so tiny that traditional arrayed waveguide gratings (AWGs) cannot be used to directly multiplex the channels. Combining using multi-port WSSs also posses problems in terms of limited resolution unless a splitting loss is accepted. Channel combining using passive splitters will add a 1/N loss, which grows rapidly as the superchannel incorporates more and more channels. Favorable trade-offs can be made using two AWGs and a passive 3 dB splitter to reduce the total combining loss while still maintain compatibility with very dense channel spacing. Similarly, at the receiver side, channels cannot easily be individually selected. This problem is the opposite of the transmitter-side channel combination issue and a similar approach with a combination of a 3 dB splitter and two AWGs can be used. While this makes the design more cumbersome, the fact that all channels are treated as a unit and routed together can enable new superchannel-DSP [323, 325], as further discussed in Section 5.3.3.

5.1.2 Space Division Multiplexing

From the discussion of using multiple channels for scaling the capacity linearly and increasing the network efficiency using superchannels, it is natural to seek other dimensions for additional parallelization. In SMFs, all four degrees of freedom available are used and the only way to increase the system throughput linearly is to scale the bandwidth further. One such approach is to, in addition to the C+L-band, use the S-band for communication. This is beyond the reach of EDFAs but broad-band SOAs can realize simultaneous amplification over 100 nm [326, 327]. However, even extreme bandwidth scaling such as moving into X-ray wavelengths, would only result in about 10 times more capacity compared to standard C-band transmission unless prohibitively large powers are used [328]. Worth mentioning here is the possibility to use hollow-core fibers, avoiding the issue with nonlinearity and supporting significantly larger bandwidth with theoretically lower loss [329–331].

The only way forward then is to go to ”space”. Space in this regards referrers to using multiple spatially separated paths, such as multiple parallel transmission fibers [96], a multi-core fiber (MCF) [332], a multi-mode fiber (MMF) [333] or combinations of any of these technologies. Without going into details, we make a rough separation between spatially separated transmission, such as a fiber bundle or a MCF, and spatially coupled transmission such as MMF and coupled-core MCF (CC-MCF) [334]. Uncoupled transmission does not require any additional signal processing compared to SMF and can therefore be viewed as a simple extension to

add more dimensions. In this case, MCF offer higher density but at the expense of some cross-talk compared to a fiber bundle [335–337]. Important here is that for submarine cables, which are power limited, SDM can be used to increase the throughput by allocating power over more spatial paths [338, 339]. We also note that the large increase in available dimensions can be used to create SDM-ROADMs, enabling significantly more paths to improve network efficiency [97, 340].

In the case of coupled systems it is naturally to talk about spatial superchannels [97]. Space can also be combined with wavelength to form spectral-spatial superchannels. The key difference here is that MIMO signal processing is needed to separate the different spatial paths at the receiver, following coupling in the fiber [341]. MIMO is typically implemented using DSP [161, 342–344] but can also be implemented using optical filters [345]. From the capacity argument, MMF offers the highest available density of spatial paths but is also one of the most challenging to exploit as large mode-dependent loss (MDL) and differential mode-group delay (DMGD) tends to result in non-unitary channel impulse responses with long time memory, which are challenging to process in DSP [343, 346, 347].

SDM has nevertheless been the key enabler for today's Pb/s throughput records over a single fiber (defined as sharing the same cladding) by either using many cores [348–350] or combining MCF with each core supporting multiple spatial modes [99, 351]. Using a MMF supporting 45 spatial modes [333], an SE >200 bits/s/Hz for a single core was demonstrated using 90×90 MIMO processing [101]. Such links could also be designed using optical DMGD compensation to reduce the length of the impulse response [352]. The CC-MCF hybrid provides a way of reducing penalties from fiber nonlinearities [353] and the strong coupling reduce the impulse response duration [334]. This can enable an increase in launch power, realizing larger throughput compared to a system using high-performance ULA SMF (same design as one of the cores in the 7-core CC-MCF) [103].

Finally, we note that while the transmission schemes used for SDM so far are very similar to the ones used for SMF, SDM requires new components that support multiple spatial paths and successful development of such components is essential to realize an SDM system. One key component is the SDM amplifier, which has the potential to enable energy savings via sharing of resources [97]. SDM EDFAs have been developed for various SDM systems including EDFAs for MCF [354–357], CC-MCF [358, 359], MMF [360–362] and hybrids such as MCF with MMF cores [363]. In addition, when using MCF or CC-MCF, fan in/out devices are needed. Many designs exist including fiber tapering [364], stacking of fibers inside a tailor-made capillary [365], free-space coupling [366] and 2D/3D waveguides [367] fabricated using techniques such as laser inscription or multi-layer stacking [368]. In analog with this, mode multiplexers are needed to excite the different orthogonal spatial modes in MMF transmission. Techniques for doing this include free-space multiplexing using fixed phase-plates [161] and liquid crystal on silicon (LCOS) displays [369], spot-based mode excitation [370], photonic lanterns (PLs) [371] and multi-plane light propagation (MPLC) [372]. An important aspect here is that in

communication, mode-selectivity is typically not needed as the MIMO DSP will sort out the different channels [373]. However, this also results in the highest DSP complexity. Attempts to reduce this using partial MIMO processing [374] or simply mode-group division multiplexing [375] have been investigated but these demand mode selectivity in the MUX/DEMUX. LCOS-based systems are re-programmable, mode selective and highly flexible, enabling flexible change of modal basis and characterization of the complete transfer matrix even for fibers supporting hundreds of modes [376, 377]. However, just as phase-plate-based multiplexing, this technique suffers from beam-splitter loss when adding every mode, limiting the number of modes that can be simultaneously used. PLs are default non-mode-selective but adiabatic and theoretically loss-less [371]. In practice, the insertion loss is about 0.6 dB [378] and devices have been scaled to support up to 15 modes [379], although theoretical investigations reveal that even more modes should be possible [380, 381]. In addition, PLs can be made mode selective [382]. The most promising technique to scale to significantly higher mode counts available today is MPLC. Today, prototypes supporting 210 spatial modes [383] have been developed. In addition, packaged devices supporting 45 modes are commercially available [384]. To support SDM networks, extending WSSs to SDM is needed. While a multi-core solution is trivial in this regard, realizing switches for MMF fiber transmission is more challenging. Designing MMF-compatible WSSs is not straight forward and they are a frequent source of additional MDL. Approaches include using demux the modes into N Gaussian beams at the switch input [385, 386] and designing a WSS for a MMF input array [387, 388]. Finally, we note that while the components presented here are only a subset of everything needed for a true SDM network, demonstrations combining various SDM technologies in a joint network have been performed [389].

5.2 Comb-Based Transmission Systems

Studying the WDM system shown in Fig. 5.2, one can intuitively understand how frequency combs can play a role in future WDM systems. If the large number of independent lasers needed could be replaced with a single multi-wavelength light source, one can envision significant energy savings [315]. The principle of an optical communication system using frequency combs is shown in Fig. 5.3. Replacing a laser array with a single comb has long been investigated in optical communications even before the year of 2000 [390]. Numerous follow-up demonstrations using direct detection have been performed including the use supercontinum combs source to realize parallel transmission of more than 1000 wavelength channels [391, 392]. Direct direction using EO combs have also been investigated [393, 394] and WDM transmission covering the S-,C- and L-band was demonstrated in [262].

Following the shift towards coherent transmission, various comb technologies have been investigated. These include the use of combs based on the Kerr effect

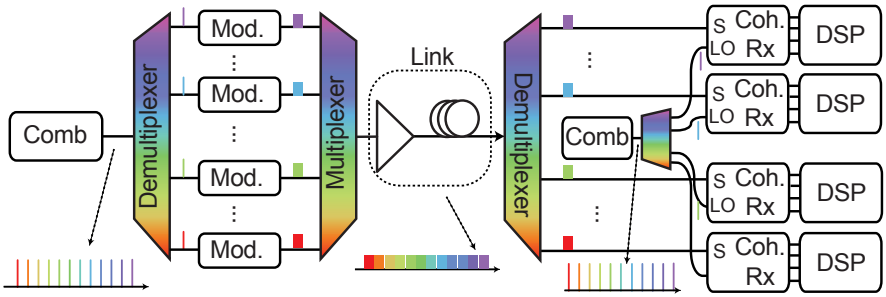

Fig. 5.3. Illustration of a comb-based WDM system. All channels originates from a common comb-source and the receiver LO lines are generated from a receiver combs. Modulation and receiver processing is typically done independent for each wavelength channel.

in micro-ring resonators (MRR) [315], mode-locked lasers [395], EO combs [393] and parametric mixers [396]. Several recent demonstrations have shown promising results for integrated multi-wavelength sources using MRR-generated combs. These include the first demonstration of transmission using a low-noise MRR-based comb at distances reaching 300 km [397], dense WDM transmission using two interleaved combs and the use of MRR-based combs both in the transmitter and receiver [315], communication over trance-oceanic distances [314] and compatibility with higher-order modulation formats by demonstrating transmission with PM-64QAM [316]. Mode-locked lasers have long been considered for use in optical communication [247, 395, 398] and recent advantages using external cavities demonstrated compatibility with PM-32QAM, overcoming classical linewidth issues using mode-locked lasers [399]. Dense WDM transmission using EO combs was investigated in [394]. They are also the basis of the parametric combs in [396], in which an EO comb is used to generate an initial comb from which two (or a few) lines are selected and sent through a parametric mixer to create ultra-flat combs exceeding 100 nm BW [259, 396]. The minimum carrier OSNR of such parametric combs can exceed 45 dB with minimum line power exceeding 5 dBm [400], enabling a record demonstration of 2.15 Pb/s throughput over a 22-core fiber [349]. The high OSNR has also enabled transmission of PM-256QAM [401].

However, while a comb with Δf matching the used grid could be used to light up all transceivers in a point-to-point link, such configuration have limited flexibility in a network with optical routing. If we instead focus on flexible networks using superchannels, a very promising use-case for combs in coherent transmission arises. This is the comb-based superchannel, one of the main focus of this thesis. With the introduction of comb-based superchannels, the unique properties of frequency combs can then be exploited to enable new signal-processing functionalities, as further

discussed in Section 5.3. However, there are also challenges with introducing combs.

The first one is the limited line power inherent in a multi wavelength source. This can be directly observed by comparing the transmitter in Fig. 5.2 and 5.3 In the case of a laser array, each laser is directly connected to the modulator and the required input power P_{Mod} is therefore only dependent on the modulator insertion loss IL_{Mod} (including limited drive and modulation loss), the MUX loss from forming the superchannel, which can be added as extra modulator insertion loss, and the required output OSNR, OSNR_{Req} (see Section 2.4). However, in the case of a comb, it depends on the number of lines sharing the power N, as well as the flatness of the frequency comb $P_{\text{Line Diff.}}$, in addition to the modulator performance. For large number of lines, additional amplification is usually needed prior to demuxing the lines, further limiting the OSNR due to amplifier noise NF_{EDFA}. This difference can be summarized according to

$$P_{\text{Mod}} = \text{OSNR}_{\text{Req}} + \text{IL}_{\text{Mod}} - 58\,\text{dBm}, \tag{5.1}$$

$$P_{\text{Comb}} = \text{OSNR}_{\text{Req}} + 10 \cdot \log_{10}(N) + \text{IL}_{\text{Comb}} + \tag{5.2}$$

$$P_{\text{Line Diff.}} + \text{NF}_{\text{EDFA}} + \text{IL}_{\text{Mod}} - 58\,\text{dBm}. \tag{5.3}$$

This makes comb-based transmitters sensitive to OSNR limitations, which can easily induce penalties, especially for higher order modulation formats [402, 403]. In addition, phase-noise scaling with the line number is typically present for frequency combs [404]. The phase noise of the n:th mode from a frequency comb can be expressed as [405]

$$\theta_n(t) = \Delta\phi(t) + 2\pi n \Delta T(t) \Delta f, \tag{5.4}$$

with $\Delta\phi(t)$ now being time variant to account for phase fluctuations (compare with Eq.4.10) and $\Delta T(t)$ denoting time-varying timing jitter, both causing a linewidth broadening. While techniques to control the timing jitter are developed and essential for metrology [406], it is often overlooked in communications. The exact line shape will depend on an interplay between the frequency content of both the phase noise and timing jitter (a convolution in the frequency domain) [405] and in-depth discussions of this are beyond the scope of this work. Instead, we note that phase-locked properties of the carriers results in a joint phase-noise evolution, which can be completely characterized if the phase evolution of any two carriers are known. Denoting the known carriers m,n the phase evolution of carrier k can be expressed as [407]

$$\theta_k(t) = \theta_n(t) + \frac{k-n}{m-n}\left(\theta_m(t) - \theta_n(t)\right), \tag{5.5}$$

clearly showing the phase-noise scaling inherent from the intrinsic phase locking. However, we do note that the exact spectral shape of the lines and how it scales with line number will depend on the kind of comb source used [404, 405, 408, 409]. As a result of this, measuring the frequency noise rather than simply estimating the width of the beating between two lines and performing a Lorentzian fit is

essential to accurately estimate the phase noise and judge its implications for coherent communications [404, 410]. While the scaling is a challenge, the phase-locked nature can also be used to jointly compensate phase noise to increase DSP performance [407].

5.3 Exploiting Unique Comb Properties in Coherent Optical Communications

The combined research efforts have been successful in validating the possibility of using frequency combs as WDM sources in optical communications. Depending on the target application, various comb technologies (mentioned in Section 5.2) have proved to meet the demands, potentially replacing the use of independent free-running lasers in WDM applications. Simply replacing free-running lasers has the potential of enabling energy savings [315, 316] but such arguments depend a lot on the feasibility of integrated comb together with necessary co-packaging to realize future on-chip superchannel transceivers.

However, in the scope of this thesis, we assume that we have access to a comb-based superchannel transmitter and receiver pair, both utilizing a frequency comb. We then aim at providing insights to answering the question of "What unique features can a comb-based superchannel enable, which cannot be enabled using alternative technologies?". This question is, of course, very complicated to answer and there are numerous different areas to target. One example of pioneering work on this was done in [213] where the authors demonstrated two-folded reach-increase by using transmitter-side digital pre-compensation of fiber nonlinearities. This compensation was enabled by exploiting the property of frequency locked carriers from an optical comb and the benefit of the scheme would be lower if implemented with free-running lasers [214].

In the following sections we will go through the different experiments and techniques developed throughout this thesis to exploit the unique frequency comb properties.

5.3.1 Exploiting the Intrinsic Line Stability

As previously discussed, the first application of combs is as a replacement for a laser array in a WDM/superchannel system. However, there are noticeable differences in doing so as lasers from an array will drift in an uncorrelated way, in contrast with the lines from a frequency comb that are frequency locked. For a laser array, guard-bands of a few GHz are needed to avoid catastrophic channel overlaps. These can make up 10% of the available spectrum for symbol rates of about 30 Gbaud and external frequency locking is therefore needed to maximize SE [174].

If we instead use a frequency comb, the guard-bands can be further reduced and optimized to balance cross-talk and overhead in order to maximize the SE.

Such optimization was performed in Paper III (see supplementary information). When using the comb, a guard-band of about 600 MHz was needed, drastically reducing the associated overhead. It is important to note here and hard to evaluate in laboratory experiments, that the guard-bands are needed to ensure long-term stability. To realize the high SE in Paper III, the microcomb was tailored to a line spacing of 22.1 GHz, matching well the EO comb spacing of 25 GHz used in Papers II, IV-VIII. This, in combination with the flat comb envelope enabled taking the full advantage of the comb bandwidth for realizing a superchannel with SE and transmission quality for the first time being compatible with that performance of traditional comb sources.

5.3.2 Locking Combs using Optical Pilot tones

In the early days of coherent optical communication, self-homodyne (SH) detection was proposed as a way of overcoming the laser phase noise and to avoid the need for complex DSP-based carrier recovery (as described in Section 3.4.2) [411]. Instead of using a free-running laser as LO, a copy of the transmitter laser is send as a pilot tone (PT) and used as LO. This avoids the need for FOE and, in the ideal case, completely removes any laser phase noise. Conventionally, the orthogonal polarization is used for PT transmission implying a 50% loss in SE. In addition, the PT is subjected to noise and nonlinear impairments from propagation (see Section 2.2.3). SNR dependence of PT filtering was investigated in [412] and capabilities for SH systems to cancel out nonlinear signal distortions was demonstrated in [413]. Despite the clear advantages of reduced DSP complexity, the loss in SE hindered SH systems and to combat this, interleaved PT transmission was proposed, reducing the overhead to 33% [414]. Generally to minimize OH it is desired to share PTs amongst as many channels as possible.

On way to achieve this is to extend SH detection to SDM transmission systems. The many spatial dimensions available allows for effectively sharing of a pilot tone by using the high correlation among separate cores within a multi-core fiber [415]. This was demonstrated in [416] where the authors used a 19 core fiber with one core dedicated for PT transmission. The capabilities of the scheme were later used in a high throughput experiment demonstrating 210 Tb/s throughput using high-linewidth laser by combining the SH detection with WDM [417]. Cross-talk dependence and correlations within multi-core fiber were investigated more in-depth in [337].

Frequency Comb Regeneration

While exploiting the high correlation of spatial dimensions using SDM fiber allowed for SH detection with low overhead, the number of WDM channel still exceeds the number of available SDM channels [416], even in record experiments combining both multi-mode and multi-core transmission [99]. Moreover, as the number of

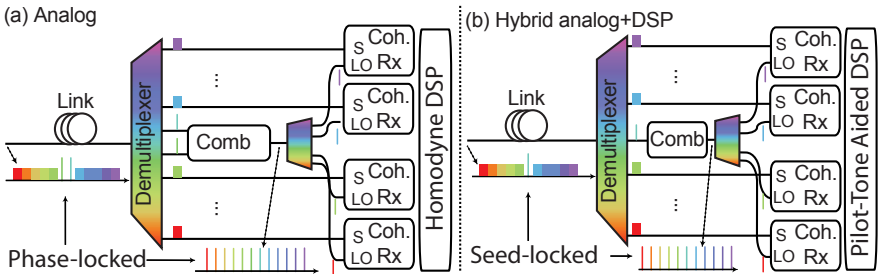

Fig. 5.4. Comparing comb regeneration using one and two pilot tones. (a) Two pilot tones are used to lock both f_0 and Δf between the transmitter comb, providing a fully SH system which eliminates the requirement of DSP-based carrier recovery. (b) A single pilot tone is used to lock f_0 while Δf is left without synchronization. However, the comb stability is order of magnitude better than the stability of the seed lasers (assuming standard lasers) and the residual offsets can easily be tracked using DSP.

wavelength channels is very high in fully loaded systems, the complexity is still high if using one PT per wavelength channel. As briefly outlined in Section 5.2, frequency combs are highly correlated among channels in the spectral domain. Comb-based superchannels can therefore be treated in similar ways to spatial superchannels. This implies that gains and sharing can be exploited also in SMF technology, making comb-based superchannels compatible with existing infrastructure.

The idea of exploiting this coherence was first proposed in [247] where the authors proposed locking a transmitter and receiver comb using two unmodulated PTs. The requirement of using two tones can be understood by considering the definitions of combs presented in Chapter 4. One PT is sufficient to directly extract the center frequency f_0 and the beating between two neighboring tones gives the spacing Δf. The first system study of properties for a comb-based SH system was in [418]. The experiment was done in back-to-back configuration and the authors only considered recovering the central tone of the frequency comb, or equivalently, locking f_0 of the two frequency combs. As only one tone was used, the same RF-clock reference Δf was used in both the transmitter and receiver to enable full phase coherence. This issue was solved in [419] which studied the use of two PTs, enabling recovery of both f_0 and Δf, creating a fully SH system. The effects of dispersive walk-off between the PTs (similar to skews in the case of multi-core fiber) were highlighted and experimentally verified [419]. Using Brillouin amplification to provide narrow optical filtering and avoid excessive phase noise on the regenerated comb, we demonstrated the first transmission experiment using frequency comb regeneration for self-homodyne detection [420]. The superchannel consisted of 24×20 Gbaud PM-32QAM channels.

To suppress penalties from the line-width scaling with comb line number reported in [420], Paper IV demonstrated regeneration using a receiver EO frequency comb. While the Brillouin amplifiers in [420] provided a filtering BW around 20 MHz, Paper IV introduced the use of an electrical phase-locked loop (PLL) that enabled orders of magnitude more narrower filtering. The comb regeneration can therefore be performed with higher quality. This enabled both a doubling of the number of regenerated lines and an increase in modulation format from PM-32QAM to PM-64QAM, resulting in a combined superchannel throughput of 10 Tb/s with a spectral overhead of 4% for self-homodyne detection.

However, in the case of EO combs or other stable platforms such as soliton microcombs, carrier offsets caused by non-ideal synchronization of f_0 and Δf result in very different impairments. Not locking the central carrier f_0 simply creates an intradyne system, similar to the ones described in Section 2, requiring DSP-based carrier recovery as outlined in Section 3.4. If f_0 is locked but not Δf, the requirements for DSP-based carrier recovery are dictated by the clock (comb) stability instead of the comb seed lasers. While impairments from not knowing Δf also will result in additional frequency offset and phase noise, RF-clocks are orders of magnitude more stable compared to standard free-running lasers.

The effective gain from going from intradyne to a single PT is therefore much larger than that of going from one to two PTs, both in terms of DSP complexity and performance. A single PT used to lock f_0 removes the need for FOE and, depending on laser quality and path-matching, suppresses phase noise. At the same time, a single pilot tone is robust to nonlinear distortions and avoids the additional complexity of using phase-locked loops to lock the frequency spacing. The single tone scheme was first proposed in Paper V. Here the tone was assisted by a slow blind DSP-based phase tracker to compensate the residual carrier offsets, something that was not feasible without the PT. The inherent resilience to both dispersive delays and nonlinear distortions compared to the 2 PT scheme was further investigated in Paper VI, demonstrating high SE transmission over distances reaching 1000 km using a single shared PT.

However, to further increase the spectral efficiency beyond what was reached in Paper V, new DSP was needed. Although the PT made carrier recovery possible, which also helped improve the DD-LMS-based equalization, the equalizer performance was still not good enough to enable reliable transmission of PM-256QAM. As a result, a hybrid analog PT+ DSP pilots was developed in Paper VII. Here the PT provided a frequency locking in line with Paper V but each channel further had DSP pilots for equalization and residual phase tracking. The joint OH was optimized to maximize the SE, enabling the 12 bits/s/Hz SE over the C-band.

5.3.3 Comb-based Superchannels with Joint DSP

Following the results in Paper II and VII, the power of pilot-based DSP became evident and further work was focused on improving its performance and develop

a complete pilot-based DSP chain aiming at high SE transmission using higher-order modulation formats. Following this work, it is natural to ask "How can this DSP be extended to exploit the unique properties of a frequency comb?". The aim of Paper VIII is to provide insights to this question by designing a tailored multi-channel DSP exploiting the comb properties. In the DSP designed here, we make a key distinction compared to previous work. Previously, the phase coherence of combs were exploited to perform joint CPE [223, 407, 421]. The superchannel adaptations using master-slave or joint processing presented in [407, 422] are completely analogous to the scheme presented in [420] and Paper IV. As a result, it also suffer from similar issues with dispersive delays [419]. In addition, we note from Paper II that the OH associated with CPE is about 0.4%, even for formats reaching up to 256QAM.

In contrast, the DSP presented in Paper VIII only requires frequency locked, rather than strictly phase-locked light sources. As a result, we here allow for each channel to have its own independent CPE and acknowledge that the OH or performance can be improved depending on reach and presence of nonlinear effects. A practical implication of significant importance following this assumption is that no path-matching is needed in the system, simplifying both experimental evaluation and, more importantly, system implementation. We note that while superchannel DSPs have previously been investigated [110, 325, 423, 424], no transmission system with such DSP has been demonstrated. While experimental work in B2B configuration has shown promising results [325], this was done using independent lasers in a homodyne configuration. In addition, we note that most of these schemes focused on NRZ-shaped pulses, naturally implying significantly more crosstalk and loss in SE compared to Nyquist-shaped transmission.

The work presented in Paper VIII aimed at overcoming these limitations and implement a superchannel transmitter-receiver system using frequency combs with multi-channel detection. We use the high-performance pilot-based DSP developed in Paper II both as base for the DSP development and as a reference source providing state-of-the-art performance. The key block of the DSP developed in Paper VIII is a multi-channel equalizer capable of mitigating inter-channel-interference (ICI). This scheme relies on an aliasing approach to avoid additional oversampling, as further presented in Paper VIII. Beyond the joint equalization block, joint FOE is a necessary to maintain the frequency locked grid. All in all, this enables increasing the SNR by about 1 dB compared to state-of-the-art single channel performance, which considering how close systems like this are to theoretical limits, is to be considered surprisingly much. Furthermore, while the gain of course can be higher for systems that are severely limited by cross-talk, as investigated in [110, 325, 424], the presented performance gain here is at the optimal channel spacing. Finally we note that the scheme in Paper VIII can directly be extended to improve the performance of DSP-based nonlinear mitigation schemes using multi-channel processing, similar to [206, 211].

Chapter 6

Future Outlook

There are numerous interesting follow-up projects relating to the work presented in this thesis. Since aiming for presenting a complete list is out of the scope, the purpose of this chapter is to briefly discuss a few key research opportunities that are particularly related to the work presented in Paper I-VIII.

Dense Comb-Based Transmitter Using a Single Modulator The results presented in Paper I demonstrates the first scheme capable of modulating independent data onto wavelength-separated carriers without the use of a MUX-DEMUX combination. This proof-of-principle demonstrations provides new, essential, insights to the basics of modulating superchannels. However, more experimental work and prototyping is needed to understand the applicability of this for broader superchannels with higher-order modulation formats. Especially important here is to investigate the performance of a straight-line modulator configuration, rather than the recirculating loop.

In addition, it would be interesting to understand the theoretical bounds on temporal modulation using the proposed structure by analyzing the amount of uncertainty put into the system via the cascaded phase modulators. Understanding this would help put realistic bounds on the number of channels and formats that can be used with a realistic number of stages.

Lossless Unitary Transformations for Quantum Optics Another key aspect of the work presented in Paper I is the ability to, at least in theory, perform lossless temporal modulation. This has been a goal for applications in quantum optics for a long time. However, the kind of transforms investigated there are different that the ones corresponding to modulate a random data signal investigated in Paper I. Using fewer stages and integrated designs, it should be possible to drastically reduce the losses of the system to go far beyond that of conventional

modulators, something that would allow new applications and scientific studies in this area.

Pilot- and DSP-free Locking of Transmitter and Receiver Combs
The single pilot scheme presented in Paper V was introduced as a hybrid between full locking and individual DSP. Relating to this, it is interesting to think of approaches to achieve locking of f_0 without the use of optical pilots. One way to do this would be to use multi-channel DSP to feedback the difference and try to adjust the center frequency of the receiver comb to the transmitter comb. The challenge of this scheme would be to accurately extract the parameters from the DSP in line with the challenges faced in Paper V, it is clear that an pilot-based approach based on Paper II and VIII would likely be needed to achieve sufficient performance to match an optical locking. Still, this should be possible but requires extracting knowledge from the DSP and feedback it to the combs, thus requiring multi-channel DSP.

However, there is an even nicer way of solving this problem, which can be seen by looking at the alternative definition of a comb using its carrier envelope offset and line spacing. Locking of f_0, as was done using the optical pilot in paper IV-VII, could also be achieved without any kind of synchronization between the two combs by instead having two self-referenced combs. In this case, the center frequency of both combs are absolutely referenced to 0 frequency. This would clearly be the most beautiful locking scheme to achieve synchronization between the two combs. In addition, as the most difficult part to control usually is the carrier envelope offset, the line spacing could also be locked and a homodyne system is achieved (neglecting phase noise induced from fiber nonlinearities and similar effects).

There are also challenges with such designs, especially as self-referencing requires an octave-spanning frequency comb and having many lines separated by $\Delta f \approx 25 - 50\,\mathrm{GHz}$ would imply having a poor starting OSNR and this would degrade the full system performance. Luckily, there are ways around this too. If we instead use a master comb having broad line spacing, say 500 GHz to THz, significantly fewer lines are needed. In addition, this larger line spacing is more favorable for microcombs, making the scheme perfectly compatible with having two master microcombs. A system like this is illustrated in Fig. 6.1.

To achieve high spectral efficiency, the spacing is then filled out with additional EO combs that form the comb-based superchannels. The aspect of having an EO-comb here also solves another problem as controlling Δf is not trivial for combs with very large line spacing. Using an EO comb, the line spacing can be downconverted and extract locked to an harmonic of the EO comb, which is great for our application. The output of each EO comb is then modulated using a multiwavelength modulator, such as the one presented in Paper I to avoid additional splitting and combining losses and allow for minimal guardband transmission. At the receiver side, a second master comb - EO comb is used to generate the local oscillator lines. The channels are demultiplexed and joint processing, similar to the one in Paper VIII is used to minimize any penalties from the minimal guardbands.

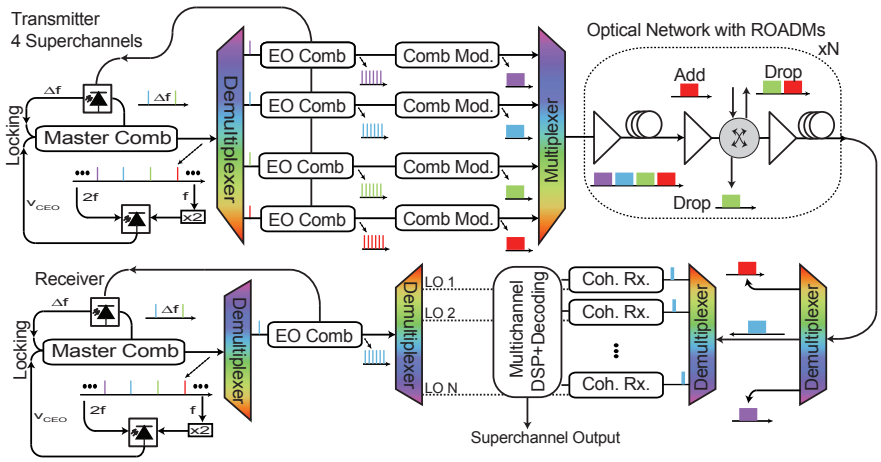

Fig. 6.1. Illustration of a future comb-based transmission system having a locked frequency grid without the use of any pilots. Both the transmitter and receiver use frequency combs that are referenced to zero.

The scheme proposed here has several advantages compared to today's schemes. Without going into detail, we just mention a few key examples. First, the gain of this scheme is equivalent to that using optical pilot tones without any required overhead. So the DSP complexity reduction facilitated by the pilots is available at no cost in terms of SE. In addition, each node will have a locked frequency comb, which is a very accurate clock, so timing synchronization can be much more accurate compared to using lower distributed RF signals or GPS locking. This clock could also be used to synchronize other clocks in the local area. Clock synchronization is essential for multiple other systems, such as wireless communication, and having a comb-based optical backbone network could help to improve the accuracy. Finally, we note that considering the development of hollowcore fiber it is not unrealistic that future fibers will have a significant broader bandwidth compared to today's system. While it will be challenging to have light sources that are continuously tunable from conventional bands all the way up to 2µm, having a broad-band comb source would directly solve this problem.

Nonlinearity Compensation for Superchannels The ability to mitigate nonlinear distortion is something that would be of indisputable importance to future optical networks. This task is very hard for a number of reasons outlined in this thesis. However, superchannels and frequency combs can likely at least improve the performance of these mitigation schemes. Key demonstrations in this area, where

gains have been shown, relied on multichannel processing and channel stitching, either on the transmitter or receiver side. Based on the DSP methods presented in Paper VIII, this is a topic of high relevance that could further be investigated and in most case, very little adaptation is needed. The equalizer used in Paper VIII could directly be replaced with say a 4×4 real-valued equalizer per channel to form a 12×4 MIMO problem. Such an equalizer will have more flexibility to track nonlinear polarization and phase noise.

Superchannels with Non-Uniform Performance A key point of superchannels that is yet to be exploited is the ability to jointly optimize the performance. In the next step of joint superchannel DSP, processing steps can be shared among multiple channels to optimize for maximum performance. Similar to the previously mentioned expansion of Paper VIII to include nonlinearity compensation, a more holistic view to joint processing would most likely be very interesting. Estimate of system and fiber parameters could then be improved. Another thing one could think of here is to modulate and use FEC that connects the multiple dimensions. Such approaches would definitely help gaining tolerance to filtering impairments from ROADMs by improving the performance of the edge channels. For broader superchannels, this could also help with balancing performance if the allocated slot is towards the edges of the EDFA gain bandwidth, where the performance is worse.

Spectral-Spatial Superchannels As this work focused on spectral superchannels, the clear next step is to go to space and combine the results with SDM. In this space, there are key differences, which enable very interesting studies. In the spectral superchannels considered here, the signal space is very homogeneous and the performance of the channels are therefore similar. While this is favorable, it is hard to find clear gains in terms of working with the joint signal space compared to that of individual channels. As presented in Paper II, the pilot overhead can be very low on a per-channel basis and even if it is possible to further reduce this using joint processing, the gains will be marginal.

However, in the spatial domain, the performance for difference channels can differ significantly. Especially in multimode transmission, when the modes couple, this poses several interesting problem relating to signal processing as the basic assumption of unitary rotations and low mode-dependent loss traditionally used when designing DSP are no longer true. In terms of superchannel, joint processing (using pilot or blind algorithms) can likely significantly improve the DSP performance. This can further be combined with joint modulation and coding to globally optimize the performance over the bigger, non-uniform signal space. Based on this, it is likely that the area of large gains from joint processing is in these massive superchannels.

In addition, it would be very interesting to study this from a networking perspective and considering switching and routing of superchannels. After all, the key gain behind superchannels are found in a networking environment and studies should therefore also consider these aspects. Relating to this, accurate

development of model and detailed characterization of SDM systems will be needed to properly understand the pros and cons of jointly distributing the information in spectra-spatial superchannels.

Superchannels for Free-space Communications In line with the potential for spectral-spatial superchannels in fibers, it is interesting to investigate how such systems would behave in a different channel. One such example would be free-space communications, which differs significantly from the traditional fiber channel. The presence of turbulence introduce mode coupling. The variations in this channel are different in nature from those of its fiber counterpart and few experiments have been aiming at developing transmission schemes tailored for this environment. Superchannels for this channel are interesting and optimal designs likely differ from the ones suitable for fiber transmission. Especially in terms of joint DSP, combining both information and pilots over multiple spectrally separated channels might be a way to increase tolerance to the fading nature of the channel.

Chapter 7

Summary of Papers

Paper I

Multi-wavelength arbitrary waveform generation through spectro-temporal unitary transformations
Under Review, 2019.

This paper presents a novel approach to realizing the most general temporal transformations available. Using multiple cascaded stages of phase modulation and dispersive all-pass filtering, the energy is temporally redistributed into the target shape. Each segment can be seen as a generalized time lens, allowing for arbitrary transformations and is in principle loss-less. This allows for realizing a theoretically loss-less IQ-modulator, something previously not feasible. In addition, we demonstrate that modulation using the proposed structure enable encoding of independent waveforms onto spectrally separated input laser lines. This feat, previously viewed as impossible, provides new essential insights to multi-wavelength modulation and broadband arbitrary waveform generation.

My contribution: I and N. K. F. developed the concept of multi-wavelength information processing using temporal unitary transformations. I built the experimental setup with assistance from N. K. F, R. R. and H. C. I processed the measurement data. I and J. S. wrote the paper with assistance from N. K. F.

Paper II

Overhead-optimization of pilot-based digital signal processing for flexible high spectral efficiency transmission
Optics Express, Vol. 27, no. 17, pp. 24654–24669, 2019.

This paper presents and evaluates a fully pilot-based DSP tailored for high spectral efficiency transmission systems using advanced higher-order modulation formats. A complete DSP chain is presented and the individual pilot-based algorithms are discussed and compared to traditional blind algorithms using numerical simulations. Overhead optimization is then performed for a 50×24 Gbaud PM-64QAM superchannel for transmission distances up to about 1000 km. The optimal B2B overhead was found to be 2.4% with only a weak dependence on distance, resulting in the same optima being optimal for all investigated distances. This highlights the power and flexibility enabled by pilot-based DSP.

My contribution: I, designed and wrote the DSP following input from T. Y and A. L-R. I, following discussions with J. S. designed and built the experimental setup. I performed all the measurement and analyzed the data. I wrote the paper with assistance from J. S. and A. L-R

Paper III

High spectral efficiency coherent superchannel transmission with soliton microcombs
Under Review, 2019.

This papers demonstrates the first microcomb-based transmission system capable of reaching comparable performance to bulk-optic combs. Using an optimized soliton microcomb with 22.1 GHz spacing allowed for reducing guardbands with more than one order of magnitude compared to previous soliton microcomb transmission experiments. This enabled significantly improved spectral efficiency by exploiting both better DAC/ADC performance and reduced guardband overhead. We report the first microcomb-based transmission experiment achieving >10 bits/s/Hz spectral efficiency and the first high spectral efficiency long-haul transmission experiments using a microcomb.

My contribution: I designed and built the transmission system. I assisted A. F. with with designing the long-term stabilization. I performed all the transmission measurements and processed the measurement data. I and M.-G. S. wrote the paper with assistance from A. F., J. S., P. A. A. and K. J. V.

Paper IV

10 Tb/s Self-Homodyne PM-64QAM Superchannel Transmission with 4% Spectral Overhead
Journal of Lightwave Technology, Vol. 36, no. 16, pp. 3176-3184, 2018.

This paper demonstrates self-homodyne detection of a comb-based superchannel using frequency comb regeneration. The regeneration is enabled by transmitting two unmodulated tones which are used in the receiver to regenerate the transmitter comb. The regeneration is implemented using a novel electrical phase-locked loop which enables narrow-band filtering and avoids additional penalty from linewidth scaling. The concept is demonstrated using a 50×20 Gbaud PM-64QAM superchannel with a total throughput of 10 Tb/s. The comb-based regeneration enabled record-low spectral overhead of 4% for self-homodyne detection.

My contribution: I developed the idea of electrical regeneration and, together with A. L-R., built the measurement setup. I wrote the DSP and processed the measurement data. I wrote the paper.

Paper V

High Spectral Efficiency PM-128QAM Comb-Based Superchannel Transmission Enabled by a Single Shared Optical Pilot Tone
Journal of Lightwave Technology, Vol. 36, no. 6, pp. 1318 - 1325, 2018

This paper demonstrates the use of a single pilot tone to enable the use of blind DSP in superchannels using advanced modulation formats. The single-pilot scheme is shown to facilitate the use of blind DSP while adding minimum spectral overhead. The combination enabled 10.3 bits/s/Hz spectral efficiency for a 54×24 Gbaud PM-128QAM superchannel.

My contribution: I, together with A. L-R. and J. S., developed the idea of the single-pilot scheme and built the measurement setup. I and J. S. wrote the DSP. I did all the measurements and processed the measurement data. I wrote the paper.

Paper VI

Experimental Investigation of Link Impairments in Pilot Tone Aided Superchannel Transmission
IEEE Photonics Technology Letters, Vol. 31, no. 6, pp. 459-462, 2019.

This paper investigates the proposed single-pilot scheme for transmission distances reaching up to 1000 km. The paper investigates both stability requirements for the transmitter and the receiver comb as well as the sensitivity to distortions on the pilot tone from transmission. The results presented verifies that the single pilot-tone scheme is tolerant to transmission-induced impairments and that DSP complexity reduction can be exploited also for longer distances. The total superchannel spectral efficiency was 9.6 bits/s/Hz (8.4 bits/s/Hz) after 480 (960) km of transmission, respectively.

My contribution: I, together with all co-authors, decided on the the scope of the paper. I built the measurement setup, wrote the DSP and performed all measurements. I wrote the paper.

Paper VII

12 bits/s/Hz Spectral Efficiency Over the C-band Based on Comb-Based Superchannels
Journal of Lightwave Technology, Vol. 37, no. 2, pp. 411 - 417, 2019.

This paper exploits the low overhead of the single pilot-tone scheme and combines it with pilot-DSP-based equalization and residual phase-noise tracking to enable detection of PM-256QAM with minimal overhead. Combining three comb-based superchannel covering the full C-band, a record high spectral efficiency of 11.5 bits/s/Hz for is demonstrated, corresponding to 12 bits/s/Hz in achievable information rate.

My contribution: I, with assistance from J. S. built the measurement setup. I wrote the DSP with input from T. Y. I performed all the measurement and analyzed the data. I wrote the paper with assistance from J. S. and A. L-R

Paper VIII

Joint Superchannel Digital Signal Processing for Ultimate Bandwidth Utilization
Manuscript Submitted, 2019.

This paper presents a joint DSP scheme for comb-based superchannel transceivers. The core of the presented DSP is a joint inter-channel-interference cancellation scheme aiming at mitigating linear cross-talk enabled by exploiting the unique line stability from optical frequency combs. Good agreement is found between numerical simulations accounting for limited transceiver performance and the experimental measurements, showing feasible gains of up to 0.8 dB in signal to noise ratio. The practical gain can be even higher when reducing the symbol rate, following the combination of better transceiver electronics and higher guardband overhead. Single span transmission also verifies that the scheme can cope with the additional distortions induced by fiber transmission.

My contribution: I conceived the concept and the design of the aliasing-assisted equalization scheme. I wrote the complete DSP and performed all numerical simulations. I designed and built the experiment and analyzed all measurement data. I wrote the main part of the manuscript with assistance from J. S., M. K. and P. A. A.

References

[1] A. Jones, *Historical Sketch of the Electric Telegraph: Including Its Rise and Progress in the United States*. GP Putnam, 1852.

[2] A. G. Bell, *Improvement in telegraphy*, US Patent 174,465, 1876.

[3] A. G. Bell and T. S., *Photo phone-transmitter*, US Patent 235,496, 1876.

[4] G. P. Agrawal, *Fiber-optic communication systems*. John Wiley & Sons, 2012, vol. 222.

[5] A. L. Schawlow and C. H. Townes, "Infrared and optical masers", *Physical Review*, vol. 112, no. 6, pp. 1940–1949, 1958.

[6] H. Rowe, "Frequency or phase modulation with a noise carrier", *Proceedings of the IEEE*, vol. 52, no. 4, pp. 396–408, 1964.

[7] K. C. Kao and G. A. Hockham, "Dielectric-fibre surface waveguides for optical frequencies", *Proceedings of the Institution of Electrical Engineers*, vol. 113, no. 7, pp. 1151–1158, 1966.

[8] ——, "Dielectric-fibre surface waveguides for optical frequencies", *IEE Proceedings J - Optoelectronics*, vol. 133, no. 3, pp. 191–198, 1986.

[9] A. Beck, "An experimental gas lens optical transmission line (correspondence)", *IEEE Transactions on Microwave Theory and Techniques*, vol. 15, no. 7, pp. 433–434, 1967.

[10] D. Gloge, "Experiments with an underground lens waveguide", *Bell System Technical Journal*, vol. 46, no. 4, pp. 721–735, 1967.

[11] D. Gloge and W. H. Steier, "Pulse shuttling in a half-mile optical lens guide", *Bell System Technical Journal*, vol. 47, no. 5, pp. 767–782, 1968.

[12] K. C. Kao and T. W. Davies, "Spectrophotometric studies of ultra low loss optical glasses i: Single beam method", *Journal of Physics E: Scientific Instruments*, vol. 1, no. 11, pp. 1063–1068, 1968.

[13] K. KAO, T. Davies, and R. Worthington, "Coherent light scattering measurements on single and cladded optical glass fibres", *Radio and Electronic Engineer*, vol. 39, no. 2, pp. 105–111, 1970.

[14] D. Keck, R. Maurer, and P. Schultz, "On the ultimate lower limit of attenuation in glass optical waveguides", *Applied Physics Letters*, vol. 22, no. 7, pp. 307–309, 1973.

[15] R. Maurer, "Glass fibers for optical communications", *Proceedings of the IEEE*, vol. 61, no. 4, pp. 452–462, 1973.

[16] M.-J. Li and D. A. Nolan, "Optical transmission fiber design evolution", *Journal of Lightwave Technology*, vol. 26, no. 9, pp. 1079–1092, 2008.

[17] R. Mears, L. Reekie, I. Jauncey, and D. Payne, "Low-noise erbium-doped fibre amplifier operating at 1.54μm", *Electronics Letters*, vol. 23, no. 19, pp. 1026–1028, 1987.

[18] E. Desurvire, J. R. Simpson, and P. C. Becker, "High-gain erbium-doped traveling-wave fiber amplifier", *Optics Letters*, vol. 12, no. 11, pp. 888–890, 1987.

[19] K. Suzuki, Y. Kimura, and M. Nakazawa, "Pumping wavelength dependence on gain factor of a 0.98 μm pumped Er3+ fiber amplifier", *Applied Physics Letters*, vol. 55, no. 25, pp. 2573–2575, 1989.

[20] R. Laming and D. Payne, "Noise characteristics of erbium-doped fiber amplifier pumped at 980 nm", *IEEE Photonics Technology Letters*, vol. 2, no. 6, pp. 418–421, 1990.

[21] A. Larsson, J. Cody, and R. J. Lang, "Strained-layer InGaAs/GaAs/AlGaAs single quantum well lasers with high internal quantum efficiency", *Applied Physics Letters*, vol. 55, no. 22, pp. 2268–2270, 1989.

[22] A. Larsson, S. Forouhar, J. Cody, R. Lang, and P. Andrekson, "A 980 nm pseudomorphic single quantum well laser for pumping erbium-doped optical fiber amplifiers", *IEEE Photonics Technology Letters*, vol. 2, no. 8, pp. 540–542, 1990.

[23] N. Olsson, P. Andrekson, J. Simpson, T. Tanbun-Ek, R. Logan, and K. Wecht, "Bit-error-rate investigation of two-channel soliton propagation over more than 10 000 km", *Electronics Letters*, vol. 27, no. 9, pp. 695–697, 1991.

[24] P. Andrekson and N. Olsson, "High bit-rate optical soliton communication", in *Global Telecommunications Conference*, 1992, pp. 1880–1885.

[25] P. J. Winzer, D. T. Neilson, and A. R. Chraplyvy, "Fiber-optic transmission and networking: The previous 20 and the next 20 years [invited]", *Optics Express*, vol. 26, no. 18, pp. 24 190–24 239, 2018.

[26] L. Cohen, C. Lin, and W. French, "Tailoring zero chromatic dispersion into the 1.5–1.6 μm low-loss spectral region of single-mode fibres", *Electronics Letters*, vol. 15, no. 12, pp. 334–33, 1979.

[27] M. A. Saifi, L. G. Cohen, J. Stone, and S. J. Jang, "Triangular-profile single-mode fiber", *Optics Letters*, vol. 7, no. 1, pp. 43–45, 1982.

[28] B. Ainslie, K. Beales, D. Cooper, C. Day, and J. Rush, "Monomode fibre with ultra-low loss and minimum dispersion at 1.55 μm", *Electronics Letters*, vol. 18, no. 19, pp. 842–844, 1982.

[29] C. D. Poole, K. T. Nelson, J. M. Wiesenfeld, and A. R. McCormick, "Broadband dispersion compensation by using the higher-order spatial mode in a two-mode fiber", *Optics Letters*, vol. 17, no. 14, pp. 985–987, 1992.

[30] J. M. Dugan, A. J. Price, M. Ramadan, D. L. Wolf, E. F. Murphy, A. J. Antos, D. K. Smith, and D. W. Hall, "All-optical, fiber-based 1550 nm dispersion compensation in a 10 Gbit/s, 150 km transmission experiment over 1310 nm optimized fiber", in *Proceedings of Optical Fiber Communication Conference*, paper. PD.14, 1992.

[31] C. Brackett, "Dense wavelength division multiplexing networks: Principles and applications", *IEEE Journal on Selected Areas in Communications*, vol. 8, no. 6, pp. 948–964, 1990.

[32] D. Fishman, J. Nagel, T. Cline, R. Tench, T. Pleiss, T. Miller, D. Coult, M. Milbrodt, P. Yeates, A. Chraplyvy, R. Tkach, A. Piccirilli, J. Simpson, and C. Miller, "A high capacity noncoherent FSK lightwave field experiment using Er3+-doped fiber optical amplifiers", *IEEE Photonics Technology Letters*, vol. 2, no. 9, pp. 662–664, 1990.

[33] H. Taga, Y. Yoshida, N. Edagawa, S. Yamamoto, and H. Wakabayashi, "459 km, 2.4 Gbit/s four wavelength multiplexing optical fibre transmission experiment using six Er-doped fibre amplifiers", *Electronics Letters*, vol. 26, no. 8, pp. 500–501, 1990.

[34] D. Marcuse, A. Chraplyvy, and R. Tkach, "Effect of fiber nonlinearity on long-distance transmission", *Journal of Lightwave Technology*, vol. 9, no. 1, pp. 121–128, 1991.

[35] K. S. Kim, W. A. Reed, K. W. Quoi, and R. H. Stolen, "Measurement of the nonlinear index of silica-core and dispersion-shifted fibers", *Optics Letters*, vol. 19, no. 4, p. 257, 1994.

[36] M. Tatham, G. Sherlock, and L. Westbrook, "Compensation fibre chromatic dispersion by optical phase conjugation in a semiconductor laser amplifier", *Electronics Letters*, vol. 29, no. 21, pp. 1851–1852, 1993.

[37] W. Pieper, C. Kurtzke, K. Petermann, R. Schnabel, H. Weber, R. Ludwig, and D. Breuer, "Nonlinearity-insensitive standard-fibre transmission based on optical-phase conjugation in a semiconductor-laser amplifier", *Electronics Letters*, vol. 30, no. 9, pp. 724–726, 1994.

[38] R. Tkach, A. Chraplyvy, F. Forghieri, A. Gnauck, and R. Derosier, "Four-photon mixing and high-speed WDM systems", *Journal of Lightwave Technology*, vol. 13, no. 5, pp. 841–849, 1995.

[39] M. Hayee and A. Willner, "Pre- and post-compensation of dispersion and nonlinearities in 10-Gb/s WDM systems", *IEEE Photonics Technology Letters*, vol. 9, no. 9, pp. 1271–1273, 1997.

[40] P. Winzer and R.-J. Essiambre, "Advanced optical modulation formats", *Proceedings of the IEEE*, vol. 94, no. 5, pp. 952–985, 2006.

[41] R. Griffin and A. Carter, "Optical differential quadrature phase-shift key (oDQPSK) for high capacity optical transmission", in *Proceedings of Optical Fiber Communication Conference*, paper. WX6, 2002.

[42] J. McNicol, M. O'Sullivan, K. Roberts, A. Comeau, D. McGhan, and L. Strawczynski, "Electrical domain compensation of optical dispersion [optical fibre communication applications", in *Proceedings of the Optical Fiber Communication Conference*, 2005.

[43] H. Sun, K.-T. Wu, and K. Roberts, "Real-time measurements of a 40 Gb/s coherent system", *Optics Express*, vol. 16, no. 2, pp. 873–879, 2008.

[44] R.-J. Essiambre, P. Winzer, X. Q. Wang, W. Lee, C. White, and E. Burrows, "Electronic predistortion and fiber nonlinearity", *IEEE Photonics Technology Letters*, vol. 18, no. 17, pp. 1804–1806, 2006.

[45] C. Laperle and M. Osullivan, "Advances in high-speed DACs, ADCs, and DSP for optical coherent transceivers", *Journal of Lightwave Technology*, vol. 32, no. 4, pp. 629–643, 2014.

[46] A. Napoli, M. M. Mezghanni, T. Rahman, D. Rafique, R. Palmer, B. Spinnler, S. Calabro, C. Castro, M. Kuschnerov, and M. Bohn, "Digital compensation of bandwidth limitations for high-speed DACs and ADCs", *Journal of Lightwave Technology*, vol. 34, no. 13, pp. 3053–3064, 2016.

[47] C. E. Shannon, "A mathematical theory of communication", *Bell System Technical Journal*, vol. 27, no. 3, pp. 379–423, 1948.

[48] A. Leven and L. Schmalen, "Status and recent advances on forward error correction technologies for lightwave systems", *Journal of Lightwave Technology*, vol. 32, no. 16, pp. 2735–2750, 2014.

[49] L. Schmalen, S. ten Brink, and A. Leven, "Advances in detection and error correction for coherent optical communications: Regular, irregular, and spatially coupled LDPC code designs", in *Enabling Technologies for High Spectral-Efficiency Coherent Optical Communication Networks*, 2016, pp. 65–122.

[50] K. Kikuchi, "Fundamentals of coherent optical fiber communications", *Journal of Lightwave Technology*, vol. 34, no. 1, pp. 157–179, 2016.

[51] Y. Tamura, H. Sakuma, K. Morita, M. Suzuki, Y. Yamamoto, K. Shimada, Y. Honma, K. Sohma, T. Fujii, and T. Hasegawa, "The first 0.14-dB/km loss optical fiber and its impact on submarine transmission", *Journal of Lightwave Technology*, vol. 36, no. 1, pp. 44–49, 2018.

[52] S. L. Olsson, J. Cho, S. Chandrasekhar, X. Chen, P. J. Winzer, and S. Makovejs, "Probabilistically shaped PDM 4096-QAM transmission over up to 200 km of fiber using standard intradyne detection", *Optics Express*, vol. 26, no. 4, pp. 4522–4530, 2018.

[53] M. Terayama, S. Okamoto, K. Kasai, M. Yoshida, and M. Nakazawa, "4096 QAM (72 gbit/s) single-carrier coherent optical transmission with a potential SE of 15.8 bit/s/Hz in all-raman amplified 160 km fiber link", in *Optical Fiber Communication Conference*, paper. Th1F.2, 2018.

[54] S. L. Olsson, J. Cho, S. Chandrasekhar, X. Chen, E. C. Burrows, and P. J. Winzer, "Record-high 17.3-bit/s/Hz spectral efficiency transmission over 50 km using probabilistically shaped PDM 4096-QAM", in *Proceedings of Optical Fiber Communication Conference*, paper. Th4C.5, 2018.

[55] S. Chandrasekhar, B. Li, J. Cho, X. Chen, E. Burrows, G. Raybon, and P. Winzer, "High-spectral-efficiency transmission of PDM 256-QAM with parallel probabilistic shaping at record rate-reach trade-offs", in *Proceedings of European Conference on Optical Communication*, paper. Th.3.C.1, 2016.

[56] L. Beygi, E. Agrell, J. M. Kahn, and M. Karlsson, "Rate-adaptive coded modulation for fiber-optic communications", *Journal of Lightwave Technology*, vol. 32, no. 2, pp. 333–343, 2014.

[57] A. Ghazisaeidi, L. Schmalen, I. F. de Jauregui Ruiz, P. Tran, C. Simonneau, P. Brindel, and G. Charlet, "Transoceanic transmission systems using adaptive multirate FECs", *Journal of Lightwave Technology*, vol. 33, no. 7, pp. 1479–1487, 2015.

[58] T. Fehenberger, A. Alvarado, G. Böcherer, and N. Hanik, "On probabilistic shaping of quadrature amplitude modulation for the nonlinear fiber channel", *Journal of Lightwave Technology*, vol. 34, no. 21, pp. 5063–5073, 2016.

[59] J. Cho and P. J. Winzer, "Probabilistic constellation shaping for optical fiber communications", *Journal of Lightwave Technology*, vol. 37, no. 6, pp. 1590–1607, 2019.

[60] A. Ghazisaeidi, I. F. de Jauregui Ruiz, L. Schmalen, P. Tran, C. Simonneau, E. Awwad, B. Uscumlic, P. Brindel, and G. Charlet, "Submarine transmission systems using digital nonlinear compensation and adaptive rate forward error correction", *Journal of Lightwave Technology*, vol. 34, no. 8, pp. 1886–1895, 2016.

[61] I. F. de Jauregui Ruiz, A. Ghazisaeidi, O. A. Sab, P. Plantady, A. Calsat, S. Dubost, L. Schmalen, V. Letellier, and J. Renaudier, "25.4-Tb/s transmission over transpacific distances using truncated probabilistically shaped PDM-64QAM", *Journal of Lightwave Technology*, vol. 36, no. 6, pp. 1354–1361, 2018.

[62] J.-X. Cai, H. G. Batshon, M. V. Mazurczyk, O. V. Sinkin, D. Wang, M. Paskov, W. W. Patterson, C. R. Davidson, P. C. Corbett, G. M. Wolter, T. E. Hammon, M. A. Bolshtyansky, D. G. Foursa, and A. N. Pilipetskii, "70.46 Tb/s over 7,600 km and 71.65 Tb/s over 6,970 km transmission in C+L band using coded modulation with hybrid constellation shaping and nonlinearity compensation", *Journal of Lightwave Technology*, vol. 36, no. 1, pp. 114–121, 2018.

[63] J.-X. Cai, H. G. Batshon, M. V. Mazurczyk, O. V. Sinkin, D. Wang, M. Paskov, C. R. Davidson, W. W. Patterson, A. Turukhin, M. A. Bolshtyansky, and D. G. Foursa, "51.5 Tb/s capacity over 17,107 km in C+L bandwidth using single-mode fibers and nonlinearity compensation", *Journal of Lightwave Technology*, vol. 36, no. 11, pp. 2135–2141, 2018.

[64] X. Chen, S. Chandrasekhar, S. Randel, G. Raybon, A. Adamiecki, P. Pupalaikis, and P. J. Winzer, "All-electronic 100-GHz bandwidth digital-to-analog converter generating PAM signals up to 190 GBaud", *Journal of Lightwave Technology*, vol. 35, no. 3, pp. 411–417, 2017.

[65] G. Raybon, A. Adamiecki, J. Cho, F. Jorge, A. Konczykowska, M. Riet, B. Duval, J.-Y. Dupuy, N. Fontaine, P. J. Winzer, S. Chandrasekhar, and X. Chen, "180-GBaud all-ETDM single-carrier polarization multiplexed QPSK transmission over 4480 km", in *Proceedings of Optical Fiber Communication Conference*, paper. Th4C.3, 2018.

[66] M. Nakamura, F. Hamaoka, M. Nagatani, Y. Ogiso, H. Wakita, H. Yamazaki, T. Kobayashi, M. Ida, H. Nosaka, and Y. Miyamoto, "192-gbaud signal generation using ultra-broadband optical frontend module integrated with bandwidth multiplexing function", in *Proceedings of Optical Fiber Communication Conference*, paper. Th4B.4, 2019.

[67] R. Maher, K. Croussore, M. Lauermann, R. Going, X. Xu, and J. Rahn, "Constellation shaped 66 GBd DP-1024QAM transceiver with 400 km transmission over standard SMF", in *Proceedings of European Conference on Optical Communication*, paper. Th.PDP.B.2, 2017.

[68] R.-J. Essiambre, G. Kramer, P. J. Winzer, G. J. Foschini, and B. Goebel, "Capacity limits of optical fiber networks", *Journal of Lightwave Technology*, vol. 28, no. 4, pp. 662–701, 2010.

[69] G. Bosco, P. Poggiolini, A. Carena, V. Curri, and F. Forghieri, "Analytical results on channel capacity in uncompensated optical links with coherent detection", *Optics Express*, vol. 19, no. 26, B440–B451, 2011.

[70] E. Agrell, A. Alvarado, G. Durisi, and M. Karlsson, "Capacity of a nonlinear optical channel with finite memory", *Journal of Lightwave Technology*, vol. 32, no. 16, pp. 2862–2876, 2014.

[71] R. Dar, M. Shtaif, and M. Feder, "New bounds on the capacity of the nonlinear fiber-optic channel", *Optics Letters*, vol. 39, no. 2, pp. 398–401, 2014.

[72] J. E. Prilepsky, S. A. Derevyanko, and S. K. Turitsyn, "Nonlinear spectral management: Linearization of the lossless fiber channel", *Optics Express*, vol. 21, no. 20, pp. 24 344–24 367, 2013.

[73] H. Bulow, "Experimental demonstration of optical signal detection using nonlinear fourier transform", *Journal of Lightwave Technology*, vol. 33, no. 7, pp. 1433–1439, 2015.

[74] E. G. Turitsyna and S. K. Turitsyn, "Digital signal processing based on inverse scattering transform", *Optics Letters*, vol. 38, no. 20, pp. 4186–4188, 2013.

[75] T. Gui, T. H. Chan, C. Lu, A. P. T. Lau, and P.-K. A. Wai, "Alternative decoding methods for optical communications based on nonlinear fourier transform", *Journal of Lightwave Technology*, vol. 35, no. 9, pp. 1542–1550, 2017.

[76] A. Buchberger, A. G. i Amat, V. Aref, and L. Schmalen, "Probabilistic eigenvalue shaping for nonlinear fourier transform transmission", *Journal of Lightwave Technology*, vol. 36, no. 20, pp. 4799–4807, 2018.

[77] S. K. Turitsyn, J. E. Prilepsky, S. T. Le, S. Wahls, L. L. Frumin, M. Kamalian, and S. A. Derevyanko, "Nonlinear fourier transform for optical data processing and transmission: Advances and perspectives", *Optica*, vol. 4, no. 3, pp. 307–32, 2017.

[78] S. A. Derevyanko, J. E. Prilepsky, and S. K. Turitsyn, "Capacity estimates for optical transmission based on the nonlinear fourier transform", *Nature Communications*, vol. 7, no. 1, 2016.

[79] S. E. Miller, "Integrated optics: An introduction", *Bell System Technical Journal*, vol. 48, no. 7, pp. 2059–2069, 1969.

[80] E. A. J. Marcatili, "Dielectric rectangular waveguide and directional coupler for integrated optics", *Bell System Technical Journal*, vol. 48, no. 7, pp. 2071–2102, 1969.

[81] S. Miller, "Survey of integrated optics", *IEEE Journal of Quantum Electronics*, vol. 7, no. 6, pp. 292–293, 1971.

[82] M. Horowitz, E. Alon, D. Patil, S. Naffziger, R. Kumar, and K. Bernstein, "Scaling, power, and the future of CMOS", in *IEEE InternationalElectron Devices Meeting, 2005. IEDM Technical Digest.*, 2005.

[83] P. Dong and S. Chandrasekhar, "Photonic integration", in *Enabling Technologies for High Spectral-Efficiency Coherent Optical Communication Networks*, 2016, pp. 447–472.

[84] B. Jalali and S. Fathpour, "Silicon photonics", *Journal of Lightwave Technology*, vol. 24, no. 12, pp. 4600–4615, 2006.

[85] R. Nagarajan, M. Kato, J. Pleumeekers, P. Evans, S. Corzine, S. Hurtt, A. Dentai, S. Murthy, M. Missey, R. Muthiah, R. A. Salvatore, C. Joyner, R. Schneider, M. Ziari, F. Kish, and D. Welch, "InP photonic integrated circuits", *IEEE Journal of Selected Topics in Quantum Electronics*, vol. 16, no. 5, pp. 1113–1125, 2010.

[86] P. Dong, X. Liu, S. Chandrasekhar, L. L. Buhl, R. Aroca, and Y.-K. Chen, "Monolithic silicon photonic integrated circuits for compact 100+gb/s coherent optical receivers and transmitters", *IEEE Journal of Selected Topics in Quantum Electronics*, vol. 20, no. 4, pp. 150–157, 2014.

[87] R. W. Going, M. Lauermann, R. Maher, H.-S. Tsai, A. Hosseini, M. Lu, N. Kim, P. Studenkov, S. W. Corzine, J. Summers, M. Anagnosti, M. Montazeri, J. Zhang, B. Behnia, J. Tang, S. Buggaveeti, T. Vallaitis, J. Osenbach, M. Kuntz, X. Xu, K. Croussore, V. Lal, P. Evans, J. T. Rahn, T. Butrie, A. Karanicolas, K.-T. Wu, M. Mitchell, M. Ziari, D. Welch, and F. Kish, "1.00 (0.88) tb/s per wave capable coherent multichannel transmitter (receiver) InP-based PICs with hybrid integrated SiGe electronics", *IEEE Journal of Quantum Electronics*, vol. 54, no. 4, pp. 1–10, 2018.

[88] H. Zhang, B. Zhu, S. Park, C. Doerr, M. Aydinlik, J. Geyer, T. Pfau, G. Pendock, R. Aroca, F. Liu, C. Rasmussen, B. Mikkelsen, P. I. Borel, T. Geisler, R. Jensen, D. W. Peckham, R. Lingle, D. Vaidya, M. F. Yan, P. W. Wisk, and D. J. DiGiovanni, "Real-time transmission of 16 tb/s over 1020km using 200gb/s CFP2-DCO", *Optics Express*, vol. 26, no. 6, pp. 6943–6948, 2018.

[89] G. T. Reed, G. Mashanovich, F. Y. Gardes, and D. J. Thomson, "Silicon optical modulators", *Nature Photonics*, vol. 4, no. 8, pp. 518–526, 2010.

[90] P. Dong, A. Maho, R. Brenot, Y.-K. Chen, and A. Melikyan, "Directly reflectivity modulated laser", *Journal of Lightwave Technology*, vol. 36, no. 5, pp. 1255–1261, 2018.

[91] K. K. Lee, D. R. Lim, L. C. Kimerling, J. Shin, and F. Cerrina, "Fabrication of ultralow-loss si/SiO_2 waveguides by roughness reduction", *Optics Letters*, vol. 26, no. 23, pp. 1888–1890, 2001.

[92] J. F. Bauters, M. J. R. Heck, D. John, D. Dai, M.-C. Tien, J. S. Barton, A. Leinse, R. G. Heideman, D. J. Blumenthal, and J. E. Bowers, "Ultra-low-loss high-aspect-ratio si_3n_4 waveguides", *Optics Express*, vol. 19, no. 4, pp. 3163–3174, 2011.

[93] N. Lindenmann, G. Balthasar, D. Hillerkuss, R. Schmogrow, M. Jordan, J. Leuthold, W. Freude, and C. Koos, "Photonic wire bonding: A novel concept for chip-scale interconnects", *Optics Express*, vol. 20, no. 16, p. 17 667, 2012.

[94] M. J. R. Heck, J. F. Bauters, M. L. Davenport, J. K. Doylend, S. Jain, G. Kurczveil, S. Srinivasan, Y. Tang, and J. E. Bowers, "Hybrid silicon photonic integrated circuit technology", *IEEE Journal of Selected Topics in Quantum Electronics*, vol. 19, no. 4, pp. 6 100 117–6 100 117, 2013.

[95] D. Thomson, A. Zilkie, J. E. Bowers, T. Komljenovic, G. T. Reed, L. Vivien, D. Marris-Morini, E. Cassan, L. Virot, J.-M. Fédéli, J.-M. Hartmann, J. H. Schmid, D.-X. Xu, F. Boeuf, P. O'Brien, G. Z. Mashanovich, and M. Nedeljkovic, "Roadmap on silicon photonics", *Journal of Optics*, vol. 18, no. 7, p. 073 003, 2016.

[96] D. J. Richardson, J. M. Fini, and L. E. Nelson, "Space-division multiplexing in optical fibres", *Nature Photonics*, vol. 7, no. 5, pp. 354–362, 2013.

[97] P. J. Winzer and D. T. Neilson, "From scaling disparities to integrated parallelism: A decathlon for a decade", *Journal of Lightwave Technology*, vol. 35, no. 5, pp. 1099–1115, 2017.

[98] D. Gloge and D. Weiner, "The capacity of multiple beam waveguides and optical delay lines", *Bell System Technical Journal*, vol. 47, no. 10, pp. 2095–2109, 1968.

[99] D. Soma, Y. Wakayama, S. Beppu, S. Sumita, T. Tsuritani, T. Hayashi, T. Nagashima, M. Suzuki, M. Yoshida, K. Kasai, M. Nakazawa, H. Takahashi, K. Igarashi, I. Morita, and M. Suzuki, "10.16-Peta-bit/s dense SDM/WDM transmission over 6-mode 19-core fiber across the C+L band", *Journal of Lightwave Technology*, vol. 36, no. 6, pp. 1362–1368, 2018.

[100] G. Rademacher, R. S. Luís, B. J. Puttnam, T. A. Eriksson, E. Agrell, R. Maruyama, K. Aikawa, H. Furukawa, Y. Awaji, and N. Wada, "159 Tbit/s C+L band transmission over 1045 km 3-mode graded-index few-mode fiber", in *Proceedings of Optical Fiber Communication Conference*, paper. Th4C.4, 2018.

[101] R. Ryf, N. K. Fontaine, S. Wittek, K. Choutagunta, M. Mazur, H. Chen, J. C. Alvarado-Zacarias, R. Amezcua-Correa, M. Capuzzo, R. Kopf, A. Tate, H. Safar, C. Bolle, D. T. Neilson, E. Burrows, K. Kim, M. Bigot-Astruc, F. Achten, P. Sillard, A. Amezcua-Correa, J. M. Kahn, J. Schroder, and J. Carpenter, "High-spectral-efficiency mode-multiplexed transmission over graded-index multimode fiber", in *Proceedings of European Conference on Optical Communication*, paper. Th3B.1, 2018.

[102] J. van Weerdenburg, R. Ryf, R. Alvarez-Aguirre, N. K. Fontaine, R.-J. Essiambre, H. Chen, J. C. Alvarado-Zacarias, R. Amezcua-Correa, S. Gross, N. Riesen, M. Withford, D. W. Peckham, A. McCurdy, R. Lingle, T. Koonen, and C. Okonkwo, "Mode-multiplexed 16-QAM transmission over 2400-km large-effective-area depressed-cladding 3-mode fiber", in *Proceedings of Optical Fiber Communication Conference*, paper. W4C.2, 2018.

[103] R. Ryf, J. C. Alvarado-Zacarias, S. Wittek, N. K. Fontaine, R.-J. Essiambre, H. Chen, R. Amezcua-Correa, H. Sakuma, T. Hayashi, and T. Hasegawa, "Coupled-core transmission over 7-core fiber", in *Proceedings of the Optical Fiber Communication Conference*, paper. Th4B.3, 2019.

[104] D. Hillerkuss and J. Leuthold, "Software-defined transceivers in dynamic access networks", *Journal of Lightwave Technology*, vol. 34, no. 2, pp. 792–797, 2016.

[105] A. Lapidoth, *A Foundation in Digital Communication*. Cambridge University Press, 2009.

[106] E. Agrell and M. Karlsson, "Power-efficient modulation formats in coherent transmission systems", *Journal of Lightwave Technology*, vol. 27, no. 22, pp. 5115–5126, 2009.

[107] A. Alvarado and E. Agrell, "Four-dimensional coded modulation with bit-wise decoders for future optical communications", *Journal of Lightwave Technology*, vol. 33, no. 10, pp. 1993–2003, 2015.

[108] D. S. Millar, T. Koike-Akino, K. Kojima, and K. Parsons, "A 24-dimensional modulation format achieving 6 dB asymptotic power efficiency", in *Advanced Photonics*, paper. SpM3D.6, 2013.

[109] R. Dar, M. Feder, A. Mecozzi, and M. Shtaif, "On shaping gain in the nonlinear fiber-optic channel", in *2014 IEEE International Symposium on Information Theory*, 2014.

[110] X. Liu, S. Chandrasekhar, and P. J. Winzer, "Digital signal processing techniques enabling multi-Tb/s superchannel transmission: An overview of recent advances in DSP-enabled superchannels", *IEEE Signal Processing Magazine*, vol. 31, no. 2, pp. 16–24, 2014.

[111] M. S. Faruk and S. J. Savory, "Digital signal processing for coherent transceivers employing multilevel formats", *Journal of Lightwave Technology*, vol. 35, no. 5, pp. 1125–1141, 2017.

[112] P. Poggiolini, A. Nespola, Y. Jiang, G. Bosco, A. Carena, L. Bertignono, S. M. Bilal, S. Abrate, and F. Forghieri, "Analytical and experimental results on system maximum reach increase through symbol rate optimization", *Journal of Lightwave Technology*, vol. 34, no. 8, pp. 1872–1885, 2016.

[113] A. Kumpera, V. Dominic, A. Awadalla, L. Dardis, J. Rahn, S. Sanders, M. Mitchell, P. Mertz, G. Shartle, S. Jackson, S. Blakey, M. Sokar, D. Krause, H. Sun, K.-T. Wu, and P. Cannon, "Real-time superchannel transmission over 10,500 km submarine link at 4.66 b/s/hz spectral efficiency", *Optics Express*, vol. 26, no. 12, pp. 15 039–15 044, 2018.

[114] F. P. Guiomar, A. Carena, G. Bosco, L. Bertignono, A. Nespola, and P. Poggiolini, "Effectiveness of symbol-rate optimization with PM-16qam subcarriers in WDM transmission", in *Optical Fiber Communication Conference*, paper. W3J.3, 2017.

[115] R. W. Schafer and A. V. Oppenheim, *Discrete-Time Signal Processing: Pearson New International Edition*. Pearson Education Limited, 2013.

[116] H. Zumbahlen *et al.*, *Linear circuit design handbook*. Newnes, 2011.

[117] R. Walden, "Analog-to-digital converter survey and analysis", *IEEE Journal on Selected Areas in Communications*, vol. 17, no. 4, pp. 539–550, 1999.

[118] A. Pilipetskii, "High-capacity undersea long-haul systems", *IEEE Journal of Selected Topics in Quantum Electronics*, vol. 12, no. 4, pp. 484–496, 2006.

[119] P. Westbergh, R. Safaisini, E. Haglund, A. Larsson, J. Gustavsson, and E. Haglund, "High-speed 850 nm VCSELs operating error free up to 57 gbit/s", *Electronics Letters*, vol. 49, no. 16, pp. 1021–1023, 2013.

[120] E. Ip, "Optical coherent detection and digital signal processing of channel impairments", in *Handbook of Optical Fibers*, 2018, pp. 1–70.

[121] M. Zhang, C. Wang, X. Chen, M. Bertrand, A. Shams-Ansari, S. Chandrasekhar, P. Winzer, and M. Lončar, "Ultra-high bandwidth integrated lithium niobate modulators with record-low v_π", in *Proceedings of Optical Fiber Communication Conference*, paper Th4A.5, 2018.

[122] K. Goi, A. Oka, H. Kusaka, Y. Terada, K. Ogawa, T.-Y. Liow, X. Tu, G.-Q. Lo, and D.-L. Kwong, "Low-loss high-speed silicon IQ modulator for QPSK/DQPSK in c and l bands", *Optics Express*, vol. 22, no. 9, pp. 10 703–10 709, 2014.

[123] Y. Ogiso, H. Wakita, M. Nagatani, H. Yamazaki, M. Nakamura, T. Kobayashi, J. Ozaki, Y. Ueda, S. Nakano, S. Kanazawa, T. Fujii, Y. Hashizume, H. Tanobe, N. Nunoya, M. Ida, Y. Miyamoto, and N. Kikuchi, "Ultra-high bandwidth InP IQ modulator co-assembled with driver IC for beyond 100-GBd CDM", in *Proceedings of Optical Fiber Communication Conference*, paper. Th4A.2, 2018.

[124] C. Haffner, W. Heni, Y. Fedoryshyn, J. Niegemann, A. Melikyan, D. L. Elder, B. Baeuerle, Y. Salamin, A. Josten, U. Koch, C. Hoessbacher, F. Ducry, L. Juchli, A. Emboras, D. Hillerkuss, M. Kohl, L. R. Dalton, C. Hafner, and J. Leuthold, "All-plasmonic mach-zehnder modulator enabling optical high-speed communication at the microscale", *Nature Photonics*, vol. 9, no. 8, pp. 525–528, 2015.

[125] C. Haffner, D. Chelladurai, Y. Fedoryshyn, A. Josten, B. Baeuerle, W. Heni, T. Watanabe, T. Cui, B. Cheng, S. Saha, D. L. Elder, L. R. Dalton, A. Boltasseva, V. M. Shalaev, N. Kinsey, and J. Leuthold, "Low-loss plasmon-assisted electro-optic modulator", *Nature*, vol. 556, no. 7702, pp. 483–486, 2018.

[126] M. Burla, C. Hoessbacher, W. Heni, C. Haffner, Y. Fedoryshyn, D. Werner, T. Watanabe, H. Massler, D. L. Elder, L. R. Dalton, and J. Leuthold, "500 GHz plasmonic mach-zehnder modulator enabling sub-THz microwave photonics", *APL Photonics*, vol. 4, no. 5, p. 056 106, 2019.

[127] K. Xu, R. Wang, Y. Dai, F. Yin, J. Li, Y. Ji, and J. Lin, "Microwave photonics: Radio-over-fiber links, systems, and applications [invited]", *Photonics Research*, vol. 2, no. 4, B54, 2014.

[128] S. Daumont, B. Rihawi, and Y. Lout, "Root-raised cosine filter influences on PAPR distribution of single carrier signals", in *2008 3rd International Symposium on Communications, Control and Signal Processing*, 2008.

[129] *Fujitsu dp-qpsk 100g ln modulator*, URL: https://www.fujitsu.com/downloads/JP/archive/imgjp/group/foc/services/100gln/ln100gdpqpsk-e-141105.pdf, Fujitsu.

[130] S. Tibuleac and M. Filer, "Transmission impairments in DWDM networks with reconfigurable optical add-drop multiplexers", *Journal of Lightwave Technology*, vol. 28, no. 4, pp. 557–598, 2010.

[131] D. Marom, D. Neilson, D. Greywall, C.-S. Pai, N. Basavanhally, V. Aksyuk, D. Lopez, F. Pardo, M. Simon, Y. Low, P. Kolodner, and C. Bolle, "Wavelength-selective 1xk switches using free-space optics and MEMS micromirrors: Theory, design, and implementation", *Journal of Lightwave Technology*, vol. 23, no. 4, pp. 1620–1630, 2005.

[132] E. Simpanen, J. S. Gustavsson, A. Larsson, M. Karlsson, W. V. Sorin, S. Mathai, M. R. Tan, and S. R. Bickham, "1060 nm single-mode VCSEL and single-mode fiber links for long-reach optical interconnects", *Journal of Lightwave Technology*, vol. 37, no. 13, pp. 2963–2969, 2019.

[133] W. S. Pelouch, "Raman amplification: An enabling technology for long-haul coherent transmission systems", *Journal of Lightwave Technology*, vol. 34, no. 1, pp. 6–19, 2016.

[134] Z. Tong, C. Lundström, P. A. Andrekson, C. J. McKinstrie, M. Karlsson, D. J. Blessing, E. Tipsuwannakul, B. J. Puttnam, H. Toda, and L. Gruener-Nielsen, "Towards ultrasensitive optical links enabled by low-noise phase-sensitive amplifiers", *Nature Photonics*, vol. 5, no. 7, pp. 430–436, 2011.

[135] C. Schubert, R. Ludwig, and H.-G. Weber, "High-speed optical signal processing using semiconductor optical amplifiers", *Journal of Optical and Fiber Communications Reports*, vol. 2, no. 2, pp. 171–208, 2005.

[136] M. Ionescu, D. Lavery, A. Edwards, E. Sillekens, L. Galdino, D. Semrau, R. Killey, W. Pelouch, S. Barnes, and P. Bayvel, "74.38 tb/s transmission over 6300 km single mode fiber with hybrid EDFA/raman amplifiers", in *Proceedings of the Optical Fiber Communication Conference*, paper. Tu3F.3, 2019.

[137] L. Galdino, D. Semrau, M. Ionescu, A. Edwards, W. S. Pelouch, S. R. Desbruslais, J. James, E. Sillekens, D. Lavery, S. Barnes, R. I. Killey, and P. Bayvel, "Study on the impact of nonlinearity and noise on the performance of high-capacity broadband hybrid raman-EDFA amplified system", *Journal of Lightwave Technology*, pp. 1–1, 2019.

[138] L. Lundberg, P. A. Andrekson, and M. Karlsson, "Power consumption analysis of hybrid EDFA/raman amplifiers in long-haul transmission systems", *Journal of Lightwave Technology*, vol. 35, no. 11, pp. 2132–2142, 2017.

[139] G. Agrawal, *Nonlinear Fiber Optics, Fifth Edition (Optics and Photonics)*. Academic Press, 2012.

[140] M. Karlsson, "Transmission systems with low noise phase-sensitive parametric amplifiers", *Journal of Lightwave Technology*, vol. 34, no. 5, pp. 1411–1423, 2016.

[141] P. Poggiolini, A. Carena, V. Curri, G. Bosco, and F. Forghieri, "Analytical modeling of nonlinear propagation in uncompensated optical transmission links", *IEEE Photonics Technology Letters*, vol. 23, no. 11, pp. 742–744, 2011.

[142] P. Poggiolini, G. Bosco, A. Carena, V. Curri, and F. Forghieri, "A simple and accurate model for non-linear propagation effects in uncompensated coherent transmission links", *Proceedings of International Conference on Transparent Optical Networks*, pp. 1–6, 2011.

[143] P. Poggiolini, G. Bosco, A. Carena, V. Curri, Y. Jiang, and F. Forghieri, "The GN-model of fiber non-linear propagation and its applications", *Journal of Lightwave Technology*, vol. 32, no. 4, pp. 694–721, 2014.

[144] A. Nespola, S. Straullu, A. Carena, G. Bosco, R. Cigliutti, V. Curri, P. Poggiolini, M. Hirano, Y. Yamamoto, T. Sasaki, J. Bauwelinck, K. Verheyen, and F. Forghieri, "GN-model validation over seven fiber types in uncompensated PM-16QAM Nyquist-WDM links", *IEEE Photonics Technology Letters*, vol. 26, no. 2, pp. 206–209, 2014.

[145] A. Carena, G. Bosco, V. Curri, Y. Jiang, P. Poggiolini, and F. Forghieri, "EGN model of non-linear fiber propagation", *Optics Express*, vol. 22, no. 13, pp. 16 335–16 362, 2014.

[146] C. Xie, "Polarization and nonlinear impairments in fiber communication systems", in *Enabling Technologies for High Spectral-Efficiency Coherent Optical Communication Networks*, 2016, pp. 201–246.

[147] J. P. Gordon and H. Kogelnik, "PMD fundamentals: Polarization mode dispersion in optical fibers", *Proceedings of the National Academy of Sciences*, vol. 97, no. 9, pp. 4541–4550, 2000.

[148] M. Karlsson and H. Sunnerud, "Effects of nonlinearities on PMD-induced system impairments", *Journal of Lightwave Technology*, vol. 24, no. 11, pp. 4127–4137, 2006.

[149] M. Karlsson, "Geometrical interpretation of second-order PMD", *Journal of Lightwave Technology*, vol. 24, no. 1, pp. 643–651, 2006.

[150] D. H. Goldstein, *Polarized Light, Third Edition*. CRC Press, 2010.

[151] P. K. A. Wai and C. R. Menyuk, "Polarization mode dispersion, decorrelation, and diffusion in optical fibers with randomly varying birefringence", *Journal of Lightwave Technology*, vol. 14, no. 2, pp. 148–157, 1996.

[152] E. Ip, A. P. T. Lau, D. J. F. Barros, and J. M. Kahn, "Coherent detection in optical fiber systems", *Optics Express*, vol. 16, no. 2, pp. 753–791, 2008.

[153] R. Maher, M. Torbatian, S. Koenig, O. Khayam, A. L. Liepvre, P. Samra, P. Day, M. Missey, Z. Wang, A. Nguyen, R. Going, S. Wolf, S. Nowierski, X. Xie, S. Tremblay, M. Ziari, F. Kish, J. Rahn, and P. Kandappan, "Constellation shaping for high symbol rate SNR limited transceivers", in *Next-Generation Optical Communication: Components, Sub-Systems, and Systems VIII*, 2019.

[154] H. C. Ji, K. J. Park, J. H. Lee, H. S. Chung, E. S. Son, K. H. Han, S. B. Jun, and Y. C. Chung, "Optical performance monitoring techniques based on pilot tones for WDM network applications", *Journal of Optical Networking*, vol. 3, no. 7, p. 510, 2004.

[155] S. O. Haykin, *Adaptive Filter Theory (5th Edition)*. Pearson, 2013.

[156] R. Kudo, T. Kobayashi, K. Ishihara, Y. Takatori, a. Sano, and Y. Miyamoto, "Coherent optical single carrier transmission using overlap frequency domain equalization for long-haul optical systems", *Journal of Lightwave Technology*, vol. 27, no. 16, pp. 3721–3728, 2009.

[157] I. Tomkos, S. Azodolmolky, J. Sole-Pareta, D. Careglio, and E. Palkopoulou, "A tutorial on the flexible optical networking paradigm: State of the art, trends, and research challenges", *Proceedings of the IEEE*, vol. 102, no. 9, pp. 1317–1337, 2014.

[158] H. Wymeersch and P. Johannisson, "Maximum-likelihood-based blind dispersion estimation for coherent optical communication", *Journal of Lightwave Technology*, vol. 30, no. 18, pp. 2976–2982, 2012.

[159] S. Yao, T. A. Eriksson, S. Fu, P. Johannisson, M. Karlsson, P. A. Andrekson, T. Ming, and D. Liu, "Fast and robust chromatic dispersion estimation based on temporal auto-correlation after digital spectrum superposition", *Optics Express*, vol. 23, no. 12, pp. 15 418–15 430, 2015.

[160] J. C. Diniz, E. P. da Silva, M. Piels, and D. Zibar, "Joint IQ skew and chromatic dispersion estimation for coherent optical communication receivers", in *Advanced Photonics*, paper. SpTu2F.2, 2016.

[161] R. Ryf, S. Randel, A. H. Gnauck, C. Bolle, A. Sierra, S. Mumtaz, M. Esmaeelpour, E. C. Burrows, R.-J. Essiambre, P. J. Winzer, D. W. Peckham, A. H. McCurdy, and R. Lingle, "Mode-division multiplexing over 96 km of few-mode fiber using coherent 6x6 MIMO processing", *Journal of Lightwave Technology*, vol. 30, no. 4, pp. 521–531, 2012.

[162] S. Ö. Arik, D. Askarov, and J. M. Kahn, "Effect of mode coupling on signal processing complexity in mode-division multiplexing", *Journal of Lightwave Technology*, vol. 31, no. 3, pp. 423–431, 2013.

[163] C. Fougstedt, A. Sheikh, P. Johannisson, A. Graell i Amat, and P. Larsson-Edefors, "Power-efficient time-domain dispersion compensation using optimized FIR filter implementation", in *Advanced Photonics 2015*, paper SpT3D.3, 2015.

[164] M. Kuschnerov, M. Chouayakh, K. Piyawanno, B. Spinnler, E. de Man, P. Kainzmaier, M. S. Alfiad, A. Napoli, and B. Lankl, "Data-aided versus blind single-carrier coherent receivers", *IEEE Photonics Journal*, vol. 2, no. 3, pp. 387–403, 2010.

[165] R. Johnson, P. Schniter, T. Endres, J. Behm, D. Brown, and R. Casas, "Blind equalization using the constant modulus criterion: A review", *Proceedings of the IEEE*, vol. 86, no. 10, pp. 1927–1950, 1998.

[166] A.-J. van der Veen and A. Paulraj, "An analytical constant modulus algorithm", *IEEE Transactions on Signal Processing*, vol. 44, no. 5, pp. 1136–1155, 1996.

[167] I. Fatadin, D. Ives, and S. Savory, "Blind Equalization and Carrier Phase Recovery in a 16-QAM Optical Coherent System", *Journal of Lightwave Technology*, vol. 27, no. 15, pp. 3042–3049, 2009.

[168] D. Godard, "Self-recovering equalization and carrier tracking in two-dimensional data communication systems", *IEEE Transactions on Communications*, vol. 28, no. 11, pp. 1867–1875, 1980.

[169] M. Ready and R. Gooch, "Blind equalization based on radius directed adaptation", in *International Conference on Acoustics, Speech, and Signal Processing*, 1990.

[170] D. Ashmawy, K. Banovic, E. Abdel-Raheem, M. Youssif, H. Mansour, and M. Mohanna, "Joint MCMA and DD blind equalization algorithm with variable-step size", in *IEEE International Conference on Electro/Information Technology*, 2009.

[171] J. M. Filho, M. T. M. Silva, and M. D. Miranda, "A family of algorithms for blind equalization of QAM signals", in *IEEE International Conference on Acoustics, Speech and Signal Processing*, 2011.

[172] E. Ip and J. M. Kahn, "Feedforward carrier recovery for coherent optical communications", *Journal of Lightwave Technology*, vol. 25, no. 9, pp. 2675–2692, 2007.

[173] X. Zhou, "Carrier recovery in coherent optical communication systems", in *Enabling Technologies for High Spectral-Efficiency Coherent Optical Communication Networks*, 2016, pp. 395–434.

[174] J. Rahn, L. Dardis, D. Krause, M. Rice, C. Berry, A. Kumpera, A. Nilsson, X. Xu, K. Croussore, P. Samra, K. Weidner, Z. Morbi, S. DeMars, A. Vasilyev, C. Chen, and P. Freeman, "DSP-enabled frequency locking for near-nyquist spectral efficiency superchannels utilizing integrated photonics", in *Proceedings of Optical Fiber Communication Conference*, paper W1B.3, 2018.

[175] G. Liu, K. Zhang, R. Zhang, R. Proietti, H. Lu, and S. J. B. Yoo, "Demonstration of a carrier frequency offset estimator for 16-/32-QAM coherent receivers: A hardware perspective", *Optics Express*, vol. 26, no. 4, pp. 4853–4862, 2018.

[176] L. B. Mercer, "1/f frequency noise effects on self-heterodyne linewidth measurements", *Journal of Lightwave Technology*, vol. 9, no. 4, pp. 485–493, 1991.

[177] K. Kikuchi, "Characterization of semiconductor-laser phase noise and estimation of bit-error rate performance with low-speed offline digital coherent receivers", *Optics Express*, vol. 20, no. 5, pp. 5291–5302, 2012.

[178] J. C. M. Diniz, J. C. R. F. de Oliveira, E. S. Rosa, V. B. Ribeiro, V. E. S. Parahyba, R. da Silva, E. P. da Silva, L. H. H. de Carvalho, A. F. Herbster, and A. C. Bordonalli, "Simple feed-forward wide-range frequency offset estimator for optical coherent receivers", *Optics Express*, vol. 19, no. 26, B323–B328, 2011.

[179] Y. Liu, Y. Peng, S. Wang, and Z. Chen, "Improved FFT-based frequency offset estimation algorithm for coherent optical systems", *IEEE Photonics Technology Letters*, vol. 26, no. 6, pp. 613–616, 2014.

[180] F. Xiao, J. Lu, S. Fu, C. Xie, M. Tang, J. Tian, and D. Liu, "Feed-forward frequency offset estimation for 32-QAM optical coherent detection", *Optics Express*, vol. 25, no. 8, pp. 8828–8839, 2017.

[181] J. Lu, X. Li, S. Fu, M. Luo, M. Xiang, H. Zhou, M. Tang, and D. Liu, "Joint carrier phase and frequency-offset estimation with parallel implementation for dual-polarization coherent receiver", *Optics Express*, vol. 25, no. 5, pp. 5217–5231, 2017.

[182] A. Meiyappan, P. Y. Kam, and H. Kim, "On decision aided carrier phase and frequency offset estimation in coherent optical receivers", *Journal of Lightwave Technology*, vol. 31, no. 13, pp. 2055–2069, 2013.

[183] M. Selmi, Y. Jaouen, and P. Ciblat, "Accurate digital frequency offset estimator for coherent polmux qam transmission systems", in *Proceedings of European Conference on Optical Communication*, paper. P3.08, 2009.

[184] I. Fatadin, D. Ives, and S. J. Savory, "Carrier phase recovery for 16-QAM using QPSK partitioning and sliding window averaging", *IEEE Photonics Technology Letters*, vol. 26, no. 9, pp. 854–857, 2014.

[185] A. Viterbi, "Nonlinear estimation of PSK-modulated carrier phase with application to burst digital transmission", *IEEE Transactions on Information Theory*, vol. 29, no. 4, pp. 543–551, 1983.

[186] Y. Gao, A. P. T. Lau, S. Yan, and C. Lu, "Low-complexity and phase noise tolerant carrier phase estimation for dual-polarization 16-QAM systems", *Optics Express*, vol. 19, no. 22, pp. 21 717–21 729, 2011.

[187] M. G. Taylor, "Phase estimation methods for optical coherent detection using digital signal processing", *Journal of Lightwave Technology*, vol. 27, no. 7, pp. 901–914, 2009.

[188] I. Fatadin, D. Ives, and S. J. Savory, "Laser linewidth tolerance for 16-QAM coherent optical systems using QPSK partitioning", *IEEE Photonics Technology Letters*, vol. 22, no. 9, pp. 631–633, 2010.

[189] T. Pfau, S. Hoffmann, and R. Noé, "Hardware-efficient coherent digital receiver concept with feedforward carrier recovery for M-QAM constellations", *Journal of Lightwave Technology*, vol. 27, no. 8, pp. 989–999, 2009.

[190] X. Zhou, "An improved feed-forward carrier recovery algorithm for coherent receivers with M-QAM modulation format", *IEEE Photonics Technology Letters*, vol. 22, no. 14, pp. 1051–1053, 2010.

[191] G. Bosco, S. M. Bilal, A. Nespola, P. Poggiolini, and F. Forghieri, "Impact of the transmitter IQ-skew in multi-subcarrier coherent optical systems", in *Proceedings of Optical Fiber Communication Conference*, paper. W4A.5, 2016.

[192] E. P. da Silva and D. Zibar, "Widely linear equalization for IQ imbalance and skew compensation in optical coherent receivers", *Journal of Lightwave Technology*, vol. 34, no. 15, pp. 3577–3586, 2016.

[193] C. R. S. Fludger and T. Kupfer, "Transmitter impairment mitigation and monitoring for high baud-rate, high order modulation systems", in *Proceedings of European Conference on Optical Communication*, paper. Tu.2.A.2, 2016.

[194] W. Cheney and D. R. Kincaid, *Linear Algebra: Theory And Applications*. Jones & Bartlett Learning, 2008.

[195] J. H. Ke, Y. Gao, and J. C. Cartledge, "400 gbit/s single-carrier and 1 tbit/s three-carrier superchannel signals using dual polarization 16-qam with look-up table correction and optical pulse shaping", *Optics Express*, vol. 22, no. 1, pp. 71–84, 2014.

[196] A. Rezania, J. C. Cartledge, A. Bakhshali, and W.-Y. Chan, "Compensation schemes for transmitter and receiver based pattern-dependent distortion", *IEEE Photonics Technology Letters*, vol. 28, no. 22, pp. 2641–2644, 2016.

[197] P. W. Berenguer, M. Nolle, L. Molle, T. Raman, A. Napoli, C. Schubert, and J. K. Fischer, "Nonlinear digital pre-distortion of transmitter components", *Journal of Lightwave Technology*, vol. 34, no. 8, pp. 1739–1745, 2016.

[198] T. Adali, P. J. Schreier, and L. L. Scharf, "Complex-valued signal processing: The proper way to deal with impropriety", *IEEE Transactions on Signal Processing*, vol. 59, no. 11, pp. 5101–5125, 2011.

[199] A. Alvarado, E. Agrell, D. Lavery, R. Maher, and P. Bayvel, "Replacing the soft-decision FEC limit paradigm in the design of optical communication systems", *Journal of Lightwave Technology*, vol. 34, no. 2, pp. 707–721, 2016.

[200] A. Alvarado, T. Fehenberger, B. Chen, and F. M. J. Willems, "Achievable information rates for fiber optics: Applications and computations", *Journal of Lightwave Technology*, vol. 36, no. 2, pp. 424–439, 2018.

[201] J. C. Cartledge, F. P. Guiomar, F. R. Kschischang, G. Liga, and M. P. Yankov, "Digital signal processing for fiber nonlinearities [invited]", *Optics Express*, vol. 25, no. 3, pp. 1916–1936, 2017.

[202] E. Ip and J. M. Kahn, "Compensation of dispersion and nonlinear impairments using digital backpropagation", *Journal of Lightwave Technology*, vol. 26, no. 20, pp. 3416–3425, 2008.

[203] F. P. Guiomar, J. D. Reis, A. L. Teixeira, and A. N. Pinto, "Mitigation of intra-channel nonlinearities using a frequency-domain volterra series equalizer", *Optics Express*, vol. 20, no. 2, pp. 1360–1369, 2012.

[204] Z. Tao, L. Dou, W. Yan, L. Li, T. Hoshida, and J. C. Rasmussen, "Multiplier-free intrachannel nonlinearity compensating algorithm operating at symbol rate", *Journal of Lightwave Technology*, vol. 29, no. 17, pp. 2570–2576, 2011.

[205] A. D. Shiner, M. Reimer, A. Borowiec, S. O. Gharan, J. Gaudette, P. Mehta, D. Charlton, K. Roberts, and M. O'Sullivan, "Demonstration of an 8-dimensional modulation format with reduced inter-channel nonlinearities in a polarization multiplexed coherent system", *Optics Express*, vol. 22, no. 17, pp. 20 366–20 374, 2014.

[206] G. Liga, T. Xu, A. Alvarado, R. I. Killey, and P. Bayvel, "On the performance of multichannel digital backpropagation in high-capacity long-haul optical transmission", *Optics Express*, vol. 22, no. 24, pp. 30 053–30 062, 2014.

[207] T. Sherborne, B. Banks, D. Semrau, R. I. Killey, P. Bayvel, and D. Lavery, "On the impact of fixed point hardware for optical fiber nonlinearity compensation algorithms", *Journal of Lightwave Technology*, vol. 36, no. 20, pp. 5016–5022, 2018.

[208] C. Fougstedt, L. Svensson, M. Mazur, M. Karlsson, and P. Larsson-Edefors, "ASIC implementation of time-domain digital back propagation for coherent receivers", *IEEE Photonics Technology Letters*, vol. 30, no. 13, pp. 1179–1182, 2018.

[209] C. S. Martins, L. Bertignono, A. Nespola, A. Carena, F. P. Guiomar, and A. N. Pinto, "Low-complexity time-domain DBP based on random step-size and partitioned quantization", *Journal of Lightwave Technology*, vol. 36, no. 14, pp. 2888–2895, 2018.

[210] C. B. Czegledi, G. Liga, D. Lavery, M. Karlsson, E. Agrell, S. J. Savory, and P. Bayvel, "Digital backpropagation accounting for polarization-mode dispersion", *Optics Express*, vol. 25, no. 3, pp. 1903–1915, 2017.

[211] N. Fontaine, S. Randel, P. Winzer, A. Sureka, S. Chandrasekhar, R. Delbue, R. Ryf, P. Pupalaikis, and X. Liu, "Fiber nonlinearity compensation by digital backpropagation of an entire 1.2-tb/s superchannel using a full-field spectrally-sliced receiver", in *Proceedings of the European Conference and Exhibition on Optical Communication (ECOC)*, paper. Mo.3.D.5, 2013.

[212] R. Dar and P. J. Winzer, "On the limits of digital back-propagation in fully loaded WDM systems", *IEEE Photonics Technology Letters*, vol. 28, no. 11, pp. 1253–1256, 2016.

[213] E. Temprana, E. Myslivets, B. P.-. P. Kuo, L. Liu, V. Ataie, N. Alic, and S. Radic, "Overcoming kerr-induced capacity limit in optical fiber transmission", *Science*, vol. 348, no. 6242, pp. 1445–1448, 2015.

[214] E. Temprana, E. Myslivets, L. Liu, V. Ataie, A. Wiberg, B. Kuo, N. Alic, and S. Radic, "Two-fold transmission reach enhancement enabled by transmitter-side digital backpropagation and optical frequency comb-derived information carriers", *Optics Express*, vol. 23, no. 16, pp. 20 774–20 783, 2015.

[215] M. Schetzeh, "Theory of pth-order inverses of nonlinear systems", *Transactions on Circuits and Systems*, vol. 23, no. 5, pp. 285–291, 1976.

[216] M. Gagni, F. P. Guiomar, S. Wabnitz, and A. N. Pinto, "Simplified high-order volterra series transfer function for optical transmission links", *Optics Express*, vol. 25, no. 3, pp. 2446–2459, 2017.

[217] M. I. Yousefi and F. R. Kschischang, "Information transmission using the nonlinear fourier transform, part i: Mathematical tools", *IEEE Transactions on Information Theory*, vol. 60, no. 7, pp. 4312–4328, 2014.

[218] S. T. Le, V. Aref, and H. Buelow, "Nonlinear signal multiplexing for communication beyond the kerr nonlinearity limit", *Nature Photonics*, vol. 11, no. 9, pp. 570–576, 2017.

[219] C. Häger and H. D. Pfister, "Nonlinear interference mitigation via deep neural networks", in *Proceedings of the Optical Fiber Communication Conference*, paper. W3A.4, 2018.

[220] C. Hager and H. D. Pfister, "Deep learning of the nonlinear schrödinger equation in fiber-optic communications", in *2018 IEEE International Symposium on Information Theory (ISIT)*, 2018.

[221] S. Zhang, F. Yaman, K. Nakamura, T. Inoue, V. Kamalov, L. Jovanovski, V. Vusirikala, E. Mateo, Y. Inada, and T. Wang, "Field and lab experimental demonstration of nonlinear impairment compensation using neural networks", *Nature Communications*, vol. 10, no. 1, 2019.

[222] C. Fougstedt, C. Hager, L. Svensson, H. D. Pfister, and P. Larsson-Edefors, "ASIC implementation of time-domain digital backpropagation with deep-learned chromatic dispersion filters", in *Proceedings of the European Conference on Optical Communication (ECOC)*, 2018.

[223] D. S. Millar, R. Maher, D. Lavery, T. Koike-Akino, M. Pajovic, A. Alvarado, M. Paskov, K. Kojima, K. Parsons, B. C. Thomsen, S. J. Savory, and P. Bayvel, "Design of a 1 Tb/s superchannel coherent receiver", *Journal of Lightwave Technology*, vol. 34, no. 6, pp. 1453–1463, 2016.

[224] G. Bosco, "Flexible transceivers and the rate/reach trade-off", in *Proceedings of Optical Fiber Communication Conference*, paper. M1G.1, 2018.

[225] R. Elschner, F. Frey, C. Meuer, J. K. Fischer, S. Alreesh, C. Schmidt-Langhorst, L. Molle, T. Tanimura, and C. Schubert, "Experimental demonstration of a format-flexible single-carrier coherent receiver using data-aided digital signal processing.", *Optics Express*, vol. 20, no. 27, pp. 28 786–28 791, 2012.

[226] F. A. Dietrich and W. Utschick, "Pilot-assisted channel estimation based on second-order statistics", *Transactions on Signal Processing*, vol. 53, no. 3, pp. 1178–1193, 2005.

[227] M. P. Yankov, E. P. da Silva, F. D. Ros, and D. Zibar, "Experimental analysis of pilot-based equalization for probabilistically shaped WDM systems with 256QAM/1024QAM", in *Proceedings of Optical Fiber Communication Conference*, paper W2A.48, 2017.

[228] A. Spalvieri and L. Barletta, "Pilot-aided carrier recovery in the presence of phase noise", *IEEE Transactions on Communications*, vol. 59, no. 7, pp. 1966–1974, 2011.

[229] M. Magarini, L. Barletta, A. Spalvieri, F. Vacondio, T. Pfau, M. Pepe, M. Bertolini, and G. Gavioli, "Pilot-symbols-aided carrier-phase Recovery for 100-G PM-QPSK digital coherent receivers", *IEEE Photonics Technology Letters*, vol. 24, no. 9, pp. 739–741, 2012.

[230] Q. Zhuge, M. Morsy-Osman, X. Xu, M. E. Mousa-Pasandi, M. Chagnon, Z. A. El-Sahn, and D. V. Plant, "Pilot-aided carrier phase recovery for m-QAM using superscalar parallelization based PLL", *Optics Express*, vol. 20, no. 17, pp. 19 599–19 609, 2012.

[231] A. F. Alfredsson, R. Krishnan, and E. Agrell, "Joint-polarization phase-noise estimation and symbol detection for optical coherent receivers", *Journal of Lightwave Technology*, vol. 34, no. 18, pp. 4394–4405, 2016.

[232] M. Pajovic, D. S. Millar, T. Koike-Akino, R. Maher, D. Lavery, A. Alvarado, M. Paskov, K. Kojima, K. Parsons, B. C. Thomsen, S. J. Savory, and P. Bayvel, "Experimental demonstration of multi-pilot aided carrier phase estimation for DP-64QAM and DP-256QAM", in *Proceedings of European Conference on Optical Communication*, paper Mo.3.3.2, 2015.

[233] I. Coddington, W. Swann, and N. Newbury, "Coherent dual-comb spectroscopy at high signal-to-noise ratio", *Physical Review A*, vol. 82, no. 4, 2010.

[234] V. Durán, S. Tainta, and V. Torres-Company, "Ultrafast electrooptic dual-comb interferometry", *Optics Express*, vol. 23, no. 23, pp. 30 557–30 569, 2015.

[235] I. Coddington, N. Newbury, and W. Swann, "Dual-comb spectroscopy", *Optica*, vol. 3, no. 4, pp. 414–426, 2016.

[236] G. Ycas, F. R. Giorgetta, E. Baumann, I. Coddington, D. Herman, S. A. Diddams, and N. R. Newbury, "High-coherence mid-infrared dual-comb spectroscopy spanning 2.6 to 5.2 μm", *Nature Photonics*, vol. 12, no. 4, pp. 202–208, 2018.

[237] N. Picqué and T. W. Hänsch, "Frequency comb spectroscopy", *Nature Photonics*, vol. 13, no. 3, pp. 146–157, 2019.

[238] A. Weiner, D. Leaird, J. Patel, and J. Wullert, "Programmable shaping of femtosecond optical pulses by use of 128-element liquid crystal phase modulator", *IEEE Journal of Quantum Electronics*, vol. 28, no. 4, pp. 908–920, 1992.

[239] S. T. Cundiff and A. M. Weiner, "Optical arbitrary waveform generation", *Nature Photonics*, vol. 4, no. 11, pp. 760–766, 2010.

[240] D. T. Spencer, T. Drake, T. C. Briles, J. Stone, L. C. Sinclair, C. Fredrick, Q. Li, D. Westly, B. R. Ilic, A. Bluestone, N. Volet, T. Komljenovic, L. Chang, S. H. Lee, D. Y. Oh, M.-G. Suh, K. Y. Yang, M. H. P. Pfeiffer, T. J. Kippenberg, E. Norberg, L. Theogarajan, K. Vahala, N. R. Newbury, K. Srinivasan, J. E. Bowers, S. A. Diddams, and S. B. Papp, "An optical-frequency synthesizer using integrated photonics", *Nature*, vol. 557, no. 7703, pp. 81–85, 2018.

[241] W. C. Swann and N. R. Newbury, "Frequency-resolved coherent lidar using a femtosecond fiber laser", *Optics Letters*, vol. 31, no. 6, pp. 826–828, 2006.

[242] I. Coddington, W. C. Swann, L. Nenadovic, and N. R. Newbury, "Rapid and precise absolute distance measurements at long range", *Nature Photonics*, vol. 3, no. 6, pp. 351–356, 2009.

[243] E. Baumann, F. R. Giorgetta, J.-D. Deschênes, W. C. Swann, I. Coddington, and N. R. Newbury, "Comb-calibrated laser ranging for three-dimensional surface profiling with micrometer-level precision at a distance", *Optics Express*, vol. 22, no. 21, pp. 24 914–24 928, 2014.

[244] V. Torres-Company and A. M. Weiner, "Optical frequency comb technology for ultra-broadband radio-frequency photonics", *Laser & Photonics Reviews*, vol. 8, no. 3, pp. 368–393, 2013.

[245] D. Marpaung, J. Yao, and J. Capmany, "Integrated microwave photonics", *Nature Photonics*, vol. 13, no. 2, pp. 80–90, 2019.

[246] A. J. Metcalf, T. Anderson, C. F. Bender, S. Blakeslee, W. Brand, D. R. Carlson, W. D. Cochran, S. A. Diddams, M. Endl, C. Fredrick, S. Halverson, D. D. Hickstein, F. Hearty, J. Jennings, S. Kanodia, K. F. Kaplan, E. Levi, E. Lubar, S. Mahadevan, A. Monson, J. P. Ninan, C. Nitroy, S. Osterman, S. B. Papp, F. Quinlan, L. Ramsey, P. Robertson, A. Roy, C. Schwab, S. Sigurdsson, K. Srinivasan, G. Stefansson, D. A. Sterner, R. Terrien, A. Wolszczan, J. T. Wright, and G. Ycas, "Stellar spectroscopy in the near-infrared with a laser frequency comb", *Optica*, vol. 6, no. 2, pp. 233–239, 2019.

[247] P. Delfyett, S. Gee, M.-T. Choi, H. Izadpanah, W. Lee, S. Ozharar, F. Quinlan, and T. Yilmaz, "Optical frequency combs from semiconductor lasers and applications in ultrawideband signal processing and communications", *Journal of Lightwave Technology*, vol. 24, no. 7, pp. 2701–2719, 2006.

[248] P. Minzioni, C. Lacava, T. Tanabe, J. Dong, X. Hu, G. Csaba, W. Porod, G. Singh, A. E. Willner, A. Almaiman, V. Torres-Company, J. Schröder, A. C. Peacock, M. J. Strain, F. Parmigiani, G. Contestabile, D. Marpaung, Z. Liu, J. E. Bowers, L. Chang, S. Fabbri, M. R. Vázquez, V. Bharadwaj, S. M. Eaton, P. Lodahl, X. Zhang, B. J. Eggleton, W. J. Munro, K. Nemoto, O. Morin, J. Laurat, and J. Nunn, "Roadmap on all-optical processing", *Journal of Optics*, vol. 21, no. 6, p. 063 001, 2019.

[249] H. Haus, "Mode-locking of lasers", *IEEE Journal of Selected Topics in Quantum Electronics*, vol. 6, no. 6, pp. 1173–1185, 2000.

[250] T. M. Fortier, A. Bartels, and S. A. Diddams, "Octave-spanning ti:sapphire laser with a repetition rate >1 GHz for optical frequency measurements and comparisons", *Optics Letters*, vol. 31, no. 7, pp. 1011–1013, 2006.

[251] L. C. Sinclair, I. Coddington, W. C. Swann, G. B. Rieker, A. Hati, K. Iwakuni, and N. R. Newbury, "Operation of an optically coherent frequency comb outside the metrology lab", *Optics Express*, vol. 22, no. 6, pp. 6996–7006, 2014.

[252] J. Chow, G. Town, B. Eggleton, M. Ibsen, K. Sugden, and I. Bennion, "Multiwavelength generation in an erbium-doped fiber laser using in-fiber comb filters", *IEEE Photonics Technology Letters*, vol. 8, no. 1, pp. 60–62, 1996.

[253] S. Joshi, C. Calò, N. Chimot, M. Radziunas, R. Arkhipov, S. Barbet, A. Accard, A. Ramdane, and F. Lelarge, "Quantum dash based single section mode locked lasers for photonic integrated circuits", *Optics Express*, vol. 22, no. 9, pp. 11 254–11 266, 2014.

[254] R. Zhou, S. Latkowski, J. O'Carroll, R. Phelan, L. P. Barry, and P. Anandarajah, "40nm wavelength tunable gain-switched optical comb source", in *Proceedings of European Conference on Optical Communication*, paper. Tu.5.LeSaleve.3, 2011.

[255] J. L. Hall, "Nobel lecture: Defining and measuring optical frequencies", *Reviews of Modern Physics*, vol. 78, no. 4, pp. 1279–1295, 2006.

[256] D. J. Jones, "Carrier-envelope phase control of femtosecond mode-locked lasers and direct optical frequency synthesis", *Science*, vol. 288, no. 5466, pp. 635–639, 2000.

[257] R. Holzwarth, T. Udem, T. W. Hänsch, J. C. Knight, W. J. Wadsworth, and P. S. J. Russell, "Optical frequency synthesizer for precision spectroscopy", *Physical Review Letters*, vol. 85, no. 11, pp. 2264–2267, 2000.

[258] A. Delmade, M. Krstić, C. Browning, J. Crnjanski, D. Gvozdić, and L. Barry, "Power efficient optical frequency comb generation using laser gain switching and dual-drive mach-zehnder modulator", *Optics Express*, vol. 27, no. 17, pp. 24 135–24 146, 2019.

[259] V. Ataie, E. Myslivets, B. P.-P. Kuo, N. Alic, and S. Radic, "Spectrally equalized frequency comb generation in multistage parametric mixer with nonlinear pulse shaping", *Journal of Lightwave Technology*, vol. 32, no. 4, pp. 840–846, 2014.

[260] S. Ozharar, F. Quinlan, I. Ozdur, S. Gee, and P. J. Delfyett, "Ultraflat optical comb generation by phase-only modulation of continuous-wave light", *IEEE Photonics Technology Letters*, vol. 20, no. 1, pp. 36–38, 2008.

[261] L. Westergren and B. Rade, *Beta Mathematics Handbook*. CRC Press, 1992.

[262] M. Fujiwara, M. Teshima, J. Kani, H. Suzuki, N. Takachio, and K. Iwatsuki, "Optical carrier supply module using flattened optical multicarrier generation based on sinusoidal amplitude and phase hybrid modulation", *Journal of Lightwave Technology*, vol. 21, no. 11, pp. 2705–2714, 2003.

[263] M. Doi, M. Sugiyama, K. Tanaka, and M. Kawai, "Advanced LiNbO/sub 3/ optical modulators for broadband optical communications", *IEEE Journal of Selected Topics in Quantum Electronics*, vol. 12, no. 4, pp. 745–750, 2006.

[264] T. Sakamoto, T. Kawanishi, and M. Izutsu, "Widely wavelength-tunable ultra-flat frequency comb generation using conventional dual-drive Mach-Zehnder modulator", *Electronics Letters*, vol. 43, no. 19, pp. 1039–1040, 2007.

[265] T. Yamamoto, T. Komukai, K. Suzuki, and A. Takada, "Spectrally flattened phase-locked multi-carrier light generator with phase modulators and chirped fibre bragg grating", *Electronics Letters*, vol. 43, no. 19, pp. 1040–1042, 2007.

[266] Y. Dou, H. Zhang, and M. Yao, "Improvement of flatness of optical frequency comb based on nonlinear effect of intensity modulator", *Optics Letters*, vol. 36, no. 14, pp. 2749–2751, 2011.

[267] M. Sugiyama, M. Doi, F. Utami, S. Watanabe, and H. Onaka, "A low drive voltage linbo3 phase and intensity integrated modulator for optical frequency comb generation and short pulse generation", in *Proceedings of European Conference on Optical Communication*, paper. Tu3.4.3, 2004.

[268] S. Xiao, L. Hollberg, N. R. Newbury, and S. A. Diddams, "Toward a low-jitter 10 GHz pulsed source with an optical frequency comb generator", *Optics Express*, vol. 16, no. 12, pp. 8498–8508, 2008.

[269] R. Slavik, F. Parmigiani, L. Gruner-Nielsen, D. Jakobsen, S. Herstrom, P. Petropoulos, and D. Richardson, "Stable and efficient generation of high repetition rate (> 160 GHz) subpicosecond optical pulses", *IEEE Photonics Technology Letters*, vol. 23, no. 9, pp. 540–542, 2011.

[270] M. Zhang, B. Buscaino, C. Wang, A. Shams-Ansari, C. Reimer, R. Zhu, J. M. Kahn, and M. Lončar, "Broadband electro-optic frequency comb generation in a lithium niobate microring resonator", *Nature*, vol. 568, no. 7752, pp. 373–377, 2019.

[271] A. J. Metcalf, V. Torres-Company, D. E. Leaird, and A. M. Weiner, "High-power broadly tunable electrooptic frequency comb generator", *Journal of Selected Topics in Quantum Electronics*, vol. 19, no. 6, pp. 231–236, 2013.

[272] V. Torres-Company, J. Lancis, and P. Andrés, "Lossless equalization of frequency combs", *Optics Letters*, vol. 33, no. 16, pp. 1822–1824, 2008.

[273] B. Kolner, "Space-time duality and the theory of temporal imaging", *IEEE Journal of Quantum Electronics*, vol. 30, no. 8, pp. 1951–1963, 1994.

[274] J. van Howe and C. Xu, "Ultrafast optical signal processing based upon space-time dualities", *Journal of Lightwave Technology*, vol. 24, no. 7, pp. 2649–2662, 2006.

[275] M. A. Foster, R. Salem, Y. Okawachi, A. C. Turner-Foster, M. Lipson, and A. L. Gaeta, "Ultrafast waveform compression using a time-domain telescope", *Nature Photonics*, vol. 3, no. 10, pp. 581–585, 2009.

[276] R. Salem, M. A. Foster, A. C. Turner-Foster, D. F. Geraghty, M. Lipson, and A. L. Gaeta, "High-speed optical sampling using a silicon-chip temporal magnifier", *Optics Express*, vol. 17, no. 6, pp. 4324–4329, 2009.

[277] V. Torres-Company, J. Lancis, and P. Andrés, "Space-time analogies in optics", in *Progress in Optics*, 2011, pp. 1–80.

[278] M. Fridman, A. Farsi, Y. Okawachi, and A. L. Gaeta, "Demonstration of temporal cloaking", *Nature*, vol. 481, no. 7379, pp. 62–65, 2012.

[279] R. Salem, M. A. Foster, and A. L. Gaeta, "Application of space–time duality to ultrahigh-speed optical signal processing", *Advances in Optics and Photonics*, vol. 5, no. 3, pp. 274–317, 2013.

[280] J. Azana, N. Berger, B. Levit, and B. Fischer, "Simplified temporal imaging systems for optical waveforms", *IEEE Photonics Technology Letters*, vol. 17, no. 1, pp. 94–96, 2005.

[281] E. Palushani, L. Oxenlowe, M. Galili, H. Mulvad, A. Clausen, and P. Jeppesen, "Flat-top pulse generation by the optical fourier transform technique for ultrahigh speed signal processing", *IEEE Journal of Quantum Electronics*, vol. 45, no. 11, pp. 1317–1324, 2009.

[282] R. Maram and J. Azaña, "Spectral self-imaging of time-periodic coherent frequency combs by parabolic cross-phase modulation", *Optics Express*, vol. 21, no. 23, pp. 28 824–28 835, 2013.

[283] P. A. Andrekson, "Linear propagation of optical picosecond pulse trains over oceanic distances", *Optics Letters*, vol. 18, no. 19, pp. 1621–1623, 1993.

[284] J. Azaña and M. A. Muriel, "Temporal talbot effect in fiber gratings and its applications", *Applied Optics*, vol. 38, no. 32, pp. 6700–6704, 1999.

[285] J. Azana and M. Muriel, "Temporal self-imaging effects: Theory and application for multiplying pulse repetition rates", *IEEE Journal of Selected Topics in Quantum Electronics*, vol. 7, no. 4, pp. 728–744, 2001.

[286] B. Zheng, Q. Xie, and C. Shu, "Comb spacing multiplication enabled widely spaced flexible frequency comb generation", *Journal of Lightwave Technology*, vol. 36, no. 13, pp. 2651–2659, 2018.

[287] B. E. Saleh and M. C. Teich, *Fundamentals of photonics*. John Wiley & Sons, 1991.

[288] A. W. Lohmann and D. Mendlovic, "Temporal filtering with time lenses", *Applied Optics*, vol. 31, no. 29, pp. 6212–6219, 1992.

[289] C. Bennett and B. Kolner, "Principles of parametric temporal imaging. i. system configurations", *IEEE Journal of Quantum Electronics*, vol. 36, no. 4, pp. 430–437, 2000.

[290] N. R. Newbury, "Searching for applications with a fine-tooth comb", *Nature Photonics*, vol. 5, no. 4, pp. 186–188, 2011.

[291] H. Murata, A. Morimoto, T. Kobayashi, and S. Yamamoto, "Optical pulse generation by electrooptic-modulation method and its application to integrated ultrashort pulse generators", *Journal of Selected Topics in Quantum Electronics*, vol. 6, no. 6, pp. 1325–1331, 2000.

[292] R. Slavik, S. G. Farwell, M. J. Wale, and D. J. Richardson, "Compact optical comb generator using InP tunable laser and push-pull modulator", *IEEE Photonics Technology Letters*, vol. 27, no. 2, pp. 217–220, 2015.

[293] J. Pfeifle, A. Coillet, R. Henriet, K. Saleh, P. Schindler, C. Weimann, W. Freude, I. V. Balakireva, L. Larger, C. Koos, and Y. K. Chembo, "Optimally coherent kerr combs generated with crystalline whispering gallery mode resonators for ultrahigh capacity fiber communications", *Physical Review Letters*, vol. 114, no. 9, 2015.

[294] T. Herr, V. Brasch, J. D. Jost, C. Y. Wang, N. M. Kondratiev, M. L. Gorodetsky, and T. J. Kippenberg, "Temporal solitons in optical microresonators", *Nature Photonics*, vol. 8, no. 2, pp. 145–152, 2013.

[295] X. Xue, Y. Xuan, Y. Liu, P.-H. Wang, S. Chen, J. Wang, D. E. Leaird, M. Qi, and A. M. Weiner, "Mode-locked dark pulse kerr combs in normal-dispersion microresonators", *Nature Photonics*, vol. 9, no. 9, pp. 594–600, 2015.

[296] X. Yi, Q.-F. Yang, K. Y. Yang, M.-G. Suh, and K. Vahala, "Soliton frequency comb at microwave rates in a high-q silica microresonator", *Optica*, vol. 2, no. 12, pp. 1078–1085, 2015.

[297] V. Brasch, M. Geiselmann, T. Herr, G. Lihachev, M. H. P. Pfeiffer, M. L. Gorodetsky, and T. J. Kippenberg, "Photonic chip-based optical frequency comb using soliton cherenkov radiation", *Science*, vol. 351, no. 6271, pp. 357–360, 2015.

[298] P.-H. Wang, J. A. Jaramillo-Villegas, Y. Xuan, X. Xue, C. Bao, D. E. Leaird, M. Qi, and A. M. Weiner, "Intracavity characterization of micro-comb generation in the single-soliton regime", *Optics Express*, vol. 24, no. 10, pp. 10 890–10 897, 2016.

[299] C. Joshi, J. K. Jang, K. Luke, X. Ji, S. A. Miller, A. Klenner, Y. Okawachi, M. Lipson, and A. L. Gaeta, "Thermally controlled comb generation and soliton modelocking in microresonators", *Optics Letters*, vol. 41, no. 11, pp. 2565–2568, 2016.

[300] T. J. Kippenberg, A. L. Gaeta, M. Lipson, and M. L. Gorodetsky, "Dissipative kerr solitons in optical microresonators", *Science*, vol. 361, no. 6402, eaan8083, 2018.

[301] F. Leo, S. Coen, P. Kockaert, S.-P. Gorza, P. Emplit, and M. Haelterman, "Temporal cavity solitons in one-dimensional kerr media as bits in an all-optical buffer", *Nature Photonics*, vol. 4, no. 7, pp. 471–476, 2010.

[302] P. Trocha, M. Karpov, D. Ganin, M. H. P. Pfeiffer, A. Kordts, S. Wolf, J. Krockenberger, P. Marin-Palomo, C. Weimann, S. Randel, W. Freude, T. J. Kippenberg, and C. Koos, "Ultrafast optical ranging using microresonator soliton frequency combs", *Science*, vol. 359, no. 6378, pp. 887–891, 2018.

[303] M.-G. Suh and K. J. Vahala, "Soliton microcomb range measurement", *Science*, vol. 359, no. 6378, pp. 884–887, 2018.

[304] M.-G. Suh, Q.-F. Yang, K. Y. Yang, X. Yi, and K. J. Vahala, "Microresonator soliton dual-comb spectroscopy", *Science*, vol. 354, no. 6312, pp. 600–603, 2016.

[305] A. Dutt, C. Joshi, X. Ji, J. Cardenas, Y. Okawachi, K. Luke, A. L. Gaeta, and M. Lipson, "On-chip dual-comb source for spectroscopy", *Science Advances*, vol. 4, no. 3, e1701858, 2018.

[306] C. Bao, M.-G. Suh, and K. Vahala, "Dual-comb imaging using soliton microcombs", in *Proceedings of the Conference on Lasers and Electro-Optics (CLEO)*, 2019.

[307] ——, "Microresonator soliton dual-comb imaging", *arXiv pre-print: 1809.09766v1*, 26, 2018.

[308] M.-G. Suh, X. Yi, Y.-H. Lai, S. Leifer, I. S. Grudinin, G. Vasisht, E. C. Martin, M. P. Fitzgerald, G. Doppmann, J. Wang, D. Mawet, S. B. Papp, S. A. Diddams, C. Beichman, and K. Vahala, "Searching for exoplanets using a microresonator astrocomb", *Nature Photonics*, vol. 13, no. 1, pp. 25–30, 2018.

[309] E. Obrzud, M. Rainer, A. Harutyunyan, M. H. Anderson, J. Liu, M. Geiselmann, B. Chazelas, S. Kundermann, S. Lecomte, M. Cecconi, A. Ghedina, E. Molinari, F. Pepe, F. Wildi, F. Bouchy, T. J. Kippenberg, and T. Herr, "A microphotonic astrocomb", *Nature Photonics*, vol. 13, no. 1, pp. 31–35, 2018.

[310] Z. L. Newman, V. Maurice, T. Drake, J. R. Stone, T. C. Briles, D. T. Spencer, C. Fredrick, Q. Li, D. Westly, B. R. Ilic, B. Shen, M.-G. Suh, K. Y. Yang, C. Johnson, D. M. S. Johnson, L. Hollberg, K. J. Vahala, K. Srinivasan, S. A. Diddams, J. Kitching, S. B. Papp, and M. T. Hummon, "Architecture for the photonic integration of an optical atomic clock", *Optica*, vol. 6, no. 5, pp. 680–685, 2019.

[311] B. Stern, X. Ji, Y. Okawachi, A. L. Gaeta, and M. Lipson, "Battery-operated integrated frequency comb generator", *Nature*, vol. 562, pp. 401–405, 2018.

[312] N. Volet, X. Yi, Q.-F. Yang, E. J. Stanton, P. A. Morton, K. Y. Yang, K. J. Vahala, and J. E. Bowers, "Micro-resonator soliton generated directly with a diode laser", *Laser & Photonics Reviews*, vol. 12, no. 5, p. 1 700 307, 2018.

[313] M.-G. Suh, C. Y. Wang, C. Johnson, and K. J. Vahala, "Directly pumped 10 GHz microcomb modules from low-power diode lasers", *Optics Letters*, vol. 44, no. 7, pp. 1841–1843, 2019.

[314] A. Fülöp, M. Mazur, A. Lorences-Riesgo, T. A. Eriksson, P.-H. Wang, Y. Xuan, D. E. Leaird, M. Qi, P. A. Andrekson, A. M. Weiner, and V. Torres-Company, "Long-haul coherent communications using microresonator-based frequency combs", *Optics Express*, vol. 25, no. 22, pp. 26 678–26 688, 2017.

[315] P. Marin-Palomo, J. N. Kemal, M. Karpov, A. Kordts, J. Pfeifle, M. H. Pfeiffer, P. Trocha, S. Wolf, V. Brasch, M. H. Anderson, R. Rosenberger, V. Kovendhan, W. Freude, T. J. Kippenberg, and C. Koos, "Microresonator-based solitons for massively parallel coherent optical communications", *Nature*, vol. 546, no. 7657, pp. 274–279, 2017.

[316] A. Fülöp, M. Mazur, A. Lorences-Riesgo, Ó. B. Helgason, P.-H. Wang, Y. Xuan, D. E. Leaird, M. Qi, P. A. Andrekson, A. M. Weiner, and V. Torres-Company, "High-order coherent communications using mode-locked dark-pulse kerr combs from microresonators", *Nature Communications*, vol. 9, p. 1598, 2018.

[317] G. Raybon, B. Guan, A. Adamiecki, P. J. Winzer, N. K. Fontaine, S. Chen, P. Papalaikis, R. Delbue, K. Doshi, B. Bhat, A. Blankman, A. Konczykowska, J.-Y. Dupuy, and F. Jorge, "160-Gbaud coherent receiver based on 100-GHz bandwidth, 240-GS/s analog-to-digital conversion", in *Proceedings of Optical Fiber Communication Conference*, paper. M2G.1, 2015.

[318] E. Agrell, M. Karlsson, A. R. Chraplyvy, D. J. Richardson, P. M. Krummrich, P. Winzer, K. Roberts, J. K. Fischer, S. J. Savory, B. J. Eggleton, M. Secondini, F. R. Kschischang, A. Lord, J. Prat, I. Tomkos, J. E. Bowers, S. Srinivasan, M. Brandt-Pearce, and N. Gisin, "Roadmap of optical communications", *Journal of Optics*, vol. 18, no. 6, p. 063 002, 2016.

[319] A. Castro, L. Velasco, M. Ruiz, M. Klinkowski, J. P. Fernández-Palacios, and D. Careglio, "Dynamic routing and spectrum (re)allocation in future flexgrid optical networks", *Computer Networks*, vol. 56, no. 12, pp. 2869–2883, 2012.

[320] D. Rafique, T. Rahman, A. Napoli, M. Kuschnerov, G. Lehmann, and B. Spinnler, "Flex-grid optical networks: Spectrum allocation and nonlinear dynamics of super-channels", *Optics Express*, vol. 21, no. 26, pp. 32 184–32 191, 2013.

[321] T. A. Strasser and J. L. Wagener, "Wavelength-selective switches for ROADM applications", *IEEE Journal of Selected Topics in Quantum Electronics*, vol. 16, no. 5, pp. 1150–1157, 2010.

[322] A. Morea, J. Renaudier, T. Zami, A. Ghazisaeidi, and O. Bertran-Pardo, "Throughput comparison between 50-GHz and 375-GHz grid transparent networks [invited]", *Journal of Optical Communications and Networking*, vol. 7, no. 2, A293, 2014.

[323] C. Liu, J. Pan, T. Detwiler, A. Stark, Y.-T. Hsueh, G.-K. Chang, and S. E. Ralph, "Super receiver design for superchannel coherent optical systems", in *Next-Generation Optical Communication: Components, Sub-Systems, and Systems*, 2012.

[324] P. Abolghasem, L. Dardis, A. Diba, T. Frost, B. Ellis, R. Going, X. Xu, A. Dentai, L. C. Chuang, S. Corzine, S. Murthy, M. Kuntz, J. Zhang, P. Samra, V. Lal, D. Pavinski, T. Butrie, S. DeMars, J. Rahn, V. Dominic, P. Evans, M. Ziari, and F. Kish, "Monolithically integrated L-band PICs and transceiver modules with 6λ x 200 Gbps (12 Tbps) for C + L band communication systems", *Optics Express*, vol. 27, no. 12, pp. 16 483–1649, 2019.

[325] C. Liu, J. Pan, T. Detwiler, A. Stark, Y.-T. Hsueh, G.-K. Chang, and S. E. Ralph, "Joint digital signal processing for superchannel coherent optical communication systems", *Optics Express*, vol. 21, no. 7, pp. 8342–8356, 2013.

[326] J. Renaudier, A. C. Meseguer, A. Ghazisaeidi, P. Tran, R. R. Muller, R. Brenot, A. Verdier, F. Blache, K. Mekhazni, B. Duval, H. Debregeas, M. Achouche, A. Boutin, F. Morin, L. Letteron, N. Fontaine, Y. Frignac, and G. Charlet, "First 100-nm continuous-band WDM transmission system with 115Tb/s transport over 100km using novel ultra-wideband semiconductor optical amplifiers", in *2017 European Conference on Optical Communication (ECOC)*, paper. Th.PDP.A.3, 2017.

[327] J. Renaudier, A. Arnould, D. L. Gac, A. Ghazisaeidi, P. Brindel, M. Makhsiyan, A. Verdier, K. Mekhazni, F. Blache, H. Debregeas, A. Boutin, N. Fontaine, D. Neilson, R. Ryf, H. Chen, M. Achouche, and G. Charlet, "107 tb/s transmission of 103-nm bandwidth over 3×100 km SSMF using ultra-wideband hybrid raman/SOA repeaters", in *Optical Fiber Communication Conference (OFC) 2019*, 2019.

[328] P. J. Winzer, "Would scaling to extreme ultraviolet or soft x-ray communications resolve the capacity crunch?", *Journal of Lightwave Technology*, vol. 36, no. 24, pp. 5786–5793, 2018.

[329] F. Poletti, "Nested antiresonant nodeless hollow core fiber", *Optics Express*, vol. 22, no. 20, pp. 23 807–23 828, 2014.

[330] B. Debord, A. Amsanpally, M. Chafer, A. Baz, M. Maurel, J. M. Blondy, E. Hugonnot, F. Scol, L. Vincetti, F. Gérôme, and F. Benabid, "Ultralow transmission loss in inhibited-coupling guiding hollow fibers", *Optica*, vol. 4, no. 2, pp. 209–217, 2017.

[331] H. Sakr, T. D. Bradley, Y. Hong, G. T. Jasion, J. R. Hayes, H. Kim, I. A. Davidson, E. N. Fokoua, Y. Chen, K. R. H. Bottrill, N. Taengnoi, P. Petropoulos, D. J. Richardson, and F. Poletti, "Ultrawide bandwidth hollow core fiber for interband short reach data transmission", in *Proceedings of the Optical Fiber Communication Conference*, paper. Th4A.1, 2019.

[332] T. Hayashi, T. Taru, O. Shimakawa, T. Sasaki, and E. Sasaoka, "Design and fabrication of ultra-low crosstalk and low-loss multi-core fiber", *Optics Express*, vol. 19, no. 17, pp. 16 576–16 592, 2011.

[333] P. Sillard, D. Molin, M. Bigot-Astruc, A. Amezcua-Correa, K. de Jongh, and F. Achten, "50 µm multimode fibers for mode division multiplexing", *Journal of Lightwave Technology*, vol. 34, no. 8, pp. 1672–1677, 2016.

[334] T. Hayashi, Y. Tamura, T. Hasegawa, and T. Taru, "Record-low spatial mode dispersion and ultra-low loss coupled multi-core fiber for ultra-long-haul transmission", *Journal of Lightwave Technology*, vol. 35, no. 3, pp. 450–457, 2017.

[335] J. M. Fini, B. Zhu, T. F. Taunay, M. F. Yan, and K. S. Abedin, "Crosstalk in multicore fibers with randomness: gradual drift vs. short-length variations.", *Optics Express*, vol. 20, no. 2, pp. 949–59, 2012.

[336] K. Saitoh, M. Koshiba, K. Takenaga, and S. Matsuo, "Crosstalk and core density in uncoupled multicore fibers", *IEEE Photonics Technology Letters*, vol. 24, no. 21, pp. 1898–1901, 2012.

[337] R. S. Luıs, B. J. Puttnam, A. V. T. Cartaxo, W. Klaus, J. M. D. Mendinueta, Y. Awaji, N. Wada, T. Nakanishi, T. Hayashi, and T. Sasaki, "Time and modulation frequency dependence of crosstalk in homogeneous multi-core fibers", *Journal of Lightwave Technology*, vol. 34, no. 2, pp. 441–447, 2016.

[338] R. Dar, P. J. Winzer, A. R. Chraplyvy, S. Zsigmond, K.-Y. Huang, H. Fevrier, and S. Grubb, "Cost-optimized submarine cables using massive spatial parallelism", *Journal of Lightwave Technology*, vol. 36, no. 18, pp. 3855–3865, 2018.

[339] J. K. Perin, J. M. Kahn, J. D. Downie, J. Hurley, and K. Bennett, "Importance of amplifier physics in maximizing the capacity of submarine links", *Journal of Lightwave Technology*, vol. 37, no. 9, pp. 2076–2085, 2019.

[340] L. E. Nelson, M. D. Feuer, K. Abedin, X. Zhou, T. F. Taunay, J. M. Fini, B. Zhu, R. Isaac, R. Harel, G. Cohen, and D. M. Marom, "Spatial superchannel routing in a two-span ROADM system for space division multiplexing", *Journal of Lightwave Technology*, vol. 32, no. 4, pp. 783–789, 2014.

[341] P. J. Winzer and G. J. Foschini, "MIMO capacities and outage probabilities in spatially multiplexed optical transport systems", *Optics Express*, vol. 19, no. 17, pp. 16 680–16 696, 2011.

[342] R. Ryf, R.-J. Essiambre, S. Randel, A. H. Gnauck, P. J. Winzer, T. Hayashi, T. Taru, and T. Sasaki, "MIMO-based crosstalk suppression in spatially multiplexed 3x56-gb/s PDM-QPSK signals for strongly coupled three-core fiber", *IEEE Photonics Technology Letters*, vol. 23, no. 20, pp. 1469–1471, 2011.

[343] S. Arik, K.-P. Ho, and J. Kahn, "Group delay management and multiinput multi-output signal processing in mode-division multiplexing systems", *Journal of Lightwave Technology*, vol. 34, no. 11, pp. 2867–2880, 2016.

[344] S. Randel, S. Corteselli, D. Badini, D. Pilori, S. Caelles, S. Chandrasekhar, J. Gripp, H. Chen, N. K. Fontaine, R. Ryf, and P. J. Winzer, "First real-time coherent MIMO-DSP for six coupled mode transmission", in *2015 IEEE Photonics Conference (IPC)*, 2015.

[345] N. K. Fontaine, C. R. Doerr, M. A. Mestre, R. Ryf, P. Winzer, L. Buhl, Y. Sun, X. Jiang, and R. Lingle, "Space-division multiplexing and all-optical MIMO demultiplexing using a photonic integrated circuit", in *Proceedings of Optical Fiber Communication Conference*, paper PDP5B.1, 2012.

[346] S. O. Arik, K.-P. Ho, and J. M. Kahn, "Delay spread reduction in mode-division multiplexing: Mode coupling versus delay compensation", *Journal of Lightwave Technology*, vol. 33, no. 21, pp. 4504–4512, 2015.

[347] K. Choutagunta, I. Roberts, and J. M. Kahn, "Efficient quantification and simulation of modal dynamics in multimode fiber links", *Journal of Lightwave Technology*, vol. 37, no. 8, pp. 1813–1825, 2019.

[348] H. Takara, A. Sano, T. Kobayashi, H. Kubota, H. Kawakami, A. Matsuura, Y. Miyamoto, Y. Abe, H. Ono, K. Shikama, Y. Goto, K. Tsujikawa, Y. Sasaki, I. Ishida, K. Takenaga, S. Matsuo, K. Saitoh, M. Koshiba, and T. Morioka, "1.01-Pb/s (12 SDM/222 WDM/456 Gb/s) crosstalk-managed transmission with 91.4-b/s/Hz aggregate spectral efficiency", in *Proceedings of the European Conference on Optical Communication*, paper. Th.3.C.1, 2012.

[349] B. Puttnam, R. Luis, W. Klaus, J. Sakaguchi, J.-M. D. Mendinueta, Y. Awaji, N. Wada, Y. Tamura, T. Hayashi, M. Hirano, and M. J., "2.15 Pb/s transmission using a 22 core homogeneous single-mode multi-core fiber and wideband optical comb", in *Proceedings of European Conference on Optical Communication*, paper. PDP3.1, 2015.

[350] T. Kobayashi, M. Nakamura, F. Hamaoka, K. Shibahara, T. Mizuno, A. Sano, H. Kawakami, A. Isoda, M. Nagatani, H. Yamazaki, Y. Miyamoto, Y. Amma, Y. Sasaki, K. Takenaga, K. Aikawa, K. Saitoh, Y. Jung, D. J. Richardson, K. Pulverer, M. Bohn, M. Nooruzzaman, and T. Morioka, "1-pb/s (32 SDM/46 WDM/768 gb/s) c-band dense SDM transmission over 205.6-km of single-mode heterogeneous multi-core fiber using 96-gbaud PDM-16qam channels", in *Optical Fiber Communication Conference Postdeadline Papers*, 2017.

[351] R. S. Luis, G. Rademacher, B. J. Puttnam, T. A. Eriksson, H. Furukawa, A. Ross-Adams, S. Gross, M. Withford, N. Riesen, Y. Sasaki, K. Saitoh, K. Aikawa, Y. Awaji, and N. Wada, "1.2 pb/s throughput transmission using a 160 um cladding, 4-core, 3-mode fiber", *Journal of Lightwave Technology*, vol. 37, no. 8, pp. 1798–1804, 2019.

[352] P. Sillard, D. Molin, M. Bigot-Astruc, A. Amezcua-Correa, K. de Jongh, and F. Achten, "DMGD-compensated links", in *Proceedings of the Optical Fiber Communication Conference*, paper. Tu2J.4, 2017.

[353] R. Ryf, N. K. Fontaine, H. Chen, and R.-J. Essiambre, "Coupled-core fibers: Where mode scrambling mitigates nonlinear effects", in *Advanced Photonics*, paper. NeTh2B.2, 2017.

[354] K. S. Abedin, T. F. Taunay, M. Fishteyn, D. J. DiGiovanni, V. Supradeepa, J. M. Fini, M. F. Yan, B. Zhu, E. M. Monberg, and F. Dimarcello, "Cladding-pumped erbium-doped multicore fiber amplifier", *Optics Express*, vol. 20, no. 18, pp. 20 191–20 200, 2012.

[355] J. Sakaguchi, W. Klaus, B. J. Puttnam, J. M. D. Mendinueta, Y. Awaji, N. Wada, Y. Tsuchida, K. Maeda, M. Tadakuma, K. Imamura, R. Sugizaki, T. Kobayashi, Y. Tottori, M. Watanabe, and R. V. Jensen, "19-core MCF transmission system using EDFA with shared core pumping coupled via free-space optics", *Optics Express*, vol. 22, no. 1, pp. 90–95, 2013.

[356] C. Matte-Breton, H. Chen, N. K. Fontaine, R. Ryf, R.-J. Essiambre, C. Kelly, C. Jin, Y. Messaddeq, and S. LaRochelle, "Demonstration of an erbium-doped fiber with annular doping for low gain compression in cladding-pumped amplifiers", *Optics Express*, vol. 26, no. 20, pp. 26 633–26 645, 2018.

[357] B. J. Puttnam, G. Rademacher, R. S. Luis, T. A. Eriksson, W. Klaus, Y. Awaji, N. Wada, K. Maeda, S. Takasaka, and R. Sugizaki, "0.715 pb/s transmission over 2,009.6 km in 19-core cladding pumped EDFA amplified MCF link", in *Optical Fiber Communication Conference Postdeadline Papers 2019*, 2019.

[358] J. C. Alvarado-Zacarias, N. K. Fontaine, H. Chen, J. E. Antonio-Lopez, S. Wittek, J. Li, S. Gausmann, R. Ryf, C. Gonnet, A. Amezcua-Correa, M. Bigot, A. Schülzgen, G. Li, P. Sillard, and R. Amezcua-Correa, "Coupled-core EDFA compatible with FMF transmission", in *Proceedings of hte Optical Fiber Communication Conference*, paper. Th4A.3, 2018.

[359] J. C. Alvarado-Zacarias, C. Matte-Breton, R. Ryf, N. K. Fontaine, H. Chen, S. Wittek, H. Sakuma, T. Ohtsuka, T. Hayashi, T. Hasegawa, S. LaRochelle, and R. Amezcua-Correa, "Characterization of coupled-core fiber amplifiers using swept-wavelength interferometer", in *Proceedings of the Optical Fiber Communication Conference*, paper. Th1B.6, 2019.

[360] N. Spellmeyer, "Communications performance of a multimode EDFA", *IEEE Photonics Technology Letters*, vol. 12, no. 10, pp. 1337–1339, 2000.

[361] C. Simonneau, P. Genevaux, G. Le Cocq, Y. Quiquempois, L. Bigot, A. Boutin, M. Bigot-Astruc, P. Sillard, and G. Charlet, "5-Mode amplifier with low modal crosstalk for spatial mode multiplexing transmission with low signal processing complexity", *Proceedings of European Conference on Optical Communication*, vol. 2015-Novem, no. 1, pp. 11–13, 2015.

[362] R. Ryf, N. K. Fontaine, H. Chen, A. H. Gnauck, Y. Jung, Q. Kang, J. K. Sahu, S. U. Alam, D. J. Richardson, Y. Sun, X. Jiang, L. Gruner-Nielsen, R. V. Jensen, and R. Lingle, "72-Tb/s transmission over 179-km all-fiber 6-mode span with two cladding pumped in-line amplifiers", *Proceedings of European Conference on Optical Communication*, vol. 2015-Novem, no. 1, pp. 6–8, 2015.

[363] H. Chen, C. Jin, B. Huang, N. K. Fontaine, R. Ryf, K. Shang, N. Grégoire, S. Morency, R.-J. Essiambre, G. Li, Y. Messaddeq, and S. LaRochelle, "Integrated cladding-pumped multicore few-mode erbium-doped fibre amplifier for space-division-multiplexed communications", *Nature Photonics*, vol. 10, no. 8, pp. 529–533, 2016.

[364] L. Yuan, Z. Liu, and J. Yang, "Coupling characteristics between single-core fiber and multicore fiber.", *Optics Letters*, vol. 31, no. 22, pp. 3237–3239, 2006.

[365] K. Watanabe and T. Saito, "Compact fan-out for 19-core multicore fiber, with high manufacturability and good optical properties", in *Proceeedings of the Opto-Electronics and Communications Conference (OECC)*, 2015.

[366] Y. Tottori, H. Tsuboya, and T. Kobayashi, "Improved return loss of fan-in/fan-out device for circular core array multi-core fiber using free space optics", in *Proceedings of the Photonics Society Summer Topical Meeting Series*, paper. 92, 2014.

[367] R. R. Thomson, R. J. Harris, T. A. Birks, G. Brown, J. Allington-Smith, and J. Bland-Hawthorn, "Ultrafast laser inscription of a 121-waveguide fan-out for astrophotonics", *Optics Letters*, vol. 37, no. 12, pp. 2331–2333, 2012.

[368] S. J. B. Yoo, B. Guan, and R. P. Scott, "Heterogeneous 2D/3D photonic integrated microsystems", *Microsystems & Nanoengineering*, vol. 2, no. 1, 2016.

[369] J. Carpenter, B. C. Thomsen, and T. D. Wilkinson, "Degenerate mode-group division multiplexing", *Journal of Lightwave Technology*, vol. 30, no. 24, pp. 3946–3952, 2012.

[370] R. Ryf, N. K. Fontaine, and R.-J. Essiambre, "Spot-based mode couplers for mode-multiplexed transmission in few-mode fiber", *IEEE Photonics Technology Letters*, vol. 24, no. 21, pp. 1973–1976, 2012.

[371] T. A. Birks, I. Gris-Sánchez, S. Yerolatsitis, S. G. Leon-Saval, and R. R. Thomson, "The photonic lantern", *Advances in Optics and Photonics*, vol. 7, no. 2, pp. 107–167, 2015.

[372] J.-F. Morizur, L. Nicholls, P. Jian, S. Armstrong, N. Treps, B. Hage, M. Hsu, W. Bowen, J. Janousek, and H.-A. Bachor, "Programmable unitary spatial mode manipulation", *Journal of the Optical Society of America A*, vol. 27, no. 11, pp. 2524–2531, 2010.

[373] S. Randel, R. Ryf, A. Sierra, P. J. Winzer, A. H. Gnauck, C. A. Bolle, R.-J. Essiambre, D. W. Peckham, A. McCurdy, and R. Lingle, "6x56-gb/s mode-division multiplexed transmission over 33-km few-mode fiber enabled by 6x6 MIMO equalization", *Optics Express*, vol. 19, no. 17, pp. 16 697–16 707, 2011.

[374] D. Soma, S. Beppu, Y. Wakayama, K. Igarashi, T. Tsuritani, I. Morita, and M. Suzuki, "257-Tbit/s weakly coupled 10-mode C + L-band WDM transmission", *Journal of Lightwave Technology*, vol. 36, no. 6, pp. 1375–1381, 2018.

[375] K. Benyahya, C. Simonneau, A. Ghazisaeidi, P. Jian, J.-F. Morizur, G. Labroille, M. Bigot, P. Sillard, J. Renaudier, and G. Charlet, "High-speed bi-directional transmission over multimode fiber link in IM/DD systems", *Journal of Lightwave Technology*, vol. 36, no. 18, pp. 4174–4180, 2018.

[376] J. Carpenter, B. J. Eggleton, and J. Schröder, "110x110 optical mode transfer matrix inversion", *Optics Express*, vol. 22, no. 1, pp. 96–101, 2013.

[377] ——, "Complete spatiotemporal characterization and optical transfer matrix inversion of a 420 mode fiber", *Optics Letters*, vol. 41, no. 23, pp. 5580–5583, 2016.

[378] B. Huang, N. K. Fontaine, R. Ryf, B. Guan, S. G. Leon-Saval, R. Shubochkin, Y. Sun, R. Lingle, and G. Li, "All-fiber mode-group-selective photonic lantern using graded-index multimode fibers", *Optics Express*, vol. 23, no. 1, pp. 224–234, 2015.

[379] N. K. Fontaine, R. Ryf, H. Chen, A. V. Benitez, B. Guan, R. Scott, B. Ercan, S. J. B. Yoo, L. E. Grüner-Nielsen, Y. Sun, R. Lingle, E. Antonio-Lopez, and R. Amezcua-Correa, "30x30 MIMO transmission over 15 spatial modes", in *Proceedings of Optical Fiber Communication Conference*, paper. Th5C.1, 2015.

[380] N. K. Fontaine, R. Ryf, J. Bland-Hawthorn, and S. G. Leon-Saval, "Geometric requirements for photonic lanterns in space division multiplexing", *Optics Express*, vol. 20, no. 24, pp. 27 123–27 132, 2012.

[381] A. M. Velázquez-Benıtez, J. E. Antonio-López, J. C. Alvarado-Zacarıas, N. K. Fontaine, R. Ryf, H. Chen, J. Hernández-Cordero, P. Sillard, C. Okonkwo, S. G. Leon-Saval, and R. Amezcua-Correa, "Scaling photonic lanterns for space-division multiplexing", *Scientific Reports*, vol. 8, no. 1, 2018.

[382] S. G. Leon-Saval, N. K. Fontaine, J. R. Salazar-Gil, B. Ercan, R. Ryf, and J. Bland-Hawthorn, "Mode-selective photonic lanterns for space-division multiplexing", *Optics Express*, vol. 22, no. 1, pp. 1036–1044, 2014.

[383] N. K. Fontaine, R. Ryf, H. Chen, D. T. Neilson, K. Kim, and J. Carpenter, "Laguerre-gaussian mode sorter", *Nature Communications*, vol. 10, no. 1, 2019.

[384] S. Bade, B. Denolle, G. Trunet, D. Allioux, P. Jian, O. Pinel, and G. Labroille, "Fabrication and Characterization of a Mode-selective 45-Mode Spatial Multiplexer based on Multi-Plane Light Conversion", arXiv:1803.07907, 2018.

[385] J. Carpenter, S. G. Leon-Saval, J. R. Salazar-Gil, J. Bland-Hawthorn, G. Baxter, L. Stewart, S. Frisken, M. A. F. Roelens, B. J. Eggleton, and J. Schröder, "1x11 few-mode fiber wavelength selective switch using photonic lanterns", *Optics Express*, vol. 22, no. 3, pp. 2216–2221, 2014.

[386] N. K. Fontaine, R. Ryf, C. Liu, B. Ercan, J. R. S. Gil, S. G. Leon-Saval, J. Bland-Hawthorn, and D. T. Neilson, "Few-mode fiber wavelength selective switch with spatial-diversity and reduced-steering angle", in *Proceedings of the Optical Fiber Communication Conference*, paper. Th4A.7, 2014.

[387] K.-P. Ho, J. M. Kahn, and J. P. Wilde, "Wavelength-selective switches for mode-division multiplexing: Scaling and performance analysis", *Journal of Lightwave Technology*, vol. 32, no. 22, pp. 4326–4337, 2014.

[388] D. M. Marom, J. Dunayevsky, D. Sinefeld, M. Blau, R. Ryf, N. K. Fontaine, M. Montoliu, S. Randel, C. Liu, B. Ercan, M. Esmaeelpour, S. Chandrasekhar, A. H. Gnauck, S. G. Leon-Saval, J. Bland-Hawthorn, J. R. Salazar-Gil, Y. Sun, L. Grüner-Nielsen, and R. Lingle, "Wavelength-

selective switch with direct few mode fiber integration", *Optics Express*, vol. 23, no. 5, p. 5723, 2015.

[389] N. K. Fontaine, T. Haramaty, R. Ryf, H. Chen, L. Miron, L. Pascar, M. Blau, B. Frenkel, L. Wang, Y. Messaddeq, S. LaRochelle, R. J. Essiambre, Y. Jung, Q. Kang, J. K. Sahu, S. U. Alam, D. J. Richardson, and D. M. Marom, "Heterogeneous space-division multiplexing and joint wavelength switching demonstration", in *Optical Fiber Communication Conference Post Deadline Papers*, 2015.

[390] J. Veselka and S. Korotky, "A multiwavelength source having precise channel spacing for WDM systems", *IEEE Photonics Technology Letters*, vol. 10, no. 7, pp. 958–960, 1998.

[391] H. Takara, T. Ohara, K. Mori, K. Sato, E. Yamada, Y. Inoue, T. Shibata, M. Abe, T. Morioka, and K.-I. Sato, "More than 1000 channel optical frequency chain generation from single supercontinuum source with 12.5 GHz channel spacing", *Electronics Letters*, vol. 36, no. 25, pp. 2089–2090, 2000.

[392] T. Ohara, H. Takara, T. Yamamoto, H. Masuda, T. Morioka, M. Abe, and H. Takahashi, "Over-1000-channel ultradense WDM transmission with supercontinuum multicarrier source", *Journal of Lightwave Technology*, vol. 24, no. 6, pp. 2311–2317, 2006.

[393] M. Fujiwara, J. Kani, H. Suzuki, K. Araya, and M. Teshima, "Flattened optical multicarrier generation of 12.5 GHz spaced 256 channels based on sinusoidal amplitude and phase hybrid modulation", *Electronics Letters*, vol. 37, no. 15, pp. 967–968, 2001.

[394] W. Mao, P. A. Andrekson, and J. Toulouse, "Investigation of a spectrally flat multi-wavelength dwdm source based on optical phase- and intensity-modulation", in *Proceedings of Optical Fiber Communication Conference*, paper. MF78, 2004.

[395] J. N. Kemal, J. Pfeifle, P. Marin-Palomo, M. D. G. Pascual, S. Wolf, F. Smyth, W. Freude, and C. Koos, "Multi-wavelength coherent transmission using an optical frequency comb as a local oscillator", *Optics Express*, vol. 24, no. 22, pp. 25 432–25 445, 2016.

[396] V. Ataie, E. Temprana, L. Liu, E. Myslivets, B. P.-P. Kuo, N. Alic, and S. Radic, "Ultrahigh count coherent WDM channels transmission using optical parametric comb-based frequency synthesizer", *Journal of Lightwave Technology*, vol. 33, no. 3, pp. 694–699, 2015.

[397] J. Pfeifle, V. Brasch, M. Lauermann, Y. Yu, D. Wegner, T. Herr, K. Hartinger, P. Schindler, J. Li, D. Hillerkuss, R. Schmogrow, C. Weimann, R. Holzwarth, W. Freude, J. Leuthold, T. J. Kippenberg, and C. Koos, "Coherent terabit communications with microresonator Kerr frequency combs", *Nature Photonics*, vol. 8, no. 5, pp. 375–380, 2014.

[398] V. Vujicic, C. Calo, R. Watts, F. Lelarge, C. Browning, K. Merghem, A. Martinez, A. Ramdane, and L. P. Barry, "Quantum dash mode-locked lasers for data centre applications", *Journal of Selected Topics in Quantum Electronics*, vol. 21, no. 6, pp. 53–60, 2015.

[399] J. N. Kemal, P. Marin-Palomo, K. Merghem, A. Guy, cosimo calo, R. Brenot, F. Lelarge, A. Ramdane, S. Randel, W. Freude, and C. Koos, "32QAM WDM transmission using a quantum-dash passively mode-locked laser with resonant feedback", in *Proceedings of Optical Fiber Communication Conference*, paper. Th5C.3, 2017.

[400] B. P.-P. Kuo, E. Myslivets, V. Ataie, E. G. Temprana, N. Alic, and S. Radic, "Wideband parametric frequency comb as coherent optical carrier", *Journal of Lightwave Technology*, vol. 31, no. 21, pp. 3414–3419, 2013.

[401] E. Temprana, B.-P. Kuo, N. Alic, S. Radic, and S. Grubb, "400 gb/s WDM DP-256-QAM transmission with 50 GHz channel separation", in *IEEE Photonics Conference*, 2016.

[402] V. Torres-Company, J. Schroder, A. Fulop, M. Mazur, L. Lundberg, O. B. Helgason, M. Karlsson, and P. A. Andrekson, "Laser frequency combs for coherent optical communications", *Journal of Lightwave Technology*, vol. 37, no. 7, pp. 1663–1670, 2019.

[403] P. Marin-Palomo, J. N. Kemal, W. Freude, S. Randel, and C. Koos, "OSNR limitations of chip-based optical frequency comb sources for wdm coherent communications", *arXiv preprint :1907.01042*, 1, 2019.

[404] A. Ishizawa, T. Nishikawa, A. Mizutori, H. Takara, A. Takada, T. Sogawa, and M. Koga, "Phase-noise characteristics of a 25-GHz-spaced optical frequency comb based on a phase- and intensity-modulated laser", *Optics Express*, vol. 21, no. 24, pp. 29 186–29 194, 2013.

[405] Y. Takushima, H. Sotobayashi, M. E. Grein, E. P. Ippen, and H. A. Haus, "Linewidth of mode combs of passively and actively mode-locked semiconductor laser diodes", in *Active and Passive Optical Components for WDM Communications IV*, 2004.

[406] R. K. Shelton, S. M. Foreman, L.-S. Ma, J. L. Hall, H. C. Kapteyn, M. M. Murnane, M. Notcutt, and J. Ye, "Subfemtosecond timing jitter between two independent, actively synchronized, mode-locked lasers", *Optics Letters*, vol. 27, no. 5, pp. 312–314, 2002.

[407] L. Lundberg, M. Karlsson, A. Lorences-Riesgo, M. Mazur, V. Torres-Company, J. Schröder, and P. Andrekson, "Frequency comb-based WDM transmission systems enabling joint signal processing", *Applied Sciences*, vol. 8, no. 5, p. 718, 2018.

[408] Z. Tong, A. O. J. Wiberg, E. Myslivets, B. P. P. Kuo, N. Alic, and S. Radic, "Spectral linewidth preservation in parametric frequency combs seeded by dual pumps", *Optics Express*, vol. 20, no. 16, pp. 17 610–17 619, 2012.

[409] A. Fülöp, M. Mazur, A. Lorences-Riesgo, P.-H. Wang, Y. Xuan, D. E. Leaird, M. Qi, P. A. Andrekson, A. M. Weiner, and V. Torres-Company, "Frequency noise of a normal dispersion microresonator-based frequency comb", in *Proceedings of the Optical Fiber Communication Conference*, paper. W2A.6, 2017.

[410] P. Marin-Palomo, J. N. Kemal, P. Trocha, S. Wolf, K. Merghem, F. Lelarge, A. Ramdane, W. Freude, S. Randel, and C. Koos, "Comb-based wdm transmission at 10 Tbit/s using a dc-driven quantum-dash mode-locked laser diode", *arXiv preprint: 1904.11952*, 22, 2019.

[411] T. Miyazaki and F. Kubota, "PSK self-homodyne detection using a pilot carrier for multibit/symbol transmission with inverse-RZ signal", *IEEE Photonics Technology Letters*, vol. 17, no. 6, pp. 1334–1336, 2005.

[412] M. Sjodin, P. Johannisson, M. Karlsson, Z. Tong, and P. A. Andrekson, "OSNR requirements for self-homodyne coherent systems", *IEEE Photonics Technology Letters*, vol. 22, no. 2, pp. 91–93, 2010.

[413] P. Johannisson, M. Sjodin, M. Karlsson, E. Tipsuwannakul, and P. Andrekson, "Cancellation of nonlinear phase distortion in self-homodyne coherent systems", *IEEE Photonics Technology Letters*, vol. 22, no. 11, pp. 802–804, 2010.

[414] M. Sjödin, E. Agrell, P. Johannisson, G.-W. Lu, P. A. Andrekson, and M. Karlsson, "Filter optimization for self-homodyne coherent WDM systems using interleaved polarization division multiplexing", *Journal of Lightwave Technology*, vol. 29, no. 9, pp. 1219–1226, 2011.

[415] B. J. Puttnam, R. S. Luis, J. M. Delgado Mendinueta, J. Sakaguchi, W. Klaus, Y. Kamio, M. Nakamura, N. Wada, Y. Awaji, A. Kanno, K. Tetsuya, and M. Tetsuya, "Self-homodyne detection in optical communication systems", in *Photonics*, vol. 1, 2014, pp. 110–130.

[416] B. J. Puttnam, J. Sakaguchi, J. M. D. Mendinueta, W. Klaus, Y. Awaji, N. Wada, A. Kanno, and T. Kawanishi, "Investigating self-homodyne coherent detection in a 19 channel space-division-multiplexed transmission link", *Optics Express*, vol. 21, no. 2, pp. 1561–1566, 2013.

[417] B. J. Puttnam, R. Luis, J.-M. Delgado-Mendinueta, J. Sakaguchi, W. Klaus, Y. Awaji, N. Wada, A. Kanno, and T. Kawanishi, "High-capacity self-homodyne PDM-WDM-SDM transmission in a 19-core fiber", *Optics Express*, vol. 22, no. 18, pp. 21 185–21 191, 2014.

[418] A. C. Bordonalli, M. J. Fice, and A. J. Seeds, "Optical injection locking to optical frequency combs for superchannel coherent detection", *Optics Express*, vol. 23, no. 2, pp. 1547–1557, 2015.

[419] A. Lorences-Riesgo, T. A. Eriksson, A. Fülöp, P. A. Andrekson, and M. Karlsson, "Frequency-comb regeneration for self-homodyne superchannels", *Journal of Lightwave Technology*, vol. 34, no. 8, pp. 1800–1806, 2016.

[420] A. Lorences-Riesgo, M. Mazur, T. A. Eriksson, P. A. Andrekson, and M. Karlsson, "Self-homodyne 24x32-QAM superchannel receiver enabled by all-optical comb regeneration using Brillouin amplification", *Optics Express*, vol. 24, no. 26, pp. 29 714–29 723, 2016.

[421] X. Yi, N. K. Fontaine, R. P. Scott, and S. Yoo, "Tb/s coherent optical OFDM systems enabled by optical frequency combs", *Journal of Lightwave Technology*, vol. 28, no. 14, pp. 2054–2061, 2010.

[422] L. Lundberg, M. Mazur, A. Mirani, B. Foo, J. Schröder, V. Torres-Company, M. Karlsson, and P. A. Andrekson, "Phase-coherent lightwave communications with frequency combs", *arXiv preprint:1905.04963*, 13, 2019.

[423] J. Pan, C. Liu, T. Detwiler, A. Stark, Y.-T. Hsueh, and S. Ralph, "Inter-channel crosstalk cancellation for nyquist-wdm superchannel applications", *Journal of Lightwave Technology*, vol. 30, no. 24, pp. 3993–3999, 2012.

[424] T. Zeng, "Superchannel transmission system based on multi-channel equalization", *Optics Express*, vol. 21, no. 12, pp. 14 799–14 807, 2013.